FABRICATION OF BIOPOLYESTER MATERIALS BY ELECTROSPINNING AS SCAFFOLDS FOR TISSUE ENGINEERING

PEDRAM AZARI

THESIS SUBMITTED IN FULFILMENT OF
THE REQUIREMENTS FOR THE DEGREE OF
DOCTOR OF PHILOSOPHY

FACULTY OF SCIENCE
UNIVERSITY OF MALAYA
KUALA LUMPUR
2016

UNIVERSITI MALAYA

ORIGINAL LITERARY WORK DECLARATION

Name of Candidate: PEDRAM AZARI (I.C/Passport No [redacted]

Registration/Matric No: SHC080025

Name of Degree: Ph.D. in Polymer chemistry

Title of Project Paper/Research Report/Dissertation/Thesis ("this Work"):

Fabrication of Biopolyester materials by Electrospinning as Scaffolds for Tissue Engineering

Field of Study:

I do solemnly and sincerely declare that:

(1) I am the sole author/writer of this Work;
(2) This Work is original;
(3) Any use of any work in which copyright exists was done by way of fair dealing and for permitted purposes and any excerpt or extract from, or reference to or reproduction of any copyright work has been disclosed expressly and sufficiently and the title of the Work and its authorship have been acknowledged in this Work;
(4) I do not have any actual knowledge nor do I ought reasonably to know that the making of this work constitutes an infringement of any copyright work;
(5) I hereby assign all and every rights in the copyright to this Work to the University of Malaya ("UM"), who henceforth shall be owner of the copyright in this Work and that any reproduction or use in any form or by any means whatsoever is prohibited without the written consent of UM having been first had and obtained;
(6) I am fully aware that if in the course of making this Work I have infringed any copyright whether intentionally or otherwise, I may be subject to legal action or any other action as may be determined by UM.

[redacted] Date

Subscribed and solemnly declared before,

[redacted]

Witness's Signature Date

Name: Dr. Gan Seng Neon
Designation: Profesor
Jabatan Kimia, Universiti Malaya
50603 Kuala Lumpur.

ABSTRACT

Tissue loss is one of the most important reasons for failure in all the living systems. With development of newer technologies, tissue regeneration seems to be a promising alternative to conventional surgical and organ donation methods without the problems of disease transmission and availability of donor. Preparation of biocompatible and biodegradable polymeric materials for scaffolding is an important part of tissue engineering. In this research, several biopolyester scaffolding materials have been developed based on polycaprolactone (PCL) and polyhydroxybutyrate (PHB) and their combination with medium chain length polyhydroxyalkanoates and bovine hydroxyapatite (BHA) at different weight ratios through electrospinning. The resulting materials were characterized using field emission scanning electron microscopy, fourier transform infrared spectroscopy, thermogravimetric analysis, differential scanning calorimetery, and wide-angle X-ray diffraction. To study cell-scaffold interaction, rat bone marrow derived stem cells were seeded on the scaffolds and cultured *in vitro* followed by carrying out cell proliferation and alkaline phosphate assays. The results showed that all the produced scaffolds are biocompatible and promote stem cell and keratocytes growth and proliferation. PCL-BHA40% and PHB-BHA10% samples showed the highest proliferation rates within 14 days. Alkaline phosphate assay showed that the combination of electrospun PHB, PCL and BHA was osteoinductive and resulted in stem cells differentiation toward Osteoblasts. The gene expression results showed that electrospun PCL promotes keratocyte growth without differentiation; the feature which is useful for drug screening applications. All the produced fulfilled the preliminary requirements of tissue engineering and can be potential candidates for more detailed *in vivo* studies.

ABSTRAK

Kehilangan tisu merupakan salah satu sebab terpenting bagi kegagalan dalam semua sistem hidup. Dengan perkembangan teknologi baharu, pertumbuhan semula tisu seolah-olah menjadi alternatif yang memberansangkan kepada kaedah pembedahan dan derma organ konvensional tanpa masalah jangkitan penyakit dan ketersediaan penderma. Penyediaan bahan polimer terbioserasian dan mesra alam untuk perancah adalah satu bahagian penting dalam kejuruteraan tisu. Dalam kajian ini, beberapa bahan perancah biopoliester berdasarkan polikaprolakton dan polihidroksibutirat telah disiasat dan gabungan kedua-duanya dengan polihidroksialkanoat berantai sederhana panjang dan hidroksiapatit pada nisbah berat yang berbeza melalui elektroputaran. Bahan yang terhasil dicirikan menggunakan mikroskopi elektron imbasan medan pemancaran , spektroskopi inframerah jelmaan fourier, analisis termogravimetri, kalorimetri imbasan pembezaan, dan pembelauan sinar-X sudut lebar. Untuk mengkaji interaksi sel-perancah, sum-sum tulang tikus yang diperolehi sel stem telah diletakkan sebagai benih pada perancah dan dikultur secara vitro serta diikuti dengan menjalankan percambahan sel dan ujian fosfat beralkali. Keputusan kajian menunjukkan bahawa perancah yang dihasilkan telah memenuhi syarat awal bagi kejuruteraan tisu dan boleh berpotensi untuk kajian yang lebih terperinci dalam aplikasi perubatan.

ACKNOWLEDGEMENT

I would like to express my sincere gratitude to my supervisors, Professor Dr. Gan seng Neon, Professor Dr. Rosiyah Yahya and Professor Dr. Wong Chiow San for their invaluable advice and guidance throughout my PhD study. I should thank Dr. Belinda-Pingguan Murphy and Dr. Ivan Djordjevic from the faculty of biomedical engineering for their generous support of this research. I would love to thank my parents Gholamreza Azari and Mahvash Rahim for their consistent support and encouraging throughout my study. The last but not the least I would like to convey my appreciation to University of Malaya for the financial support through research grant IPPP PV107-2012A.

TABLE OF CONTETS

PAGE

LIST OF FIGURES

LIST OF TABLES

LIST OF ABBREVIATIONS

ALP	Alkaline phosphate assay
BHA	Bovine Hydroxyapatite
BMSC	Bone marrow stem cells
CA	Citric acid
DMF	Dimethylformamaide
DMSO	Dimethyl sulfoxide
DSC	Differential scanning calorimetry
FESEM	Field emission scanning microscopy
FTIR	Fourier transform infra-red spectroscopy
GPC	Gel permeation chromatography
HA	Hydroxyapatite
mcl-PHA	Medium chain length polyhydroxyalkanoate
MTT	3-[4,5-dimethylthiazol-2-yl]-2,5 diphenyl tetrazolium bromide
PCL	Poly(ε-caprolactone)
PCLT	Polycaprolactone triol
PEO	Poly(ethylene oxide)
PET	Poly(ethylene terephthalate)
PHB	Poly(3-hydroxybutyrate)
PHBV	Poly (3-hydroxybutyric acid-co-3-hydroxyvaleric acid)
RT-PCR	Reverse transcription polymerase chain reaction
TGA	Thermogravimetric analysis

WAXRD	Wide angle x-ray diffraction

LIST OF SYMBOLS

ΔG	Change in Gibbs free energy
ΔH	Changes in enthalpy of mixing
$\Delta \mathbf{S}$	Changes in entropy of mixing
γ	Surface tension
g	Gravity force
h	Capillary length
R	Capillary radius
r_0	Droplet radius
T	Temperature
T_m	Melting Temperature
φ	Relative humidity
ρ	Density
P	Vapor pressure
P_s	Saturated Vapor pressure
V_c	Critical Voltage

LIST OF APPENDICES

CHAPTER 1: INTRODUCTION

1.1 Problem statement

Tissue engineering is an interdisciplinary field of science with ultimate goal of *in vitro* regeneration of the organs from cells in order to overcome the shortages caused by the unavailability of donors (Chapekar, 2000). Despite the advances in the currently available surgical therapies which have greatly improved the quality of life, the need for alternative methods has been emerging (Akram et al., 2014). An important part of tissue engineering is design and fabrication scaffolds; a 3D porous surface which serves as a temporary template for *in vitro* tissue regeneration (Hutmacher, 2000). Electrospun biopolyesters have shown promising results as scaffolding materials due to their biocompatibility, high porosity and similarity of texture to natural extracellular matrix (Azari et al., 2015; Teo et al., 2006). There are several good features with biopolyesters including relatively low cost of synthesis, ease of *in vivo* degradation through hydrolysis of ester bonds and non-toxic degradation products (Gunatillake et al., 2003a). Therefore, electrospun biopolyesters have been the subject of a lot of researches within the last decade (Araujo, 2010; Croisier et al., 2012; Doyle et al., 1991; Johnson et al., 2012). However; there is still the need for a comprehensive and comparative study on various electrospun biopolyesters in terms of chemical and morphological properties as well as biological potential. This study aims to provide a comprehensive and comparative information about the chemical and biological potential of electrospun scaffolds based on different microbial and chemical biopolyesters which are fabricated under the similar conditions. The produced scaffolds have been studied via various analytical methods which include FESEM, FTIR, WAXRD, TGA, DSC and confocal microscopy as well as cell proliferation and differentiation assays.

1.2 Scope of the research and thesis structure

This study is based on the electrospinning of PCL, PHB, PHBV and their composites with BHA to produce scaffolds for tissue engineering applications. This research consists of 6 individually connected parallel projects with a specific focus on bone tissue engineering, as outlined in Figure 1.1. The first project describes the construction and calibration of an electrospinning setup for biopolyesters. It includes the attempts to find the right processing parameters of electrospinning. The second part of this research presents a way to overcome the poor processability of PHB which is naturally rigid due to its high crystallinity. PHB has been modified through blending with mcl-PHA. Along with processing parameters, intrinsic parameters play an important role in the formation of electrospun fibers and their relevant morphology.

In project 3 and 4 various compositional ratios of PCL-BHA and PHB-BHA have been studied respectively. The goal of the study was to find the compositional ratio which is suitable for bone tissue engineering applications. The morphological and chemical properties of the scaffolds were studied. The biological evaluation was carried out using rat derived BMSCs in terms of cell proliferation and differentiation. These projects provide a comprehensive and comparative insight into concept of composite fibrous scaffolds containing BHA particles. Unlike most of the research which has been carried out so far, we used micro particles of BHA rather than nano sized which has its own advantages. The relevant results have been presented in details in 4.3 and 4.4.

The fifth project is a comparative study on the potential of PCL, PHB and PHBV to be used as *in vitro* platforms for drug screening. Rabbit corneal keratocytes were placed to evaluate their biological potential. All the three electrospun scaffolds were exposed to the same conditions and compared in terms of cell proliferation and differentiation. The electrospinning parameters were kept constant and different morphologies were obtained

to study the relationship between scaffold morphology and cell attachment and proliferation. The relevant results for this part has been presented in 4.5.

The last part of this research is introducing a new concept in the design of scaffolds for guided tissue regeneration. It also shows the flexibility of electrospinning which can be combined with other scaffolding techniques. In this part electrospinning is combined with salt leaching to fabricate a multi layered scaffold with graded concentration of the bioactive material which was HA. The graded concentration of bioactive material is presumed to direct the cell growth in the desired direction. The relevant results are shown in 4.6.

1.3 Research background

PCL, PHB and PHBV are some of the most important commercially available biopolyesters. There were separate studies on the potential of electrospun scaffolds of PCL (Cipitria et al., 2011; Johnson et al., 2012), PHB (Suwantong et al., 2007; Wang et al., 2009; Yu et al., 2008), and PHBV (Ito et al., 2005; Suwantong et al., 2007) for tissue engineering applications. However, to our knowledge there has not been any comprehensive study, which includes all of these materials being exposed to the same conditions.

The previous studies on the composite electrospun scaffolds containing HA, was based on using nano HA (Cipitria et al., 2011; Guan et al., 2008; Tehrani et al., 2010; Yang et al., 2010). While usage nano sized HA has advantages of more homogenous distribution, it has the disadvantage of low bioavailability. The diameter of electrospun fibers is far larger than the size of nanoparticles and some of the particles are lost inside the fibers considering the fact that biodegradation time of the fibers is much longer than cell culturing time. In this research we have used micro size particles of BHA which have

better bioavailability and lower cost of synthesis. The other advantage of BHA is recycling bovine bone which is a natural waste.

1.4 Objectives of the study

The current study was carried out to fulfil the following objectives:

a) To study the effect of intrinsic and processing parameters on the morphology of electrospun fibers via various analytical techniques
b) To combine bioactive micro size particles with fibers to achieve better bioavailability of particles as well as lower cost of synthesis
c) To find the compositional ratio of BHA with PCL and PHB suitable for bone tissue engineering applications
d) To study the potential of electrospun biopolyesters in terms of stem cell proliferation and differentiation
e) To study the potential of PCL, PHB and PHBV for corneal keratocytes tissue engineering

1.5 Research diagram

This study is composed of six parallel project with target application of tissue engineering. Figure 1.1 shows each one of the individual project and their interconnection with each other.

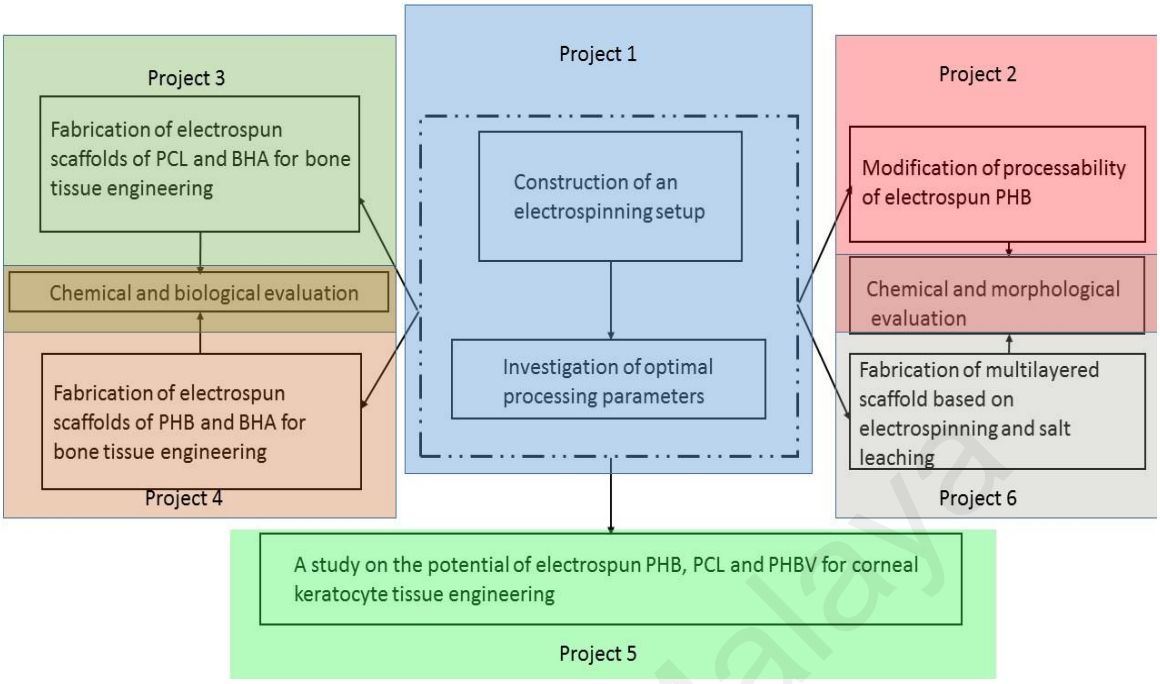

Figure 1.1 Project diagram of the thesis showing the individual projects and their connections

CHAPTER 2: LITERATURE REVIEW

2.1 Fibers

The application of fibers dates back to 3600 years ago. The first fibers which found use were natural fibers. Fibers based on their origin can be classified into natural and man-made. Natural fibers could be based either on plants or animal hair, while man-made fibers are produced by using regenerated polymers from naturally available materials or synthetic polymers (Trotman, 1984). In the production of regenerated fibers, a naturally available material is processed and fibrous structure is prepared based on it, e.g. viscose rayon. On the other hand, synthesized fibers are made of synthetic material such as PET or Nylon. Fibers, nowadays find a wide and versatile range of uses in the textile industry, specialty and biomedical applications, as well as, industrial products (Purane et al., 2007).

2.1.1 Conventional methods of fiber spinning

A number of different methods have been reported for production of fibers to date. The most prominent methods are melt spinning and solution or gel spinning of polymeric materials (Chawla, 2005). In melt spinning, the spinning dope is prepared by melting the polymer granules into a homogenous liquid. By application of mechanical force the polymer melt is passed through the spinneret followed by cooling the melt to keep the fibrous morphology (Nakajima, 1994).

In gel spinning or solution spinning, a viscous solution of the polymer is prepared and passed through the spinneret. Then there would be two options to remove the solvent. Depending on the solvent used, it could be eliminated either by hot air blowing or usage of a coagulation bath (Lemstra et al., 1987).

In both methods, the spinning dope shall be prepared by either melting the polymeric material or dissolving it in a solvent. After this step, the dope is passed through a spinneret followed by quenching or solvent removal to create fibers. In both processes, mechanical force is applied to pass the dope through the spinneret followed by drawing afterward. These two primary methods have dominated the fiber production industry for decades (Nakajima, 1994).

2.2 Nanofibers

Nanofibers are defined as fibers with diameters less than 100 nanometers. In the textile industry, this definition is often extended to include fibers up to 1000 nm (or 1 micron) diameter. When the diameter of the fibers shrink to submicron and nanometers, they show unique characteristics such as huge surface area to volume ratio (up to 1000 times of the relevant ratio of microfibers), improved mechanical properties and better surface functionality (Huang et al., 2003). These prominent characteristics of nanofibers makes them a suitable candidate for a range of applications including tissue engineering (Kroeze et al., 2009; Yoshimoto et al., 2003), filtration (Yun et al., 2007), protective clothing (Gibson et al., 2001), drug delivery systems (Kenawy et al., 2009) and nano-sensors (Wang et al., 2002).

2.2.1 Methods of production of nanofibers

By application of conventional fiber production methods, fibers with diameter finer than 2μm could not be produced. In order to produce fibers with the diameter in nanometer range, other methods are required (Andrady, 2008). A number of methods have been reported to be capable of production fibers with submicron diameters including drawing (Nain et al., 2006), self-assembly (Hartgerink et al., 2001), phase separation (Liu et al.,

2009), template synthesis (Ikegame et al., 2003) and electrospinning (Teo & Ramakrishna, 2006). Drawing is a process very similar to conventional dry spinning and as the name suggests fibers are formed by drawing a viscoelastic polymer to reach nanometer scale. This method requires a minimum level of equipment; on the other hand it is not applicable to all the materials. Only very specific materials can undergo strong drawing tensions without breaking. Self-assembly is a complex process of organizing of existing components in a desired pattern. Apart from the complexity, this process requires longer periods of time. Phase separation is a process based on separation of phases due to physical incompatibility. The steps involved in this process are polymer dissolution, gelation, solvent extraction and freeze drying. The main advantage of phase separation is the direct fabrication of the nanofibrous matrix and tailoring mechanical properties. However, it is limited to particular polymers, and the process requires long periods of time. Template synthesis applies a template to obtain the desired morphology. The polymer solution is passed through a metal oxide template containing nanoscale pores by application of water pressure. The extruded polymer solution would be passed through coagulation solution and nanofibers would be formed. Different fiber diameters could be achieved by using different templates. The main disadvantage of this process is its inability to produce continuous fibers (Huang et al., 2003; Ramakrishna et al., 2005). Among all these methods, electrospinning is the only one with the potential of industrialization. It has the benefits of being repeatable and having control on fiber diameter and process continuity (Fridrikh et al., 2003). It can be applied to a broad range of thermoplastic polymeric materials which can be dissolved in a volatile solvent. Therefore, a lot of research has been done on electrospinning over the last two decades (Subbiah et al., 2005). In the next part, electrospinning is discussed in more details.

2.3 Electrospinning

Electrospinning is a direct method for production of continuous micro and nanofibers. It was first patented by J. F. Cooley and W. J. Morton in 1902 (Ramakrishna et al., 2005). Unlike the conventional methods which apply mechanical force for drawing and fiber stretching, electrospinning uses high voltage electrostatic repulsive force (Doshi et al., 1993). This application of electrostatic force makes it possible to produce fibers with diameters in the range of nanometers (Rutledge et al., 2007). In electrospinning, high voltage (usually more than 10 kV) is applied to a polymeric solution. When the charges induced within the polymer solution reaches a critical amount, a jet will be initiated from the spinneret or capillary tip. The jet would undergo uniaxial stretching and thinning as it is moving toward the oppositely charged collecting plate while solvent evaporation is happening. By the time the jet reaches the collecting plate, all the solvent should be gone, and micro or nanofibers should be formed (Agarwal et al., 2008; Rutledge & Fridrikh, 2007). In order to produce the fibers by electrospinning, the polymeric fluid would undergo the following steps:

Droplet Generation: When a Polymer Solution is pumped at a low flow rate into the capillary, in the absence of an electric field, a droplet is formed at the tip of the capillary (Deitzel, Kleinmeyer, Harris, et al., 2001). Equation (1) shows the radius ($\boldsymbol{r_0}$) of the droplet of polymer solution with surface tension of $\boldsymbol{\gamma}$ and density □ which can be formed at the tip of a capillary with inner diameter of R, under ideal conditions when it is just exposed to the gravitational acceleration force($\boldsymbol{g}$) (Andrady, 2008):

$$r_0 = (3R\gamma/2\rho g)^{1/3} \qquad (1)$$

Taylor's Cone Formation: Under an electric field, as the electric charge is introduced to the droplet it elongates and obtains a cone-like shape known as Taylor's Cone (Yarin et al., 2001). Taylor cone is formed at a critical voltage (V_C) which is calculated from the equation (2) (Taylor, 1969) where R is the capillary radius and h is the capillary length:

$$V_C^2 = \left(\frac{2L}{h}\right)^2 \left(\ln\left(\frac{2h}{R}\right) - 1.5\right) (0.117\pi RT) \quad (2)$$

Jet initiation: At a certain voltage known as critical voltage, the electric charge induced within the polymer solution would be strong enough to overcome its surface tension. Due to the polymer solution's willingness to keep the charge the surface area has to increase in order to accommodate the charge build-up and a jet would be ejected from the cone's point (Subbiah et al., 2005).

Straight Elongation of Jet: Once the jet is ejected from the capillary tip, the columbic repulsion of surface charges present on the jet has an axial component that causes the jet to elongate in a straight passage towards the collector (Reneker et al., 2008).

Whipping Instability: With further stretching and thinning, the straight jet segment becomes unstable and starts bending on its path to the collector. Bending of jet occurs as a result of the jet tendency for charge accommodation. Therefore, it needs to increase its surface area to decrease the density of charge (Reneker et al., 2000).

Solidification of the Jet and formation of fibers: While the jet is undergoing the whipping instability, along with an increase in the surface area, the solvent evaporation rate would also increase. The jet should be dry enough when it hits the collector to dismiss any chance of deformation occurring. The fibers obtained under the optimum conditions of

electrospinning should have circular cross-section while maintaining continuous and bead free morphology (Tripatanasuwan et al., 2007).

A simple electrospinning set-up would consist of a high voltage power supply, a pump to keep the feeding rate constant, a needle or capillary as spinneret and a collecting plate. High voltage power supply oppositely charges the collecting plate and capillary. Figure 1.1 shows a schematic illustration of an electrospinning set-up (Teo & Ramakrishna, 2006).

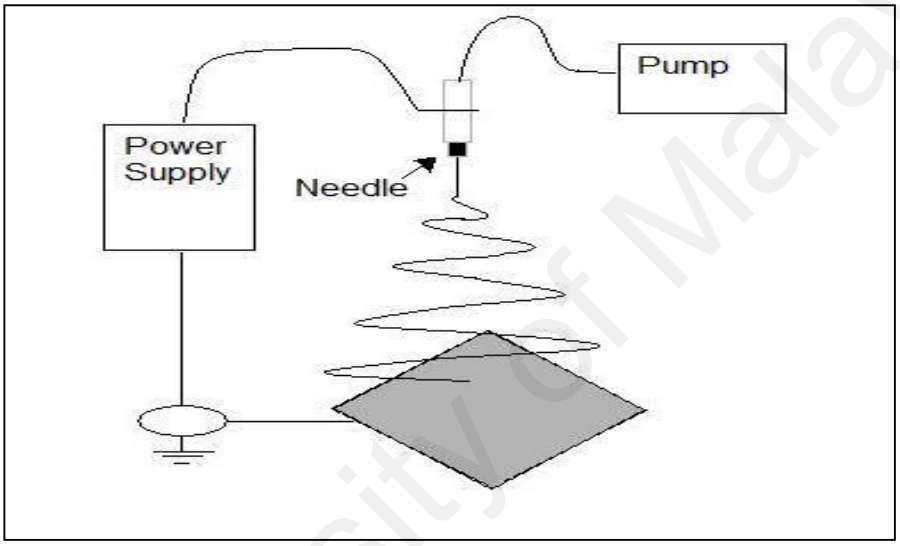

Figure 2.1 Schematic illustration of a simple electrospinning setup

2.3.1 Parameters affecting electrospinning

There are a number of parameters that can affect the electrospinning process and morphology of the electrospun products. Parameters related to the nature of polymer and the solvent are known as intrinsic parameters e.g. solution viscosity. The second group relates to the conditions being applied to the polymer solution during the electrospinning process known as process parameters e.g. applied voltage. In this part, some of the most influential electrospinning parameters are being covered.

2.3.1.1 Solution properties

In order to perform electrospinning, the polymer should be dissolved in a solvent. There has been reports of electrospun molten polymers (Dalton et al., 2007; Lyons et al., 2004); however, due to the requirement for a more complicated setup to process polymer melts, polymer solutions have been more widely used (Teo & Ramakrishna, 2006).

For dissolving a polymer in a solution, the polymer – solvent interactions should be stronger than the polymer – polymer interactions that are mainly due to van der Waals attractive forces, cross-linking, hydrogen bonding or crystallinity. The criterion for achieving a homogeneous polymeric solution is Gibbs free energy of mixing to have a negative value. Gibbs free energy is calculated from equation (3):

$$\Delta G_{mix} = \Delta H_{mix} - T\Delta S_{mix} \quad (3)$$

Where ΔH_{mix} is the enthalpy of mixing and ΔS_{mix} is the entropy of mixing at the temperature T. A good solvent will expand the polymeric chains to reduce the Gibbs free energy of the system (Adamson et al., 1967). A poor solvent is unable to reduce the Gibbs free energy of the system and the polymer chains would curl up. As could be seen in equation (3), temperature has an important role in increasing the solubility. Since the enthalpy and entropy of mixing have positive values (Hildebrand et al., 1964), by increasing the temperature, the amount of Gibbs free energy would decrease. Wannatong et al. reported that the solubility of the polymer in a solvent can affect the morphology of the electrospun fiber (Wannatong et al., 2004); therefore the choice of solvent which can provide good polymer solubility, conductivity and volatility is an important part of any electrospinning system.

Solution viscosity has a crucial effect on the morphology of the electrospun fibers (Mit-uppatham et al., 2004). The viscosity of the polymer solution is related to polymer chain entanglements. Chain entanglement is responsible for holding the solution jet together during the electrospinning. When the viscosity of the polymer solution is too low, electrospraying might happen instead of electrospinning. When the chain entanglement is not high enough, the jet will break into droplets and beaded fibers are formed (Gupta et al., 2005). The high molecular weight polymers normally have longer chains that increase the likelihood of having more chain entanglements (Fetters et al., 1994). They can provide solutions with a favorable viscosity at low concentrations of the polymer. That is the reason they are preferred for electrospinning. Increasing the polymer concentration in a solution also creates more chain entanglement. By increasing the solution concentration, at a critical point solution behavior would change from semi-dilute regime to concentrated regime. This concentration that is known as critical concentration can be measured by viscometry or light-scattering. In order to have an electrospinnable solution, the polymer concentration should be much higher than the critical concentration. The required ratio between concentration and critical concentration depends on the molecular weight of the polymer (Andrady, 2008; Gupta et al., 2005).

Another important feature in the choice of a solvent is its volatility. During electrospinning, as the jet is moving toward the collector the solvent is evaporating. By the time, the jet meets the collector the solvent should be evaporated to form the fiber. If the solvent is not gone, the wet fibers formed on the collector will join each other, and a thin layer of film would be formed on the collector. On the other hand, if the solvent evaporates too fast before reaching the collector, the jet would be unable to undergo thinning caused by the whipping instability and the fiber diameter would increase (Megelski et al., 2002). The evaporation rate of the solvent depends on factors such as

vapor pressure, boiling point, enthalpy, and heat of vaporization and surface tension. In order to improve the evaporation rate of the solvent during electrospinning, there are reports on blowing air (Kim et al., 2008) and placing dry ice (Y. Yang et al., 2006) inside the electrospinning chamber.

Polymer solution should possess sufficient conductivity to carry the charge build-up. Jet initiation depends on Coulombic repulsive forces within the solution to overcome the surface tension which is responsible for decreasing surface area per unit of mass. Most of the solvents have few free ions which result in having poor conductivity (between 10^{-3} to 10^{-9} $ohm^{-1}m^{-1}$). In order to improve the conductivity, application of co-solvent systems (Wang et al., 2008) and addition of mineral salts (Cheng et al., 2008) have been reported. Solvents with greater dielectric properties can help produce smaller diameter electrospun fibers. The whipping instability of the jet increases when the solvent has a higher dielectric properties. This was observed when the deposition area over the collector was increased (Hsu et al., 2004; Wutticharoenmongkol et al., 2006). Mineral salts can increase the charge capacity of the solution, and it has a positive effect on solution stretching when it undergoes bending instability. This increase makes formation of fibers with smaller diameters possible (Choi et al., 2004). Zhong et al. found that the size of ions present in the polymer solution can affect the size of fiber (Zong et al., 2002). When the ions have smaller atomic diameters, they have higher mobility that contributes to the electrostatic elongational force.

2.3.1.2 Processing parameters

A significant parameter in electrospinning is the electrostatic field strength which is determined by the applied voltage. The charge induced within the polymer solution along with external electric field is responsible for jet initiation. Generally a high voltage of more than 5 kV is required to stretch the solution drop into the shape of the Taylor cone

(Deitzel, Kleinmeyer, Hirvonen, et al., 2001). The applied voltage depends on the feeding rate as well. If the applied voltage is too high, the more intense electric field will cause the jet to move toward the collector faster. It can result in a less stable Taylor cone as more amount of polymer solution is taken from the capillary tip (Zong et al., 2002). Since the applied voltage has an influence on the jet stretching path and jet flight time, it can affect the electrospun fiber morphology as well. In lower viscosity solutions, the higher voltage can result in the formation of smaller diameter fibers through the increase in the jet stretching path (Lee et al., 2004). Higher voltage also makes the solvent evaporation faster and drier fibers would be formed on the collector (Subbiah et al., 2005) as well as promoting formation of secondary jets during electrospinning (Demir et al., 2002). On the other hand, higher voltage can decrease the jet flight time. A longer flight time is supposed to increase the time for jet stretching and elongation and solvent evaporation. For this reason, a voltage near the critical voltage could be helpful to increase the flight time and yield finer diameter fibers (Zhao et al., 2004). Some studies showed that at higher voltages the formation of beads will increase (Deitzel, Kleinmeyer, Hirvonen, et al., 2001; Demir et al., 2002; Zong et al., 2002). The reason was the formation of a less stable Taylor cone during the electrospinning that caused the Taylor cone to retreat inside the capillary. Krishnappa et al. in a study showed that the beads density would increase at higher voltages as the beads will join, and a bigger diameter fibers are formed (Krishnappa et al., 2003).

The high voltage not only affects the morphology but also influences the microstructure of the fibers. The tension imposed on the jet while electrospinning would cause the polymer chains obtain a better alignment in the direction of the fiber axis and increase the crystallinity. However, it only works up to a certain voltage. If the applied voltage is too high, the flight time of the jet will reduce, and the polymer chains won't get enough time to be oriented (Zhao et al., 2004). Based on what has been said, the optimum voltage

should be strong enough to initiate the jet and create the whipping instability while it is not significantly decreasing the flight time.

Another parameter that can affect fiber morphology is the feeding rate. The feeding rate has a direct effect on the Taylor cone stability. An increase in feeding rate can cause the fiber diameter become thicker and encourages the formation of beads. It is mainly due to the reason that at higher feeding rates a larger amount of solution is taken away from the capillary (Shin et al., 2001; Zuo et al., 2005). Once a larger amount of solution is drawn from the needle tip, it requires a longer time to dry. Therefore, by the time the fibers reach the collector, they might be still wet and join each other at the connection points forming beads.

The distance between the collector and needle tip has a significant influence on the jet flight time and electric field strength. When the distance between the needle tip and the collector is shortened, the jet path is reduced while electric field is intensifying. As a result, the flight time will decrease a lot, and the solvents do not have enough time to evaporate. If the distance is too low, a thin layer of film could be formed as the wet fibers would join each other (Buchko et al., 1999).

The orifice diameter of the needle was also found to influence the morphology of the fibers. Smaller diameter capillaries can reduce bead formation and solution clogging (Mo et al., 2004). A smaller droplet formed at a finer diameter needle and the reduction in solution clogging is mainly due to less exposure to the solvent. The smaller diameter droplet would require a stronger columbic repulsion force for jet initiation since its surface tension is higher than a big droplet. Therefore, under the same voltage it would resist more which gives the jet more time to undergo stretching and can result in smaller diameter fibers (Zhao et al., 2004).

2.3.1.3 Environment conditions

The ambient parameters such as relative humidity and temperature can also affect the electrospun fiber morphology. When electrospinning is carried out under normal environment, relative humidity can affect solvent evaporation and morphology of the fibers. The vapor pressure is calculated from equation *(4*) (Y. Yang et al., 2006):

$$P = \varphi . P_s \qquad (4)$$

Where P_s corresponds to saturated vapor pressure, φ is the relative humidity and P is the vapor pressure. The difference between the saturated vapor pressure and vapor pressure can increase the solvent evaporation rate. Based on equation (5) pressure difference can be increased by lowering the relative humidity.

$$\Delta P = P_s - P = (1 - \varphi) \qquad (5)$$

Yang et al. in a study showed that Polyethylene oxide (PEO) fibers could not be formed at high relative humidity when deionized water was used as a solvent. The fibers were only formed when relative humidity dropped below 50% (Y. Yang et al., 2006). Casper et al. also found that at relative humidity below 50% fiber surface is smoother and bead free. With increasing humidity, pores began to form on the surface of the fibers (Casper et al., 2004). They discovered that the depth of pores would increase in line with the increase in relative humidity and above a certain humidity nonuniform membranes would be formed instead of fibers.

Temperature can change the evaporation rate of the solvent and its viscosity. To increase the evaporation rate of the solvents, industrial heat guns and high wattage lamps have been used as external heat sources to expedite solvent evaporation rate (Subramanian et al., 2005). Heating jackets have been used to prevent the needle clogging during

electrospinning. High viscosity can create a lot of problems by disrupting the process by needle clogging. An increase in temperature will decrease the viscosity while making it easier to handle (Sombatmankhong et al., 2006). Mit-uppatham et al. reported formation of smaller diameter fibers at lower viscosity at the same concentration. In the study, he found that at lower viscosity the columbic repulses within the solution can contribute more to jet stretching (Mit-uppatham et al., 2004). So far syringe wrapping heating jackets (Sombatmankhong et al., 2006) and hot air jackets (Um et al., 2004) have been reported to control the solution viscosity.

2.4 Biodegradable polyesters

As a result of increasing environmental pollution issues caused by petrochemical products, the need in finding biodegradable replacements has been actively pursued. According to ASTM D 5488-94d a biodegradable polymer is the one that is capable of undergoing biodegradation by decomposing into carbon dioxide, methane, water and biomass (Avérous et al., 2012). Biodegradable polymers based on the chemical structures could be divided into polysaccharides, proteins, and biopolyesters. Biopolyesters have been attractive materials for biomedical applications, mainly due to their ease of degradation and the ability to tailor their structure to alter degradation rate. They degrade through hydrolysis of the ester bond, which produces resorbable degradation products through metabolic activities (Gunatillake et al., 2003b). Biopolyesters could be biologically or chemically synthesized. In the next parts, the biopolyesters used in this study have been discussed in more detail.

2.4.1.1 Polyhydroxyalkanoates (PHAs)

PHAs are microbial biopolyesters which due to their excellent biocompatibility, biodegradability and plastic like behavior have been considered as alternatives to be used in several fields of applications (Abd-el-haleem et al., 2007; Chen et al., 2005; Pouton et al., 1996). PHAs are produced by some microorganisms as food reserves when they are exposed to harsh conditions. PHAs are synthesized as intracellular carbon and energy insoluble granules when one or more of the essential nutrients such as nitrogen, phosphorous, oxygen or sulfur is not sufficiently available to them (Chan Sin et al., 2010). The interest in PHA related research has increased within the last two decades as their cost of production is decreasing, and they are seen as a replacement for non-degradable polymers in a variety of applications. PHAs could be classified based on the number of carbon atoms in their monomers as short-chain-length (scl) and medium-chain-length (mcl). Scl-PHAs do have 3-5 carbon atoms in their monomer backbone and tend to be brittle and highly crystalline. Mcl-PHAs have 6-14 carbon atoms in their monomer backbone and tend to be amorphous and elastic (Chan Sin et al., 2010, 2011). General structure of PHAs is shown below.

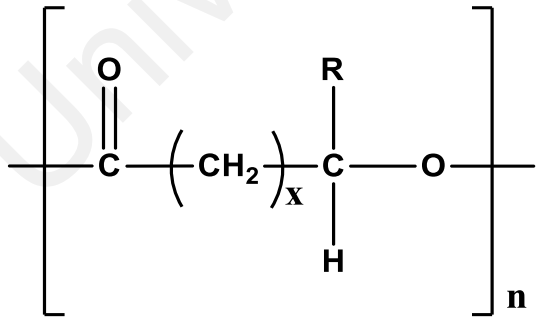

Figure 2.2 General structure of PHAs; X:1, 2 or 3; R: hydrogen or alkyl group; n: degree of polymerization

Table 2-1 summarizes the most common PHA homopolymers based on Figure 2.2 that have been produced to date.

Table 2-1- Main PHA homopolymers' structures based on Figure 1.2 source: Green nano - biocomposites (Avérous & Pollet, 2012)

Chemical name	Abbreviation	X value	R group
Poly(3-hydroxypropionate)	P(3HP)	1	Hydrogen
Poly(3-hydroxybutyrate)	P(3HB)	1	Methyl
Poly(3-hydroxyvalerate)	P(3HV)	1	Ethyl
Poly(3-hydroxyhexanoate) or Poly(3-hydroxycaproate)	P(3HHx) or P(3HC)	1	Propyl
Poly(3-hydroxyhexanoate)	P(3HH)	1	Butyl
Poly (3-hydroxyoctanoate)	P(3HO)	1	Pentyl
Poly (3-hydroxynonanoate)	P(3HN)	1	Hexyl
Poly(3-hydroxydecanoate)	P(3HD)	1	Heptyl
Poly(3-hydroxyundecanoate)	P(3HUD)	1	Octyl
Poly(3-hydroxydodecanoate)	P(3HDD)	1	Nonyl
Poly(3-hydroxyoctadecanoate)	P(3HOD)	1	Pentadecanoyl
Poly(4-hydroxybutyrate)	P(4HB)	2	Hydrogen
Poly(5-hydroxyvalerate)	P(5HV)	3	Hydrogen

2.4.1.1.1 Poly(3-hydroxybutyrate)

The most common and least costly of production in the PHA family is poly3-hydroxybutyric acid (PHB). It is a scl-PHA. PHB that is commercially available is a highly crystalline (about 50%) polyester with a melting point much higher than other microbial polyesters (T_m= 172 -180ºC). Its physical properties are comparable to some of petroleum-based polyethylene. However, its rigidity and reduced elasticity has

significantly limited its applications (Yu, 2009). To improve PHB's processability, several studies have been carried out based on copolymerization or blending. It has been copolymerized with 3-hydroxyvalerate with different proportions in the form of Poly (3-hydroxybutyrate-co-3-hydroxyvalerate). It is a polymer with a random arrangement of two monomers. Another monomer that has been copolymerized with PHB is 3-hydroxyhexanoate (3HHX) (Avérous & Pollet, 2012). However, due to the limitation in the development of new copolymers, blending it with cheaper plasticizing polymers has been a more feasible option to produce new materials with desirable properties. Blending can be carried out either by solution casting or melt mixing. Some of the biodegradable polymers which have been blended with PHB are polycaprolactone (Chun et al., 2000; Wang et al., 2007), polylactic acid (Vogel et al., 2009), chitosan (Shih et al., 2007; Veleirinho et al., 2011) and starch (Godbole et al., 2003; Thiré et al., 2006).

Godbole et al. in an study showed that blending PHB with starch in a weight ratio of 70:30 is beneficial for reducing costs as well as improved physical properties for applications such as paper or cardboard coatings for food packaging materials (Godbole et al., 2003). Blumm et al. reported that PHB is miscible with low molecular weight polylactic acid (PLA) (M_n=1759) while blends with high molecular weight PLA show biphasic separation (Blumm et al., 1995). Furukawa et al. carried out a study on the microstructure and dispersibility of PHB and PLA and copolymer of PHB-co-HHX using differential scanning calorimetry, infrared spectroscopy and wide angle x-ray diffraction (Furukawa et al., 2005). He reported that both of the systems are immiscible while blend of PLA PHB-co-HHX is somehow more compatible. Lovera et al. in a study showed that PHB is partly miscible with chemically modified low molecular weight polycaprolactone (PCL) while it remains immiscible with high molecular weight PCL (Lovera et al., 2007).

2.4.1.2 Chemically synthesized biopolyesters

A large number of biopolyesters are chemically synthesized based on petroleum based raw materials. The most important members of this category are polycaprolactone (PCL), polyesteramaide (PEA), aliphatic copolyesters based on polybutylene succinate (PBS) and aromatic copolyesters such as poly(butylene adipate-co-terephthalate) (PBAT) (Avérous & Pollet, 2012).

2.4.1.2.1 Poly(ε-caprolactone)

PCL is the most famous member of petroleum based biopolyesters. It is synthesized by ring opening polymerization of ε-caprolactone under heat and in the presence of metal alkoxide catalysts such as tin octoate (Labet et al., 2009). PCL is a low melting point (T_m =65 ˚C) aliphatic linear biopolymer which was initially used as an additive to resins for improving processing properties or a polymer plasticizer for PVC. After showing promising potential in tissue engineering and biomedical applications, PCL was the subject of many researches within the last two decades (Cipitria et al., 2011). Different grades of PCL are commercially available. Chemical structure of PCL is shown below in Figure 2.3.

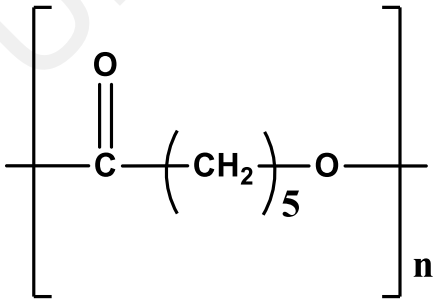

Figure 2.3 Chemical structure of poly (ε-caprolactone)

Some of the reasons for increasing popularity of PCL are its low cost of synthesis, slow degradation rate which can last up to 4 years and mechanical properties suitable for a broad range of applications (Woodruff et al., 2010). The most important reason for the popularity of PCL in biomedical applications is its rheological and viscoelastic properties which make it suitable to undergo various scaffold fabrication techniques. Electrospinning (Croisier et al., 2012), phase separation (Hutmacher, 2000), gravity spinning (Williamson et al., 2004), loaded microparticles (Balmayor et al., 2009) and rapid prototyping (Mondrinos et al., 2006) are some examples of PCL exceptional flexibility in undergoing different fabrication techniques.

PCL has the capability of being blended with other biopolymers. Biopolymers such as polylactic acid, Polyethylene glycol, chitosan and silk fibroin are some of the examples (Cipitria et al., 2011; Ghasemi-Mobarakeh et al., 2008; Lee et al., 2010).

The main disadvantage of PCL for scaffolding applications is its hydrophobicity. The hydrophobic nature of PCL reduces its wettability, which makes its biological interactions difficult to control. Surfaces hydrophobicity can result in reduced cell attachment and inadequate protein absorption (Cipitria et al., 2011). To overcome this weak point, a number of methods of surface modification have been practiced so far. Plasma treatment reduces hydrophobicity by formation of hydroxyl, carboxyl, amino and sulfate groups on the surface (Martins et al., 2009). It has the advantages of preserving the material's bulk and conformation properties as it only affects the surface. Chemical treatment with reagents such as sodium hydroxide (NaOH) is another alternative to rectify surface hydrophobicity. This method introduces hydroxyl groups and carboxylate groups by side chain modification which results in improved wettability (Cipitria et al., 2011). However; both of these methods are reversible and show hydrophobic recovery (Jokinen et al., 2012). Blending with biologically active materials is another applicable option for PCL. Bioactive materials can produce a signal for cells while improving surface properties.

Various hybrid scaffolds of PCL with bioactive materials such as collagen, hydroxyapatite and bioglass have been fabricated (Cipitria et al., 2011; Erisken et al., 2008; McClure et al., 2011). Some of the hybrid scaffolds showed improved properties. For instance, cells do have an affinity towards collagen. However, its mechanical properties are poor, and it is soluble in water-based mediums. While it is blended with PCL, mechanical properties show an improvement and through crosslinking of collagen's amide bonds to PCL's carboxylic linkage, solubility issue could be resolved (McClure et al., 2011).

2.5 Tissue engineering

Tissue engineering is an interdisciplinary research area which applies principles of life science and engineering to produce substitute tissues with an ultimate goal of improving and restoring the function of a damaged organ (Diba et al., 2012; Fabbri et al., 2010). Regenerative medicine started with the preliminary idea of reproduction of tissues or organ to replace the damaged tissues. Although current therapeutic methods such as allograft, autograft and xenograft have contributed a lot to improving the quality of life, there are still serious issues associated with them. Allograft is the transplantation of an organ or tissue from an individual to another of the same type. It has the risks of disease transmission, potential rejection of the implant as well as the problems associated with donor availability. Autograft that is the transplantation of tissue from one spot to another of the same individual has its own limitations and risks of infections. Xenograft is the surgical graft of tissue from one species to a different species has the highest risks of infection, the genetic difference, disease transmission and rejection of the implant due to incompatibility (Gualandi, 2011). Therefore, the need for novel alternative methods such as tissue engineering is highlighted.

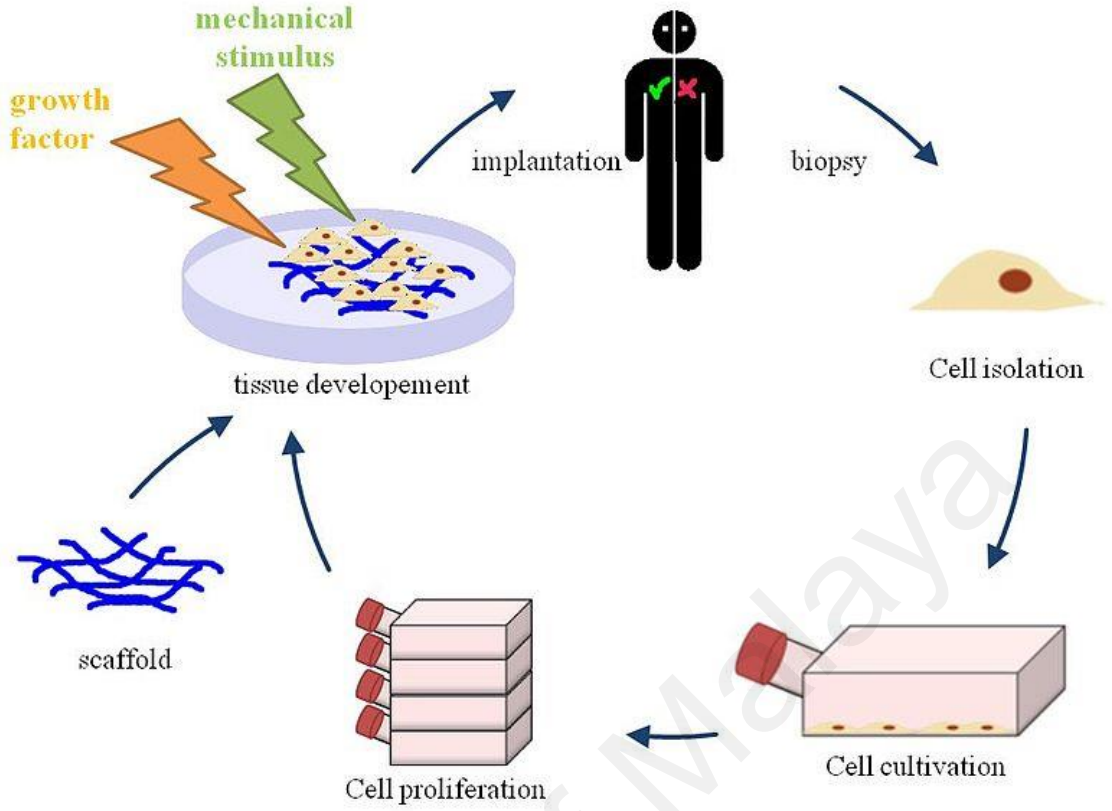

Figure 2.4 Principles of tissue engineering reprinted from Wikipedia

Figure 2.4 shows the principles being applied in tissue engineering for producing tissues and cell constructs. The isolated cells obtained from biopsy are cultured to increase in number. Cells are seeded on a porous three-dimensional biodegradable material which is known as scaffold. Once the scaffold is implanted inside human body, the scaffold would be resorbed over a period while the cells are proliferating and filling the space occupied by it. Tissue engineering is a multidisciplinary field that is not based only on medical or biological science. Synthesis and fabrication of biomaterials in the form that could benefit cell proliferation has been an important branch of chemistry and materials science within the last two decades.

2.5.1 Bone tissue engineering

Bone loss can occur for various reasons such as trauma, cancer, fractures, periodontitis, osteoporosis, and infectious disease (Kimakhe et al., 1999). Surgical approaches such as bone grafting, has improved the quality of life for many people; however the rate of success is between 50-84% and complete restoration of the bone tissue would not be possible (Stevenson et al., 1996). Due to the need for alternative methods, bone tissue engineering as a still expanding process has been the subject of a lot of researches within the last two decades (Rose et al., 2002). Bone tissue engineering is believed to be a promising method as it uses patients own tissue throughout the healing process which minimizes the risk of disease transfer. Another reason for practice of bone tissue engineering is the increasing demand for functional bone grafts. Only in US treatment of bone defects would cost more than $2.5 billion annually (Amini et al., 2012).

2.5.1.1 Bone structure and function

Bone is a composite material which provides support for various organs inside the body. Its mechanical properties are comparable to some of the man-made composites. Bone is a composite material made of collagenous fibers and nonstoichiometric calcium phosphate. There are embedded cell components such as osteoblasts and osteoclasts. These combinations make the fundamental unit of the bone structure called osteon. Bone provides support and sites of attachment for muscles as well as protecting vital organs such as brain and bone marrow (Sultana, 2013).

Bone tissue regeneration naturally takes place through a complex process called bone remodeling. It starts with the detection of remodeling signal. The signal could be a hormone or mechanical damage to begin the homeostasis change. This would cause bone remodeling to begin in the activated sites. Once the osteons are activated, bone resorption would start by osteoclast precursors recruited to the remodeling site. Osteoblasts would surpass bone resorption by occupying and trenching bone surface. They deposit

unmineralized matrix that is known as osteoid and direct formation and mineralization. Remodeling cycle would be completed once the osteoid becomes mineralized (Burr et al., 1985; Hill, 1998).

2.5.1.2 Hydroxyapatite (HA)

The naturally occurring calcium phosphate in bones and tooth is a nonstoichiometric mineral with the calcium to phosphorous ratio of 1.67 (Sobczak et al., 2009). Hydroxyapatite with the formula $Ca_{10}(PO4)_6(OH)_2$ is the most stable calcium phosphate salt in normal conditions with structural similarity to bone minerals (Koutsopoulos, 2002). The hydroxyl group can also be replaced by fluoride, chloride or carbonate (Wu et al., 2010). The pure hydroxyapatite is a white powder which is widely used in the fabrication of hybrid scaffolds with natural and synthetic biopolymers due to the similarity to the minerals found in natural bone. It is believed to be osteoinductive and osteocunductive (Ni et al., 2002; Rainer et al., 2011; Song et al., 2012). There have been several methods of production reported for hydroxyapatite including solid state reactions, layer hydrolysis of various phosphate salts, sol-gel crystallization and bone calcination (Koutsopoulos, 2002).

2.5.2 Scaffold

Scaffold is a biocompatible and biodegradable material with a porous structure that serves as a temporary template for tissue regeneration (Sultana, 2013). It should have interconnectivity of pores, bioactivity as well as appropriate mechanical properties and degradation rates to make it a suitable material for biological interactions with cells (Diba et al., 2012; Fabbri et al., 2010; Sultana, 2013). The degradation rate of the scaffold under physiological conditions should be in agreement with host tissue restoration. The porosity

of scaffold, pore size and interconnection of the pores is of significance as it facilitates the absorption of nutrients as well as metabolic waste release by the cells (Hutmacher, 2000). The mechanical properties of the scaffold should be similar to those of host tissue to make it usable as in implant in the area of defect (Liu et al., 2007). Selection of biomaterials, fabrication method, scaffold porosity and composition materials formation are some of the parameters that can be altered to achieve favorable mechanical properties of scaffolds. In order to avoid any infection during the *in-vitro* cell culturing, the scaffolds should be compatible with sterilizing methods (Zhou et al., 2007). Some of the methods such as gamma irradiation, ethylene oxide treatment and combinations of ethanol treatment and UV irradiation have been commonly used in scaffold sterilizations.

2.5.2.1 Electrospun scaffolds for bone tissue engineering

Electrospun fibers can provide morphologies and dimensions similar to that of natural extracellular matrix (ECM) (Cipitria et al., 2011). Within the last decade there has been a number of researches on electrospun fibers based on various biopolymers to serve as scaffolding materials for *In vitro* cell culturing (Hutmacher, 2000; Kroeze et al., 2009). Apart from similarity to natural ECM, electrospun fibers provide very high ratio of surface area to volume, which is suitable for cell attachment and loading of bioactive materials. The porous nature of electrospun fibers also facilitates food absorption and waste release by the cells (Kroeze et al., 2009).

Electrospun scaffolds based on biopolyesters have been used successfully for bone tissue engineering (Lee & Kim, 2010; Oh et al., 2007). Despite the success of scaffolds based on biopolyesters such as PCL and PHB (Hutmacher, 2000; Sombatmankhong et al., 2007; Tehrani & Zadhoush, 2010), incorporation of bioactive minerals inside the fibers has been a common practice. Bioactive minerals such as HA and bioglass improved cell growth and proliferation rates (Rainer et al., 2011; Song et al., 2012).

Electrospun PCL and PHB possess hydrophobic nature; therefore, incorporation of bioactive minerals in electrospun fibers can improve cell attachment through reducing scaffolds hydrophobicity (Ito et al., 2005). In the studies that stem cells were used, addition of hydroxyapatite was reported to have a positive effect on cell differentiation (Erisken et al., 2008; Song et al., 2012).

2.5.2.2 Electrospun scaffolds based on combinations of PCL/HA

Wutticharoenmongko et al. fabricated electrospun scaffolds of PCL and their blends with HA at 1% w/v and studied its potential as scaffolding material with rat derived pre-osteoblast MC3T3-E1 cell line (Wutticharoenmongkol et al., 2007). The fibrous scaffolds showed the greatest proliferation rate at day 3 once they were initially allowed for 16 h of cell attachment time. The authors observed the highest alkaline phosphatase activity in Day 5.

Yu et al. produced electrospun scaffolds with its surface mineralized with bone like apatite as bone tissue engineering substrate (Yu et al., 2009). The mineralization of electrospun PCL consisted of three steps: 1) surface activation through treatment with an alkaline solution (2N NaOH) at room temperature for 12 h 2) washing with distilled water and dipping in Ca and P solutions for 30s; while the process was repeated 6 times 3) incubation in simulated body fluid. The authors demonstrated in their work that surface mineralization improves cell attachment, proliferation and differentiation compared to untreated PCL fibers. The RT-PCR results showed that the mineralized sample maintains the genes associated with bone much better.

Li et al. reported coating of electrospun PCL with gelatin and calcium phosphate as scaffolding material for bone tissue engineering (Li et al., 2008). The PCL fibers were immersed in gelatin solution in presence of mild acidic buffer. Coating of calcium

phosphate was carried out by immersing the samples in simulated body fluid for 8 hours while the solution was changed every 2 hours. The authors concluded that the presence of gelatin contributed to homogenous deposition of calcium phosphate on the fibers. They also reported that the coatings improved cell attachment and proliferation.

Yang et al. reported fabrication of hybrid scaffolds based on electrospun PCL, gelatin and nano HA and its biological assessment with dental pulp stem cells (Yang et al., 2010). The polymer/HA weight ratio was 5:1. The authors concluded that the hybrid scaffold is capable of odontogenic differentiation of dental pulp stem cells. Addition of HA had a significant positive effect on the *in vitro* and *in vivo* differentiation of rat derived dental pulp stem cells.

Erisken et al. reported fabrication of a functionally graded electrospun scaffold based on PCL and β-tricalcium phosphate using a hybrid twin screw extrusion and electrospinning system (Erisken et al., 2008). The authors studied the mechanical properties of the samples as well as biological potential with rat derived pre-osteoblasts. The sample used for cell culturing contained 15 %wt β-tricalcium phosphate. The authors concluded that the ability to incorporate β-tricalcium phosphate in electrospun PCL in a controllable manner is an important step in mimicking morphological and compositional structure of the natural bone especially at the interfaces of bone and cartilage tissue.

2.5.2.3 Electrospun Scaffolds based on combinations of PHB/HA

It was first demonstrated by Doyle et al. that PHB and its blends with HA is capable of producing a reliable promising bone tissue adaptation without any proof of inflammatory response after a period of 12 month subsequent to implantation. Fast formation of bone tissue around the implant was observed and about 80% of the implant surface exposed to

deposition of new bone. There was no evidence of material breakdown during the period of *in vivo* study (Doyle et al., 1991).

Other studies showed that HA particles incorporated in polymeric PHB can result in formation of a bioactive composite material suitable for bone tissue regeneration or replacement applications. Formation of a bone like apatite layer was observed after the immersion of the composites in simulated body fluid (SBF) which is a sign of in vitro bioactivity of the composite (Luklinska et al., 1997; Ni & Wang, 2002). Furthermore, PHB/HA composites have a compression strength of 62 MPa which is about the same value of some human bones (Galego et al., 2000). This feature can make PHB/HA composites an interesting implant for applications such as fracture fixation.

Along with understanding of the advantages porous morphology of biomaterials to be used as scaffolding substrates, several efforts on fabrication of electrospun composite scaffolds based on PHB/HA was devoted.

Guan et al. reported fabrication of composite fibrous scaffolds based PHB and nano HA (nHA) particles through a gas-jet electrospinning system (Guan et al., 2008). Rat bone marrow stem cells were seeded on the scaffolds and cell proliferation and differentiation was studied over a period of 7 days. The study confirmed that addition of functional growth factor (nHA) had a positive effect on rat bone marrow stem cell attachment, proliferation and differentiation. The authors concluded electrospun scaffolds based on PHB/nHA possess unique morphological features combined with functional growth factors which potentially make it suitable for bone tissue engineering applications.

Tehrani et al. reported fabrication electrospun scaffolds PHB containing lower filler concentrations of nHA (Tehrani & Zadhoush, 2010). Electrospun scaffolds containing three different weight ratios of nHA (5%, 10% and 15%wt) were fabricated and studied for morphological and physical properties. The scaffold containing 5 wt% nHA showed

the highest mechanical strength while highest stiffness and elongation at break was observed in the sample containing 10wt% nHA. The authors concluded that it is possible to fabricate and tailor the mechanical properties of the samples to suit the physiological and mechanical demands of the host tissue.

Tong et al. reported *in vitro* evaluation of electrospun nanocomposite scaffolds based on PHBV and carbonated nHA (Tong et al., 2011). The carbonated nHA was synthesized through an in-house nanoemulsification process. Nanocomposite fibrous mats containing three different weight % of carbonated nHA (5%, 10% and 15%) were successfully fabricated. Human osteoblasts (SaOS-2) were seeded on the scaffolds to investigate the effect of addition of carbonated nHA over a culturing period of 14 days. For dispersion of nanoparticles inside the electrospinning solution ultrasound power was applied and the authors reported it had a positive influence on the homogenous distribution of the carbonated nHA inside the fibers. It was reported that scaffolds contacting carbonated nHA showed better wettability and osteoconductivity while not having a significant influence on the mechanical properties of the fibrous nanocomposite.

CHAPTER 3: METHODOLOGY

3.1 Introduction

This chapter describes the procedures for the preparation, fabrication and characterization methods used in the current study.

3.2 Materials

Poly[(*R*)-3-hydroxybutyric acid] (PHB), poly(3-hydroxybutyric acid-co-3-hydroxyvaleric acid) (PHBV) and polycaprolactone (Mn=80000g/mol) (PCL) were purchased from Aldrich. High purity citric acid (CA; molecular weight (Mw) = 192.13 g mol^{-1}; melting temperature (Tm = 153 °C), Polycaprolactone triol (PCLT; M_w = 300 g mol^{-1}), Hydroxyapatite (HA) and dioxane were purchased from Aldrich and used as received. (NaCl) was sieved to particles size in the range of 200-300 μm for particulate leaching.

F12: DMEM (FD) (Dulbecco's modified eagle medium: nutrient mixture F12), antibiotic-antimycotic, trypsin-EDTA glutamax and fetal bovine serum were purchased from Gibco Invitrogen, USA. 3-(4, 5-dimethylthiazolyl-2)-2, 5-diphenyltetrazolium bromide solution was purchased from Sigma Aldrich USA. Vitamin C, dimethyl sulfoxide, paraformaldehyde, Chloroform, dimethylformamide (DMF) and phosphate buffer saline were purchased from Merck Millipore, Germany. Alamar blue solution was purchased from Life Technologies, USA. TRI Reagent and polyacryl carrier were purchased from Molecular Research Center, USA. DNAse- and RNAse- free distilled water and SuperScript™ III First-Strand Synthesis SuperMix kit were purchased from Invitrogen, USA.

3.2.1 Synthesis of mcl-PHA

Mcl-PHA was produced at the Biotechnology Laboratory of the Institute of Biological Sciences, university of Malaya, by using palm kernel oil (PKO) as the fermentation substrate. Since *Pseudomonas putida* PGA1-which was used in this study- lacks lipase gene, it could not consume the highly saturated PKO directly and required a saponification pretreatment. Saponification was carried out by using an ethanolic solution of sodium hydroxide followed by drying at 65° C to obtain the sodium salt of the fatty acids which was subsequently used in batch feeding of the bacterial cell culture. The details of the process were explained in an earlier publication (Tan et al., 1997).

3.2.2 Bovine Hydroxyapatite (BHA) powder production

Bovine bone (femur, tibia and metatarsus) was obtained from the local abattoir. It was cleaned from macroscopic impurities and substances, including the ligaments and tissue stuck to the bone (Herliansyah et al., 2009) and defatted by boiling in double distilled water for 3 hours, followed by drying in an oven at 70°C for 7 days. Defatting was done to remove soot formed during the heating process (Ooi et al., 2007). The bones were ground into powder using a Schein Orthopedic machine (T2002 ULTRA) followed by sieving in the range of 25- 40 µm. The sieving size was chosen based on a previous study which reported it to have a positive effect on the cell growth (Sun et al., 1997). The sieved powder was then heated in a furnace until 1100°C at a heating rate of 10°C/min to obtain pure bovine hydroxyapatite powder (Herliansyah et al., 2009). X-Ray Diffraction and FTIR were carried out to make sure that the obtained powder was hydroxyapatite after matching with the JCPDS database.

3.3 Electrospinning setup

The experimental set up consisted of a syringe pump (Longerpump), a needle (Terumo needle, 0.45 ×13 mm) used as spinneret, a transformer (Capable of stepping up voltage up to 24 kV) and a high voltage capacitor (Maxwell Laboratories Inc. USA, capacitance 0.22 µF, Voltage: 50 kV).The polymer solution was pumped to the needle at a constant rate of 3 ml/h. The high voltage was generated by stepping up the 230 V AC voltage by using the transformer and subsequently rectified by a diode chain to produce the half-wave rectified output. The half-wave rectified output voltage was further smoothened by the high voltage capacitor. The needle was fixed at 18 cm from aluminum foil in a horizontal position. The wires from the positive and negative terminals of the capacitor were connected to the needle and aluminum foil respectively. The whole set up, except for transformer, was placed inside a clear plastic box to have a more careful control on the experiment environment. A hygrometer (Hanna Instruments HI 8564, Romania) was placed inside the box to measure relative humidity and temperature during electrospinning. The experiments were carried out at 12 kV. Relative humidity and temperature during the electrospinning time were kept in the range of 28±2°C and 61-65% respectively. The produced fiber mesh, collected on the aluminum foil, was dried in a vacuum oven for 48 hours at 40°C to remove any residual solvent.

The preliminary studies for calibration of instrument was carried out using a PEO solution mainly due to ease of handling of aqueous solutions. Later on to study the effects of processing parameters PEO were replaced by PHB as it was one of our main materials in this project. The process was optimized using PHB solutions according to the parameters reported here. Fig 2-1 shows different parts of the electrospinning setup including high voltage power supply, capacitor, and syringe pump.

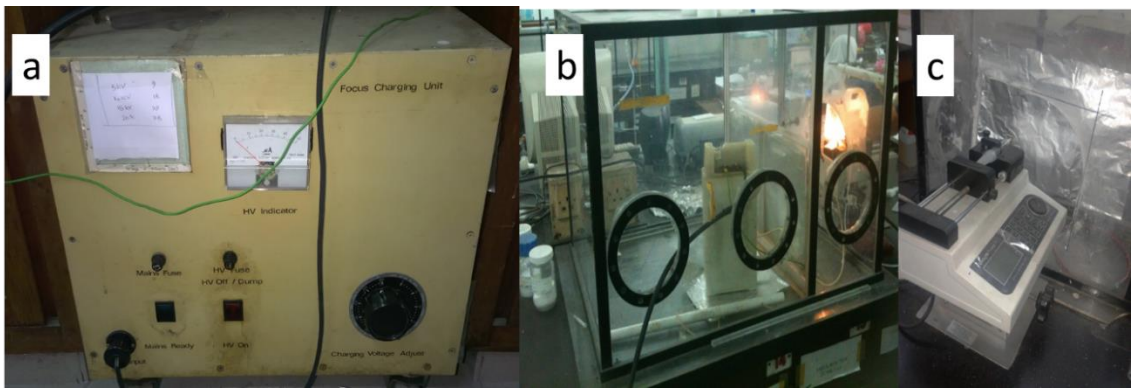

Figure 3.1 Different parts of electrospinning setup a) high voltage power supply b) high voltage capacitor c) Syringe pump

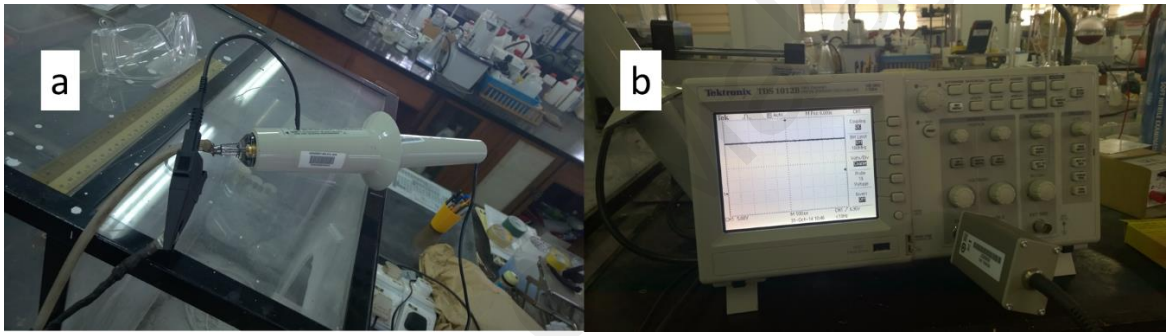

Figure 3.2 DC quality of high voltage power supply after the current being passed through capacitor a) high voltage voltmeter probe; b) high voltage voltmeter screen

3.3.1 Preparation of polymeric solutions for electrospinning

A 10% wt solution was prepared by dissolving the respective polymer (PHB, PHBV or PCL) in a solvent mixture comprising of chloroform and DMF with a ratio of 9:1. The solution was stirred at 60º C in a round bottom flask fitted with a condenser for 5 hours to reach homogeneity. The process was followed by loading the solution into a 20 ml syringe (Terumo) for electrospinning.

3.3.2 Preparation of Polymeric solutions of PHB and mcl-PHA

For blends of PHB and mcl-PHA a 10% wt solution was prepared. Blends of PHB and mcl-PHA were prepared in weight compositional ratios of 100:0, 90:10, 80:20, 70:30 and 60:40 respectively. The blend was dissolved in the solvent mixture consisting of 9 parts chloroform and 1 part DMF.

3.3.3 Preparation of polymeric suspensions of PCL and BHA

Solution Blending of PCL and BHA were carried out in weight compositional ratios of 100:0, 90:10, 80:20, 70:30, 60:40 and 50:50 respectively. PCL was first dissolved in a mixed solvent consisting of 9 parts chloroform and 1 part DMF using a magnetic stirrer at 50°C for three hours in a conical flask fitted with a condenser. After obtaining a homogenous solution, BHA was added to the solution and stirring continued for another 20 hours. In order to agitate and break the random agglomerations of BHA, the solution was sonicated for one hour before loading into the syringe.

3.3.4 Preparation of polymeric suspensions of PHB and BHA

Solution Blending of PHB and BHA were carried out in weight compositional ratios of 100:0, 90:10, 80:20, 70:30, 60:40 and 50:50 respectively. PHB was first dissolved in a mixed solvent consisting of 9 parts chloroform and 1 part DMF using a magnetic stirrer at 60°C for three hours in a condensed conical flask. After obtaining a homogenous solution, BHA was added to the solution and stirring continued for another 20 hours. In order to agitate and break the random agglomerations of BHA, the solution was sonicated for one hour before loading into the syringe.

3.4 Synthesis of PCLT-CA elastomer and fabrication of PCLT-HA composite scaffolds

Equimolar amount of PCLT and CA monomers were mixed to produce the pre-polymer. The pre-mixed monomers were reacted in a three-necked round-bottom flask and the mixture was first heated up to 160-165 °C to melt CA. The reaction was continued by mixing at 140-145 °C for 1 h under the constant stream of nitrogen. Synthesized PCLT pre-polymer was dissolved in dioxane (50% (w/w) solution), and the resulting solution was mixed with pre-calculated amounts of HA particles to obtain polymer-composites of 10, 20 and 30% wt. HA by weight relative to pure pre-polymer. Porous scaffolds were fabricated by particulate-leaching method (J. Yang et al., 2006). The sieved salt were added to the prepared solutions as a porogen. The resulting slurry (90% salt and 10% (w/w) PCLT-HA) was then poured into the Teflon™ molds and placed in an oven for solvent evaporation and polymerization (80°C, 7 days) (Djordjevic et al., 2009). Afterwards, composites of salt and PCLT-HA were soaked in distilled water for four days in order to leach out the salt. The porous scaffolds were then freeze-dried for 4 h and stored in a desiccator for further characterization. Two sets of samples including PCLT-HA10%, PCLT-HA20%, and PCLT-HA30% as reference samples as well as a single three layered scaffold containing all the three compositional HA weight ratios with electrospun PHB sheets in between as a single construct.

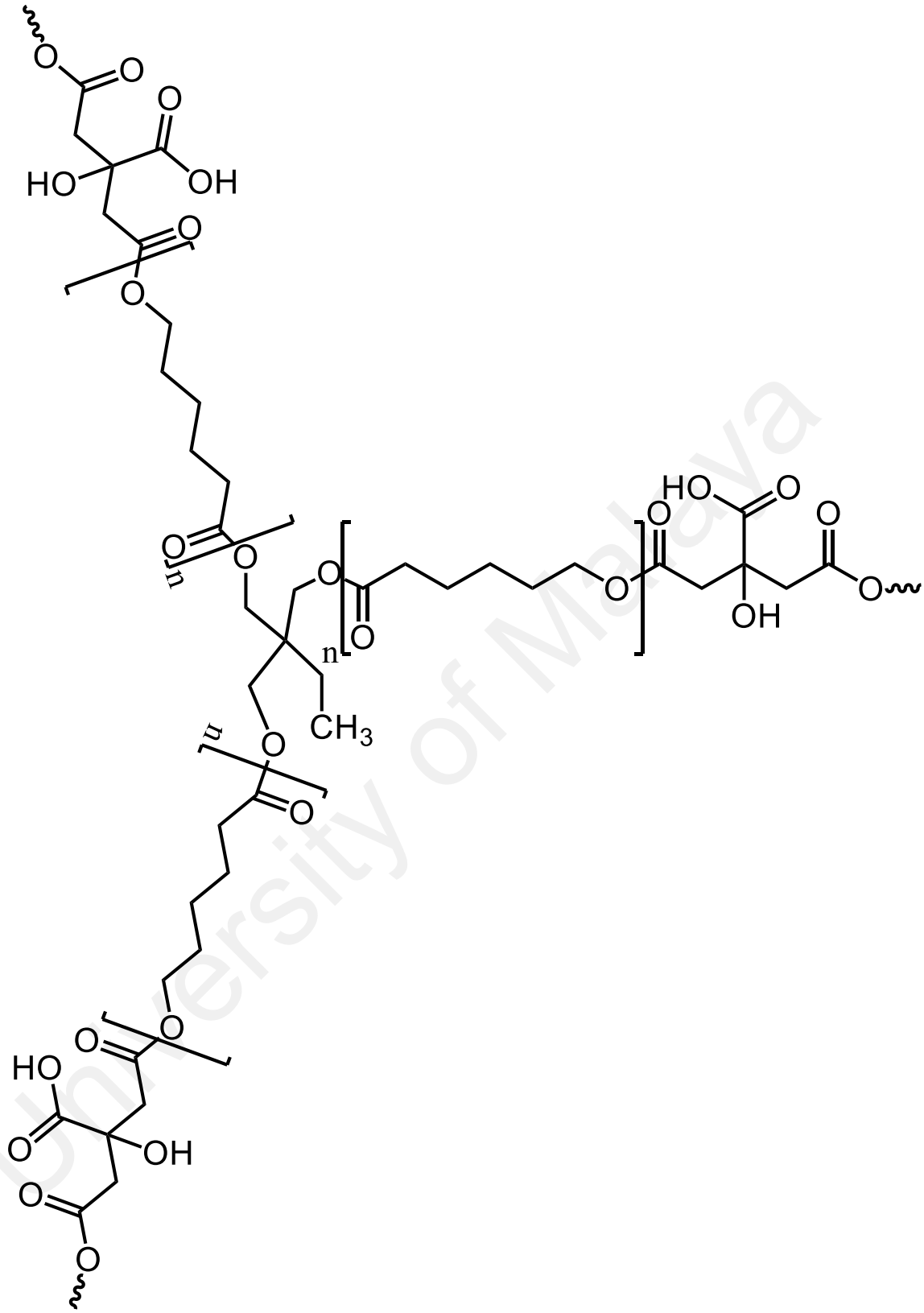

Figure 3.3 A plausible chemical structure of PCLT

3.5 Characterization methods

3.5.1 BHA Particle Size Analysis

Particle size distribution analysis was carried out using a Malvern Master Sizer-S equipped with a hydro 2000 sample dispersion unit and a laser diffraction optical bench. A sample of BHA was dispersed in distilled water while the stirrer speed was adjusted at 1800 rpm. The sample was analyzed based on equivalent sphere concept, and a volume weighted distribution of the HA particles was obtained.

3.5.2 Fourier Transform Infrared Spectroscopy (FTIR-ATR)

The produced scaffolds were analyzed using a Perkin Elmer Spectrum 400 powered by ATR technique. The spectra were collected at room temperature between 4000 and 400 cm^{-1} at a resolution of ± 2 cm^{-1}.

3.5.3 Field Emission scanning Electron Microscopy (FESEM)

The morphology of the electrospun fibers was studied using FESEM (FEI: QUANTA FEG 250). Diameter distribution patterns of fibers produced from different blending proportions were compared. FESEM micrographs were analyzed by an image analysis program (ImageJ). For each sample, diameter measurement was carried out at a minimum of 30 different random points. Fiber intersections and beads were avoided in measurements.

3.5.4 3D Confocal Laser Microscopy

In order to determine the thickness and roughness profiles of the scaffolds, 3D confocal laser microscopy (OLYMPUS: LEXT OLS4000) was also carried out on the scaffolds.

3.5.5 Thermogravimetric analysis

Thermogravimetric analysis of the scaffolds was carried out from 30ºC to 900ºC at a heating rate of 10ºC/min (Perkin Elmer TGA 4000). The temperature at which 95% of the sample weight was observed was considered as the onset of degradation. The sample weight was between 5-10 mg.

3.5.6 Differential scanning calorimetery

DSC thermograms were recorded using a Mettler Toledo DSC equipped with an inter cooler. Specimens of each sample were sealed in aluminum pans while an empty pan was used as a reference. The weight of each sample was around 6 mg. All the experiments were carried out at heating rate of 20° C /min from -50 to 200°C. Crystallinity was calculated based on enthalpy of fusion (ΔH_f) compared to a theoretical value [146 J/g] for 100% crystalline PHB ($\Delta H^o{}_m$) through equation (6) (Hahn et al., 1995).

$$X_c = \frac{\Delta H_f}{\Delta H^o{}_m} \qquad (6)$$

3.5.7 Wide angle X-ray diffraction (WAXRD)

WAXRD patterns of electrospun mats were obtained under ambient condition using an Empyrean diffractometer system operating at 45kV and 30mA; Cu Kα radiation (λ=1.54 Å). Scans were performed in a 2Θ range of 10-40°Å.

3.5.8 Contact angle measurements

Contact Angle measurements were obtained using the SCA20 software on the DataPhysics OCA35 machine.

3.6 Biological assays

3.6.1 Rat stem cell isolation, culturing and seeding

Rat Bone Marrow derived Stromal Cells (BMSCs) were obtained as previously described by our research group (Muhammad et al., 2012). Briefly BMSC were obtained from young adult 150-200g male Sprague Dawley rats with isolation protocol approved by the Animal Ethics Committee [ethics reference number no BM/10/11/2008/KBM(R)], Faculty of Medicine, University of Malaya. The cells were grown in monolayer culture in T-75 flasks (Nunc) in primary media containing DMEM with 4.5g/l glucose, L-glutamine and Sodium Pyruvate [Cellgro® #10-013-CM] with 10% FBS [SIGMA # F1051] and PSN [GIBCO # 15640]. The cells were incubated in 95% relative humidity and 5% CO_2 at 37°C. The medium was changed twice a week until confluence and cells between passage 2 and 3 were used for this experiment. The sterilized scaffolds were then placed inside 24 well plates and seeded at a density of 20,000 cells per cm^2 and cultured until Day 14.

3.6.2 Rabbit keratocyte isolation, culturing and seeding

Six New Zealand white rabbits' corneal tissues were obtained from the local animal slaughter house. The corneal tissues were processed using the techniques reported by Ghafar et al (Ghafar et al., 2007). The use of corneal cells for research purpose was approved by the Universiti Kebangsaan Malaysia animal ethic committee with approval number of: FF-092-2012. Keratocytes were harvested from the corneal stroma with 0.3% collagenase type I digestion as mentioned in a recent paper (Zainal Abidin et al., 2011). Cell cultures were maintained in F12: DMEM (FD) media supplemented with 10% fetal bovine serum (Gibco Invitrogen, USA), 1% antibiotic-antimycotic, 1% glutamax and 1% vitamin C under standard incubation at 37°C, 5% CO_2 and 95% humidity. Primary culture

(P0) was passaged at a split ratio of 1:4 when cells reached approximately 90% confluence using 0.125% trypsin-EDTA. Passage 1 culture was used in the study.

3.6.3 Cell Viability and Cytotoxicity Test

Cytotoxicity of scaffold leachate was assessed via 3-(4, 5-dimethylthiazolyl-2)-2, 5-diphenyltetrazolium bromide (MTT) assay. Passage 1 keratocytes with the seeding density of 50,000 cells/ml were seeded onto 96-well culture plate overnight. The keratocytes were treated with 10 leachate concentrations using a dilution factor of 10 in FD media for 72 hours. MTT solution was added and incubated for 4 hours at 37°C and 5% CO^2. Dimethylsulfoxide (DMSO) was added to dissolve the purple formazan before reading its absorbance at wavelength 570 nm.

3.6.4 Cell proliferation assay

3.6.4.1 Cell proliferation assay for rat BMSCs

The first step in resazurin test (also known as AlamarBlue®) is the creation of a resazurin solution. The solution was prepared by using resazurin powder purchased from Sigma Aldrich, which was reconstituted by adding 14mg of resazurin into 100ml of culture medium DMEM-LG without Phenol Red (SIGMA- D9521). The process was done according to the manufacturer's instructions. All the samples and controls (24-well plate) were then washed gently three times with pre-warmed PBS prior to the Resazurin test. After the washing, 500 µl of medium (without Phenol Red) was added to each well. 50 µL of Resazurin solution (14mg/100ml phenol red-free medium) was added subsequently. The well plate was incubated for 4 hours. 10 minutes before the incubation time ended, the plates were covered with aluminium foil and placed onto the plate shaker and shook gently for 10 minutes. After shaking, the plate was transferred into the laminar

flow hood. 100 µL from each well (24-well plate) was transferred to a 96-well plate in triplicates while still lights were off.

1. The absorbance was measured at 690 nm and 600 nm using a FLUOstar OPTIMA BMG LABTECH micro-plate reader.
2. The absorbance reading was then taken to be the metabolic activity of the cells (Fidalgo et al, 2010).

3.6.4.2 Cell proliferation assay for rabbit keratocytes

The AlamarBlue® assay was used to measure the cell proliferation continuously since the cells remained viable after performing the cytotoxicity test. Passage 1 keratocytes with a seeding density of $3.5x10^4$ cells were seeded onto the scaffolds (PCL, PHB and PHBV) respectively for 4 hours. Scaffolds were rinsed with PBS X1 in order to remove the unattached cells, then the scaffolds were transferred into new culture wells with 2ml FD+10%FBS medium. On day 1 Alamar blue assay, the culture media were removed and substituted with 550µl medium containing 10% Alamar Blue. After 4-hour incubation at 37°C and 5% CO_2, 200µl of medium was aspirated and read using ELISA microplate reader with wavelength 570nm. The Alamar Blue test was repeated for day 3, 5 and 7 cultures. On day 7, the keratocytes cultured on the scaffolds were harvested using Trypsin-EDTA 0.125% after the Alamar Blue assay. Keratocytes were centrifuged and the pellet was preserved using TRI Reagent (Molecular Research Center, Cincinnati, USA) for total RNA extraction. A standard curve was plotted based on the Alamar Blue absorbance reading in serial dilutions of cell number to obtain an equation, and to calculate the number of viable cells.

3.6.5 Alkaline phosphate assay for rat BMSCs

In order to quantify the protein produced by cells, Alkaline Phosphatase Activity was measured as previously described (Zhao et al., 2009). Alkaline Phosphatase is quantified by the rate of hydrolysis of various phosphate esters by alkaline phosphate hydrolase enzyme from many types of molecules such as nucleotides, proteins and alkaloyds. One of the most famous phosphate esters is Nitrophenyl Phosphate (pNPP) which was introduced as a substrate by Fujita in 1939. Following that, the process was reported as an endpoint procedure by Bowers and McComb in their study in 1946. In 1974, the Committee on Enzymes of the Scandinavian Society of Clinical Chemistry and Clinical Physiology approved a modification of the procedure as the recommended procedure. The same method has been followed in this thesis with some modifications suggested by Wilkinson et al. (Wilkinson et al., 1969).

Briefly, 50µl of the supernatant obtained was then added to 200µl of pNPP solution [SIGMA ALDRICH: N1591] in a 96-well plate flask [TPP Corporation] followed by incubation at room temperature for 30 minutes. The reaction was then stopped by adding 50 µl of 3M NaOH to the solution. The solution was then read at 405nm absorbance. All absorbance readings were carried out using a BMG Labtech FluoStar Optima. The absorbance reading that were obtained were then processed using the following formula (this was done in order to change the absorbance to International Units)

$$(IU/L)=\frac{Abs./Min \times 1000 \times 0.3}{18.75 \times 1 \times 0.050} = Abs./min \times 2187$$

Where Abs./min = Average absorbance change per minute (in this experiment, the samples were incubated for 30 minutes)

1000 = Conversion of IU/ml to IU/L, 0.30 = Total reaction volume (ml), 18.75 = Millimolar absorbivity of Nitrophenol, 0.050 = Sample Volume (ml), 1 = Light Path in cm.

3.6.6 Total RNA Extraction and Two-step Reverse Transcriptase Polymerase Chain Reaction (RT-PCR) for keratocytes

Total RNA extraction was carried out according to the manufacturer's protocol. Polyacryl carrier (Molecular Research Center, USA) was used for total RNA precipitation. The total RNA pellet was washed with 75% ethanol and air dried before dissolving in DNAse- and RNAse- free distilled water (Invitrogen, Carlsbad, USA). The purity and concentration of extracted total RNA was determined by Nanodrop ND-100 spectrophotometer (Wilmington DE, USA) and stored at -80°C for further use. The synthesis of complementary DNA was performed using SuperScript™ III First-Strand Synthesis SuperMix kit (Invitrogen, Carlsbad, USA) according to the manufacturer's instruction. The reverse transcription was carried out at 50°C for 30 minutes. The forward and reverse primers used in the quantitative RT-PCR were designed from the sequences obtained in NIH Genbank database using Primer-3 software as published in (Zainal Abidin et al., 2011). Glycerylaldehyde-3-phospate dehydrogenase (GAPDH) was used as housekeeping gene for the data normalisation. Two-step RT-PCR was carried out using iQSYBR Supermix in Bio-Rad iCycler (Bio-Rad, USA). The protocol conditions were initiated with the activation of Taq DNA polymerase at 94°C for 3 minutes, followed by 45 cycles of PCR amplification at 94°C for 10 seconds and 60°C for 30 seconds and then melting curve analysis. The specificity and size of PCR products were confirmed with 2% agarose gel electrophoresis.

CHAPTER 4: RESULTS AND DISCUSSION

4.1 Project 1: The effect of processing parameters on the morphology of electrospun PHB

4.1.1 Introduction

PHB was one of major materials used in fabrication of scaffolds in this thesis. Therefore it was used to obtain the optimum processing parameters for electrospinning setup. A 10 wt% solution of PHB in a co-solvent of chloroform / DMF (9:1) was exposed to various conditions. The effect of altering voltage, needle to collector distance, capillary size and feeding rate has been studied. To study the effect of parameters individually, all the parameters were kept constant except for the subject parameter. FESEM was used to study the morphology of each sample. All the samples were collected on a small piece of glass which was stuck on the aluminum foil after 15 minutes of time was devoted to electrospinning. The FESEM images were further analyzed for fiber diameter measured with ImageJ software as described in 2.4.3 and the relevant diameter distribution histograms were produced by IBM SPSS 20.

4.1.2 Effect of applied voltage

Three samples were prepared at applied voltages of 5, 10 and 15 kV while the feeding rate was kept at 3ml/h, needle to collector distance 18 cm and capillary inner diameter of 1.2 mm (20G).

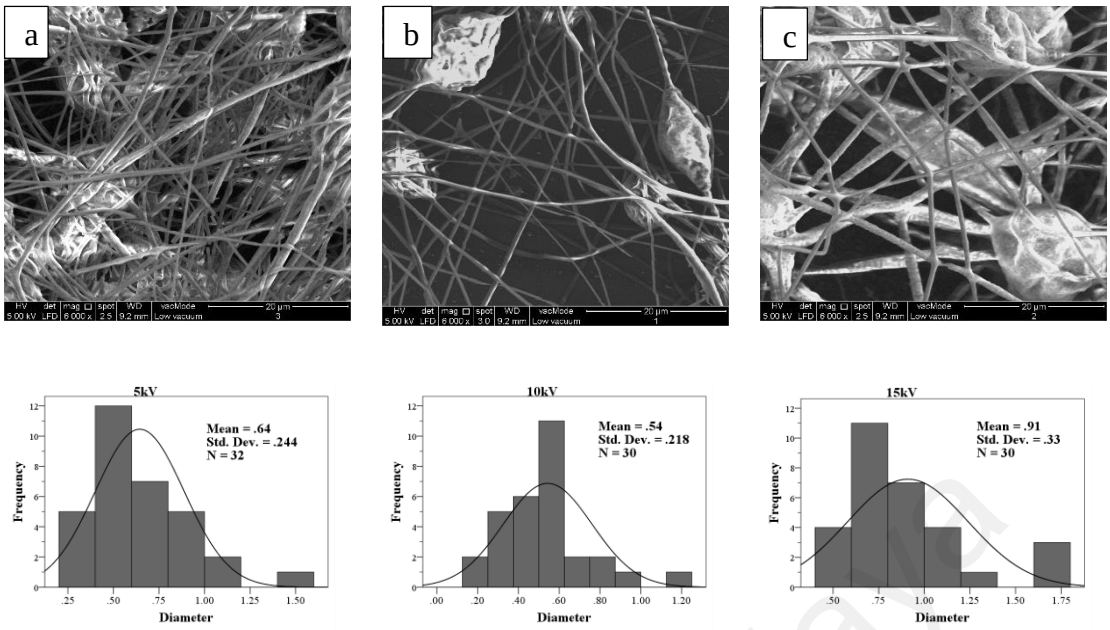

Figure 4.1 FESEM morphology of electrospun PHB at different applied voltages and their relevant fiber diameter (µm) distribution a) 5kV; b) 10kV; c) 15kV; the scale bar equals to 20 µm

The results show that the smallest average fiber diameter was obtained when 10kV was applied (0.54 µm). The diameter distribution range was also smaller compared to the two other groups and overall more uniform fibers were achieved. The largest average fiber diameter was achieved at 15kV (0.91 µm). 15kV provides a stronger electric field and the jet flight time should be reduced. Therefore, the jet had less time to undergo stretching and yielded to formation of larger fibers. At 5kV while the electric field was weaker, the jet flight time should have been increased. Despite the weaker electric field, the jet had more time to undergo stretching before hitting the collector and resulted in smaller fibers compared to 15 kV. The fibrous mesh obtained by 5kV is denser which suggests a more stable jet which covers a smaller area on the collector. The best combination of electric field strength and jet flight time was established at 10kV among all the groups. Beaded fibers were produced among all the groups which suggests another parameter other than applied voltage could be responsible for that.

4.1.3 The effect of feeding rate

Three samples were prepared at feeding rates of 1, 2 and 3 ml while the applied voltage was kept at 10kV, needle to collector distance 18 cm and capillary inner diameter of 1.2 mm (18G).

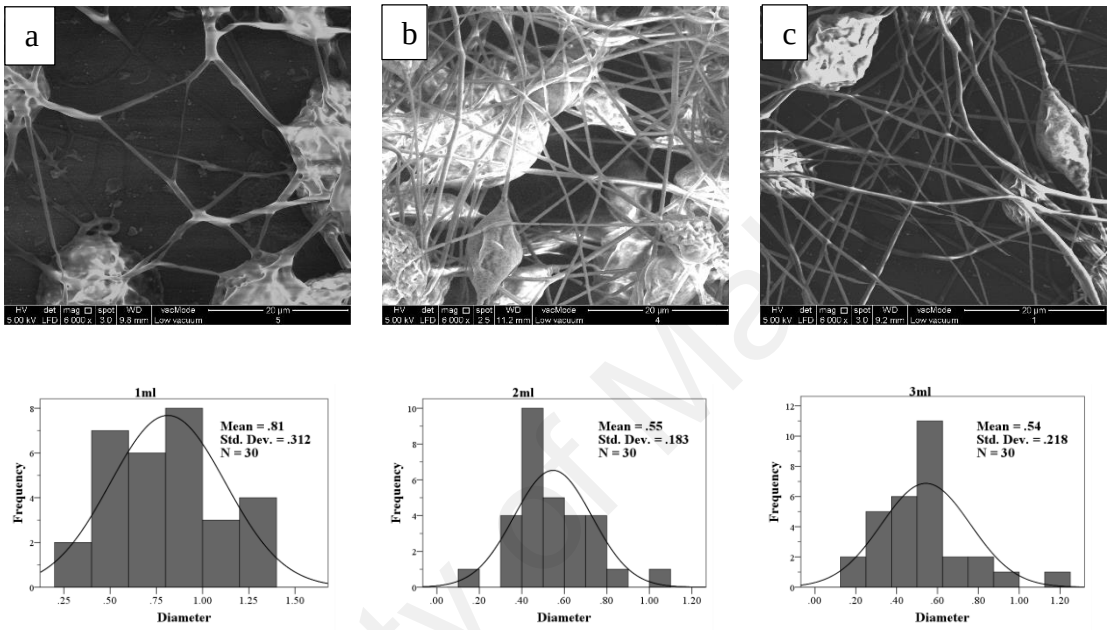

Figure 4.2 FESEM of morphology of electrospun PHB at different feeding rates and their fiber diameter (µm) distribution a) 1ml/h; b) 2ml/h; c) 3ml/h

The best result was achieved at feeding rate of 3ml/h (0.54 µm). Although the average fiber diameters at feeding rates of 2ml/h and 3ml/h are almost the same, the fibers formed at feeding speed of 3 ml/h show more uniformity with less beads. This could be due to more stability of the jet formation with less interruptions during the whipping instability stage. At feeding rate of 2 ml/h the jet becomes more unstable with more interruptions while undergoing whipping instability which resulted in formation of beaded fibers. However, the diameter of fibers is in the same range as 3ml/h. At 1ml/h only beads and non-uniform fibers are formed. The low feeding rate speed can result in more frequent jet

interruptions during the electrospinning process. The highest standard deviation (0.312) for this sample confirms the observation.

4.1.4 The effect of capillary diameter

Three samples were prepared by using needles with inner diameters of 0.7 mm (22G), 0.9 mm (20G) and 1.2 mm (18G) while the applied voltage was kept at 10kV, needle to collector distance 18 cm and the feeding rate at 3ml/h.

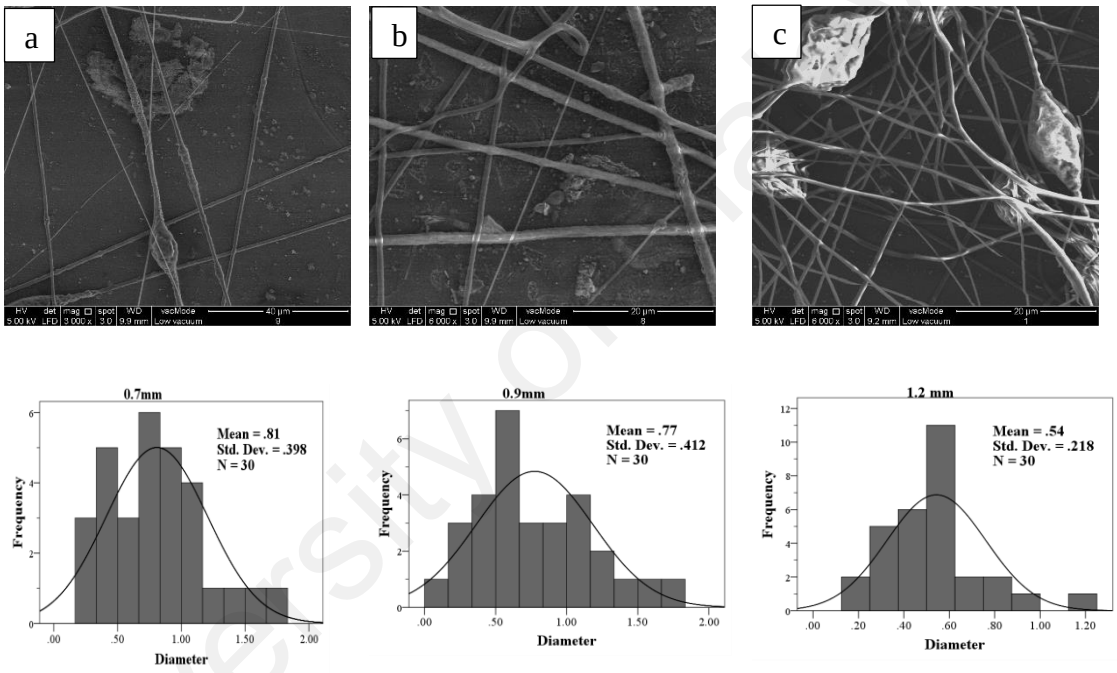

Figure 4.3 FESEM of morphology of electrospun PHB by using different needle sizes and their fiber diameter (µm) distribution, needle sizes a) 0.7mm; b) 0.9mm; c) 1.2mm

The results in figure 3-3 suggest that an increase in the inner diameter of the capillary used for electrospinning can cause a decrease in the diameter of formed fibers. The electrospun fibers produced by capillary diameter of 1.2 mm show average diameter of 0.54 µm while with 0.9mm and 0.7mm average diameters of 0.77 µm and 0.81 µm were achieved respectively. When a bigger size needle is used the droplet generated at the needle tip would be smaller at a constant feeding rate. The size of the droplet generated

is relevant to the surface tension of the droplet. An increase in the size of droplet would result in a decrease in its surface tension. The smaller droplet requires a stronger columbic force for jet initiation, and less acceleration towards the collector which provides more time for further stretching. The observation was in line with findings of Zhao et al (Zhao et al., 2004). One disadvantage of larger orifices is the formation of beads. The fibers produced by needle 20G and 22G despite having thicker diameters are bead free. Overall, the needle 20G could be considered as the best among all the groups.

4.1.5 The effect of distance between the needle tip and the collector

Three samples were prepared at needle tip to collector distances of 12, 18 and 24 cm while the applied voltage was kept at 10kV, needle inner diameter 1.2 mm and the feeding rate at 3ml/h.

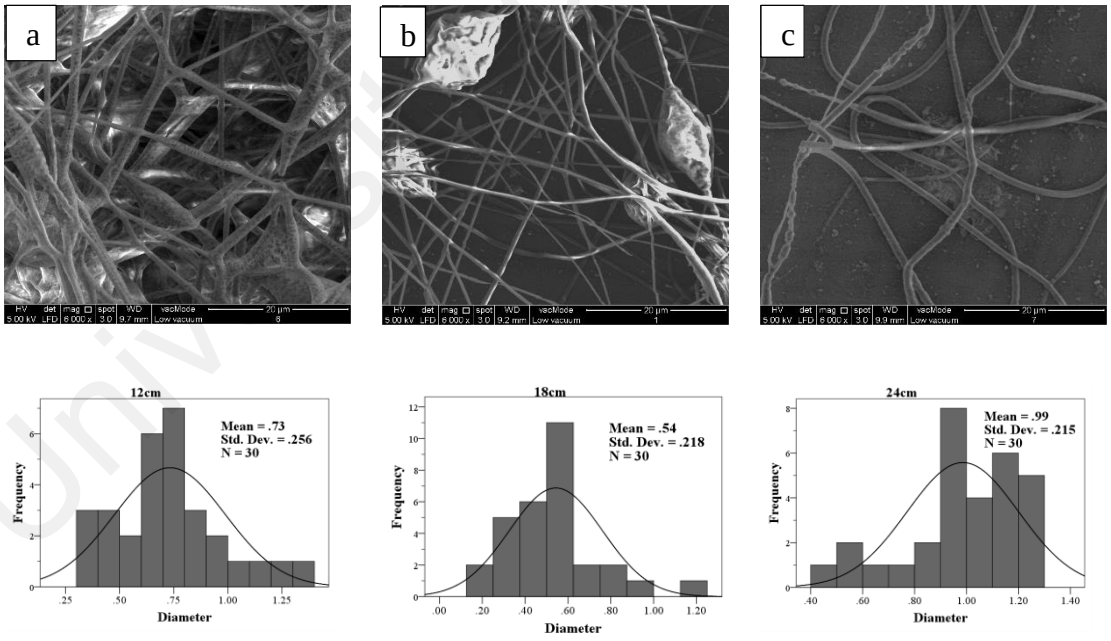

Figure 4.4 FESEM of morphology of electrospun PHB obtained through different tip to collector distances and their fiber diameter (μm) distribution a) 12cm; b) 18cm; c) 24cm

The needle to collector distance has a direct influence on the morphology of the electrospun fibers since it affects the flight time and electric field strength. According to figure 3-4, the finest fibers were obtained when collector was placed in 18 cm from the needle tip (average fiber diameter = 0.54μm). When the distance was decreased to 12 cm, the stronger electric field reduced the jet flight time and less stretching happened while undergoing the whipping instability region and the average diameter increased to 0.73 μm. By increasing the tip to collector distance to 24 cm, the electric field was weakened and less stretching happened despite the fact that it had more flight time. The longer flight path could not necessarily contribute to reduction in fiber diameter if the solvent is evaporated completely before hitting the collector and the dry jet cannot undergo any further stretching. The thickest fibers were yielded at the distance of 24 cm with average diameter of 0.99 μm. 18 cm is considered as the optimum distance between the studied groups.

4.1.6 Optimizing processing conditions

Based on the findings on processing parameters, in order to produce uniform and bead free fibrous mesh suitable for biomedical applications, the applied voltage was set at 10 kV, needle to collector distance at 18 cm, feeding rate at 3ml/h and the needle 20 G (0.9 mm) was selected. Figure 4.5 shows the FESEM images of the fibers obtained by applying above mentioned parameters.

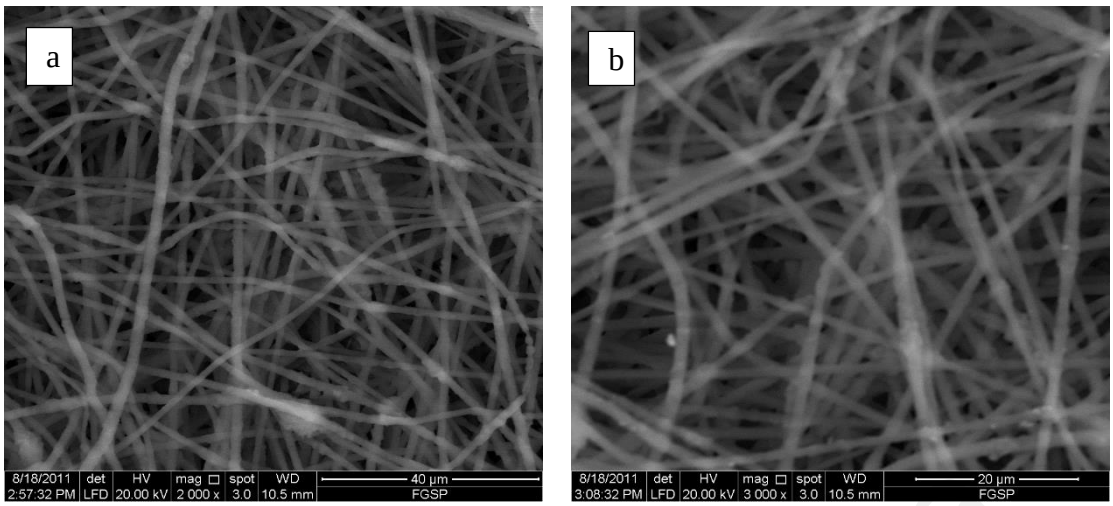

Figure 4.5 FESEM images of PHB obtained after process optimization a) magnification 2000X b) Magnification 3000X

4.2 Project 2: Improving the processability of electrospun Poly [(R)-3-hydroxybutyric acid] through blending with medium chain length Poly (3-hydroxyalkanoates)

4.2.1 Introduction

In recent years, electrospinning of PHB blends was widely carried out and the potential of nanofibers were investigated for scaffolding and other biomedical applications (Chen et al., 2011; Heidarkhan Tehrani et al., 2010; Sombatmankhong et al., 2007). In this study we have looked into the electrospinning of PHB blended with mcl-PHA biosynthesized by *Pseudomonas putida* from palm kernel oil as culturing substrate and looked into the effect of the added mcl-PHA on morphology and microstructure of electrospun fibers. Since both PHB and mcl-PHA possess good biocompatibility and biodegradability, their electrospun blends could have potential biomedical applications would possess all the advantages of pure PHB plus decreased crystallinity and improved porosity and permeability due to reduction of fiber diameter which are important factors in designing scaffolds (Chen et al., 2011). Also, researches show that less crystalline surfaces in scaffolds can improve scaffold / cell interaction of certain types of cells such as fibroblasts (Park et al., 1996).

4.2.2 Solution blending and electrospinning of PHB/ mcl-PHA

Electrospinning and blending was carried out at five different ratios of PHB/ mcl-PHA (100:0, 90:10, 80:20, 70:30, and 60:40). Solution blending was carried out at 60˚C in a condensed flask in a co-solvent of chloroform / DMF with a ration 9:1 respectively. The solutions were electrospun at 12kV with the needle to collector distance of 18cm while a capillary with internal diameter of 0.9 mm was used. The feeding rate was 3 ml/h. For more details please refer to part 3.3.13.3.

4.2.3 Differential scanning calorimetry

Figure 4.6 shows the DSC thermograms of PHB and its blends of mcl-PHA. Figure 4.7 shows the changes in enthalpy of melt against weight percentage of added mcl-PHA, measured based on DSC thermograms. As could be seen, there is a decrease in enthalpy of fusion as the weight percentage of mcl-PHA increases. Therefore, addition of mcl-PHA has decreased the crystallinity. Due to the plasticizing effects of mcl-PHA, crystal packing in PHB is reduced significantly. For example, the sample containing 40% of mcl-PHA has reduced the crystallinity of PHB from 47.2 % to 28.7%.

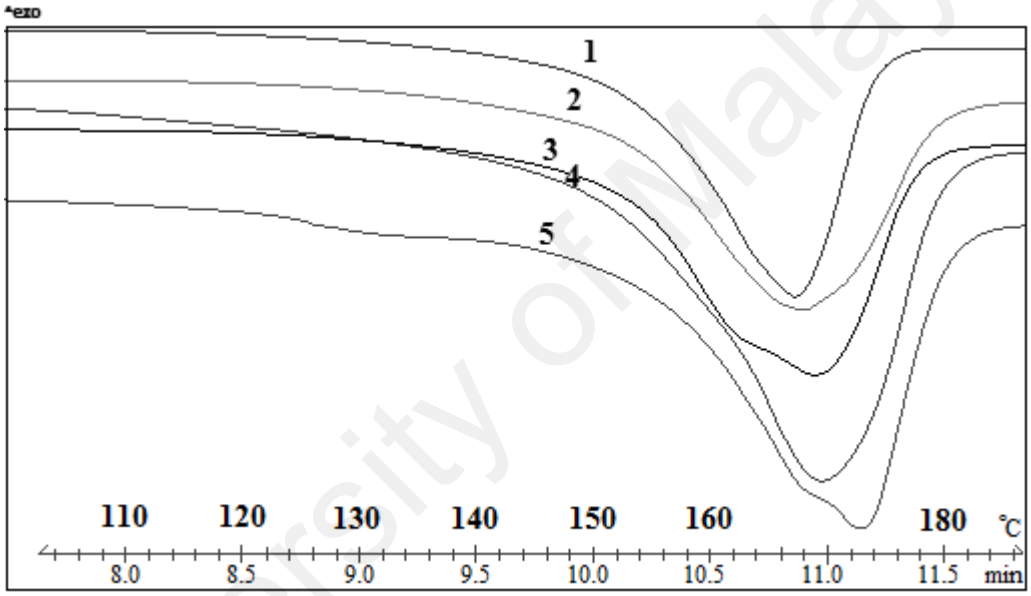

Figure 4.6 DSC thermograms of PHB and its blends with mcl-PHA 1) PHB-mcl-PHA 60:40; 2) PHB-mcl-PHA 70:30; 3) PHB-mcl-PHA 80:20; 4) PHB-mcl-PHA 90:10; 5) Pure PHB

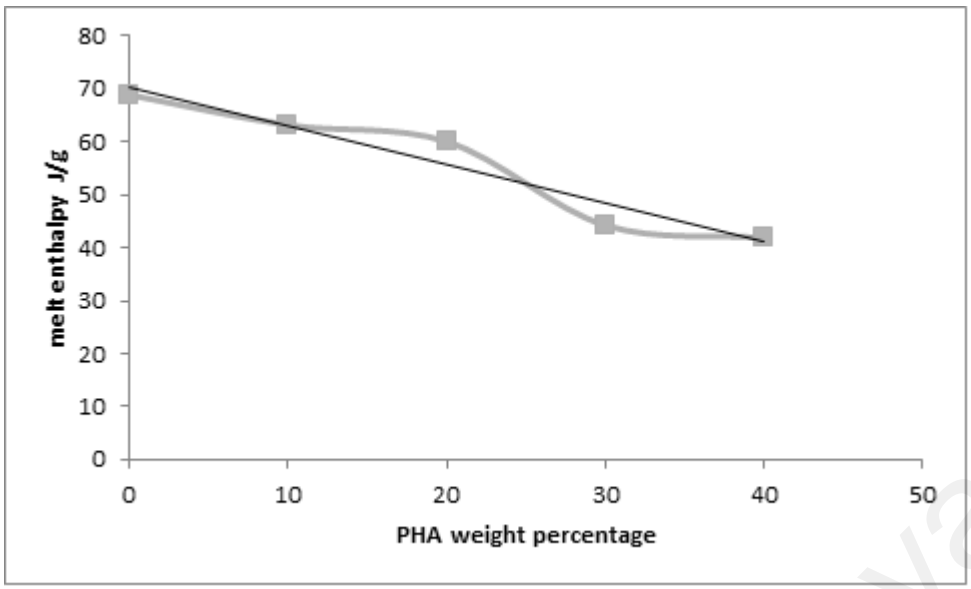

Figure 4.7 Changes of melt enthalpy plotted against weight percentage of mcl-PHA

4.2.4 Fourier transform infrared (FTIR-ATR) spectroscopy

In order to confirm that all the solvent has been evaporated after vacuum oven treatment, FTIR spectra of electrospun PHB and PHB powder were collected. As Figure 4.8 shows the spectra are identical and no proof of solvent was found.

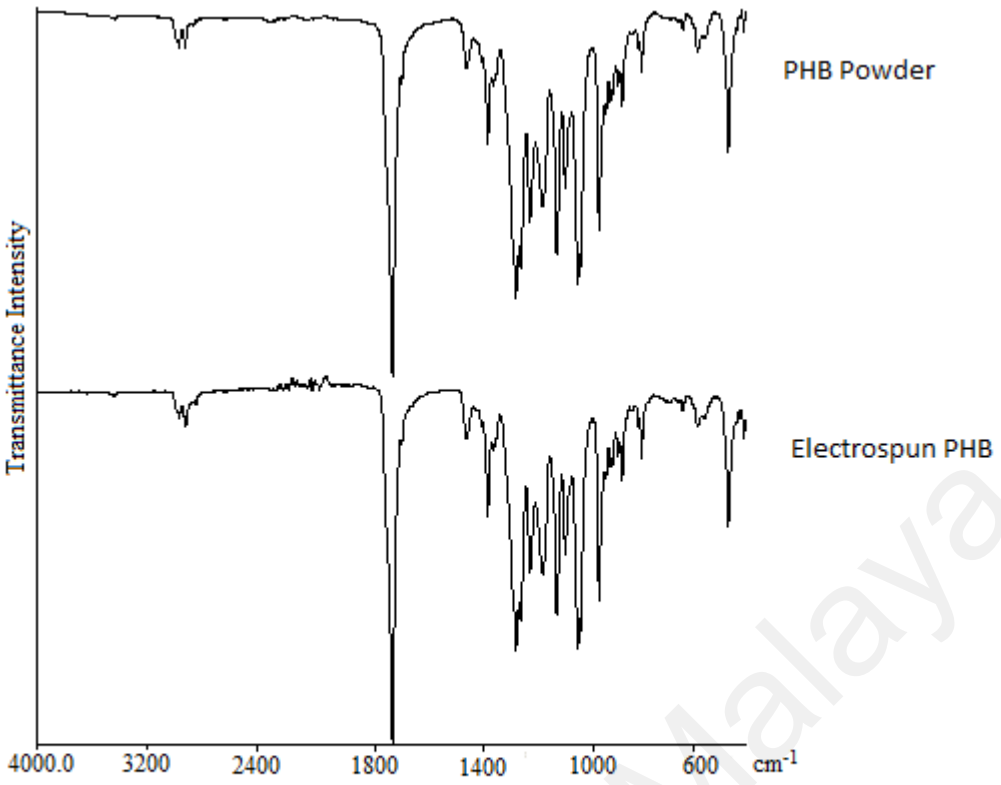

Figure 4.8 FTIR spectra of (a) PHB Powder and (b) Electrospun PHB

4.2.5 Wide angle X-ray diffraction

Figure 4.9 shows the diffraction intensity profiles of electrospun PHB and its blends with mcl-PHA. In all profiles, α-form crystals with 21 helix conformation is observed. The diffraction peak observed at 2Θ=19.6˚ is assigned to β-form crystals with planar zigzag conformation. β-form crystals were not observed in samples containing 30% and 40% mcl-PHA. It is assumed to be because of smaller degree of chain orientation in amorphous areas, since β-form crystals are contributed from the amorphous chains between lamella crystals. It is also because of increased proportion of amorphous region in the sample, which leads to lower degree of orientation.

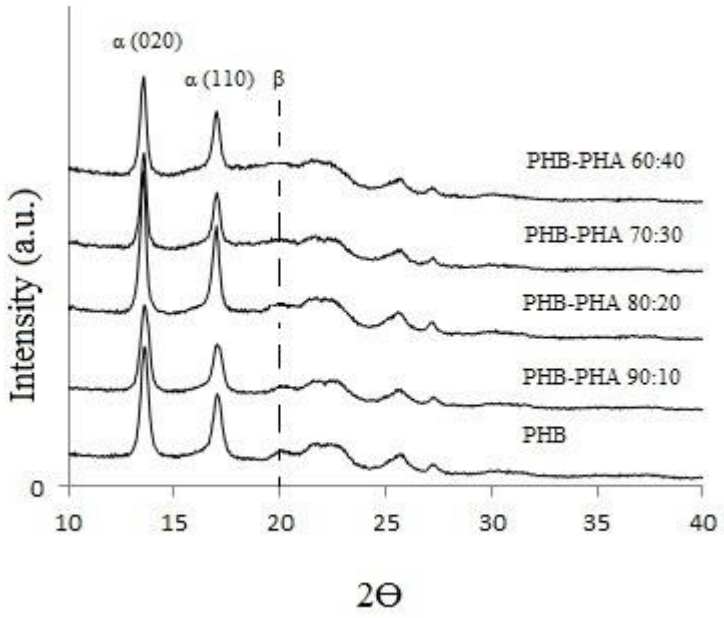

Figure 4.9 Diffraction profiles of electrospun PHB and its blends with mcl-PHA

4.2.6 FESEM Microscopy

FESEM images were taken at 2000 times magnification using a high voltage field of 20kV. The data provided in table 2 is based on 100 measurements per sample. As could be seen in Figure 4.10, the distribution patterns of fiber diameters indicate that addition of mcl-PHA had a positive effect in decreasing electrospun fiber diameter. The plasticizing effect of mcl-PHA has made the blend more flexible and stretchable to form fibers of smaller diameter using the same electrostatic field strength. Also, PHB being rigid and brittle tends to form more uniform fibers which have a lower standard deviation; while by increasing the weight ratio of mcl-PHA the distribution of fiber diameter has become broader. When the amount of mcl-PHA is increased more beads were along the fibers. It could be due to the stretchable fiber which cannot maintain a constant diameter under the slight pulsation voltage of the semi-rectified DC during spinning time. Deitzel et.al in their study (Deitzel, Kleinmeyer, Harris, et al., 2001) reported that at a higher voltage, more beads were formed, presumably the fiber flight time had decreased with increasing voltage and the solvent could not evaporated fast enough. In this case, the

lower molecular weight mcl-PHA tends to lower the viscosity of the blend solution, making it easier to flow under the electrostatic attraction. The faster movement would reduce the flight time, and consequently some formation of beads was observed.

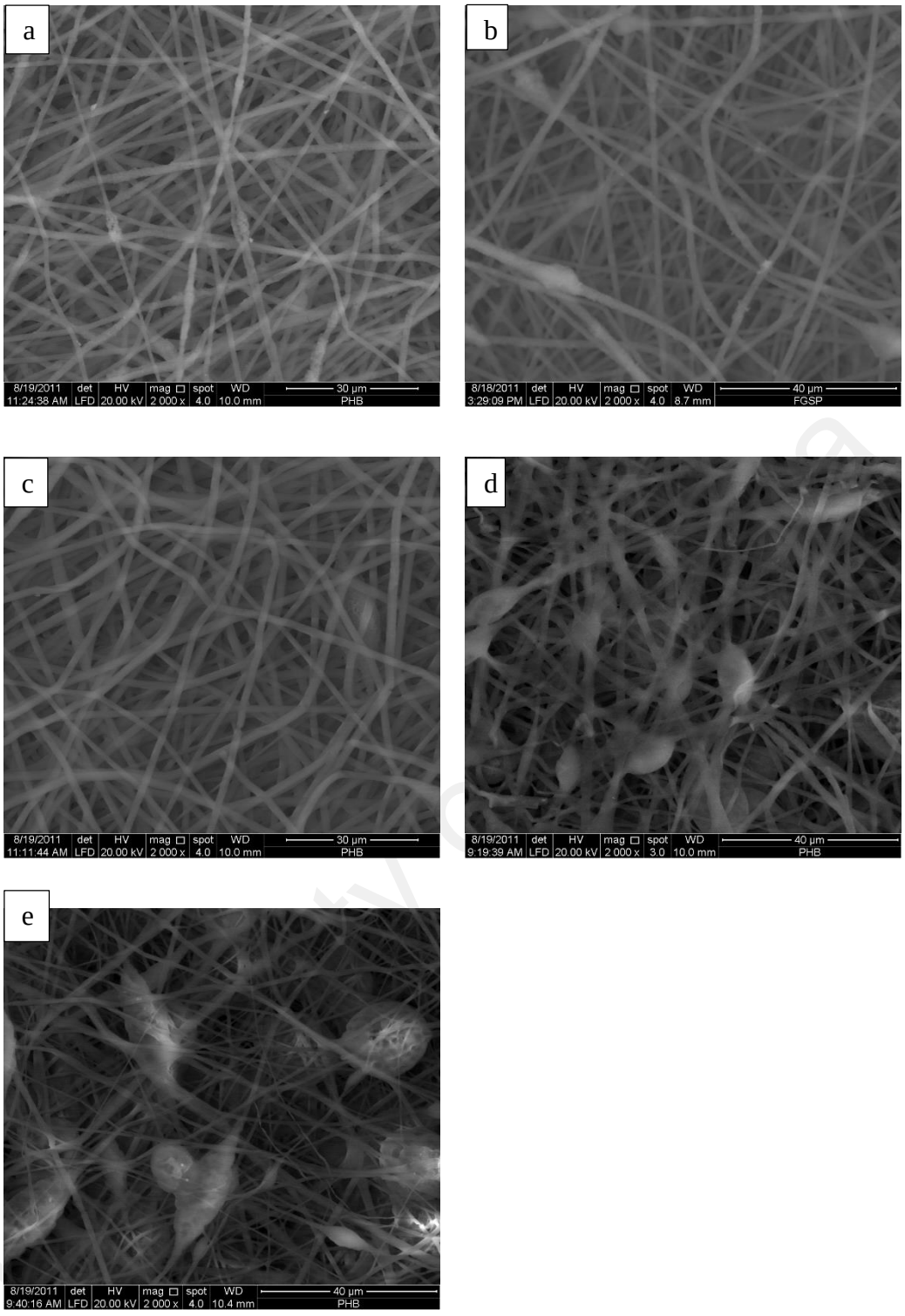

Figure 4.10 Scanning electron microscopy images of electrospun PHB and its blends with mcl-PHA along with fiber diameter (µm) distribution a) PHB b) PHB-mcl PHA 90:10 c) PHB-mcl-PHA 80:20 d) PHB-mcl-PHA 70:30 e) PHB-mcl-PHA 60:40

Table 4-1 Fiber diameter changes against weight ratio of mcl PHA

Sample	Fiber Diameter (μm)			
	Mean	Standard deviation	min	max
PHB	1.27	0.27	0.72	2.02
PHB-mcl PHA 90:10	1.31	0.29	0.52	2.55
PHB-mcl PHA 80:20	1.30	0.45	0.69	2.32
PHB-mcl PHA 70:30	1.01	0.36	0.41	2.19
PHB-mcl PHA 60:40	0.81	0.37	0.2	1.87

4.3 Project 3: An In-vitro evaluation of electrospun scaffolds of polycaprolactone containing micro hydroxyapatite particles

4.3.1 Introduction

Bone loss can occur due to various reasons, including trauma, cancer, fracture, osteoporosis, and infectious disease (Kimakhe et al., 1999). The rate of success with conventional surgical methods has been limited in terms of complete bone regeneration. Bone grafting as the most dominant surgical method has a rate of success of 50-84% (Stevenson et al., 1996). However, more feasible options has been introduced by bone tissue engineering to be fully optimized for routine clinical use. An aspect of tissue engineering (TE) is the careful design of scaffolds, microstructures which help cells build better neo-tissue, and imitate an extracellular matrix. Electrospinning which uses electrical charge to produce fine threads from a polymeric solution to form a fibrous microstructure. Scaffolds made by electrospinning have a high surface area which leads to better cellular attachment (Cipitria et al., 2011) and growth and their morphology is similar to that of extracellular matrix. In this research we have fabricated PCL scaffolds containing different weight ratios of BHA their chemical properties and biological response to rat derived bone marrow stem cells have been investigated.

The use of hydroxyapatite (HA) has been extensively documented (Shin et al., 2004; Wei et al., 2004) to fabricate scaffolds for bone tissue engineering. HA, when produced in a laboratory setting, is typically brittle and lacks the mechanical strength required for effective bone TE. Various additives and structural modifications are made in order to combat these limitations. In particular, there has been some work on the incorporation of synthetic HA into PCL (Ma et al., 2005; Nisbet et al., 2009). However, in this research we used bovine derived HA because of its quality (purity > 95%) (Lin et al., 1999), quantity (>60 wt%) and cost effectiveness as a natural waste (Lin et al., 1999; Ooi et al., 2007).

4.3.2 Characterization of BHA

4.3.2.1 Particle size analysis

The details of BHA synthesis and sieving is provided in 2.1.2 and particle size analysis in 2.4.1. As the results show (Table 4-2), the volume weighted average particle diameter for the HA is 28.5 µm (Dv50=28.5 µm), which is in line with previous sieving applied to the HA particles (20 – 40 µm). The table below summarizes the largest particle size for a given percentage of volume for the sample.

Table 4-2 Particle size analysis of BHA

Percentile of volume	Size (µm)
10%	0.58
20%	6.46
50%	22.81
80%	49.24
90%	63.69

4.3.2.2 Chemical characterization of BHA

In order to confirm that bovine bone has been successfully converted into BHA, the resulting BHA powder was analyzed by FTIR and XRD. Both of the methods showed characteristic peaks of HA.

In this research BHA was derived from three different bovine bones including femur, metatarsus and tibia. The XRD results showed that regardless of which part of the bone used BHA could be achieved before and after sintering. Figure 4.11 shows diffraction

intensity patterns of unsintered and sintered bovine which were scanned in the range of 2θ between 20° and 50°. Due to the lower crystallinity of the unsintered bone, the peaks are unclear suggests presence of impurities. However, the peaks of the sintered bovine bone match the JCPDS database for HA. When the XRD peaks of all the sintered BHA were indexed on the basis of the hexagonal crystal system of space group $P6_3\ m^{-1}$ with respect to the JCPDS database, the Bragg peaks of sintered BHA powder at ~22, 23, 26, 28, 29, 30–35, 39, 40, 42, 46, 48 and 49° (2θ) were similar to the characteristics peaks of HA, which means HA could be obtained from a bovine source.

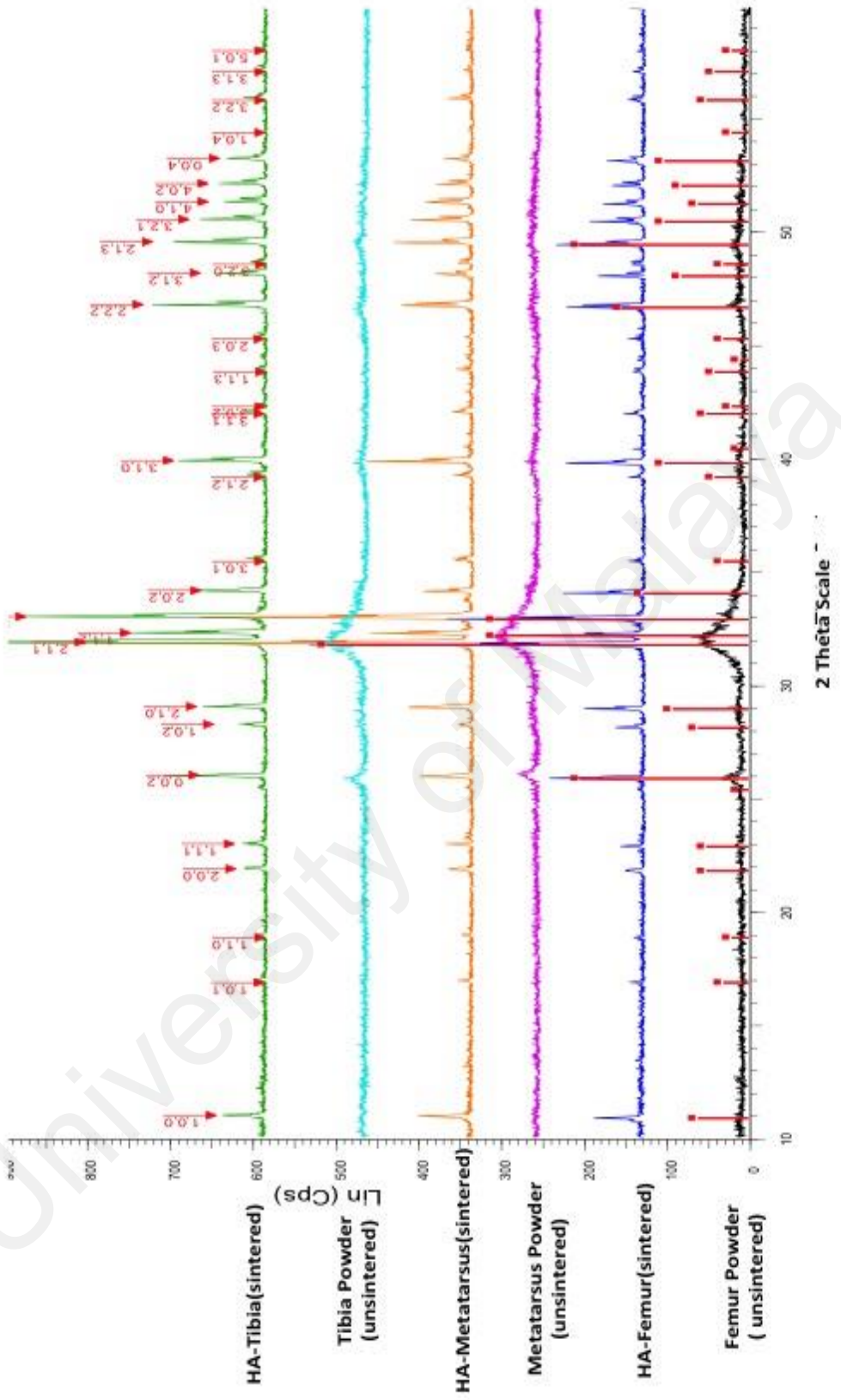

Figure 4.11 XRD profile of sintered and unsintered bovine bones from different spots

The FT-IR results (Figure 4.12) show that the band of OH^- at 3290 cm^{-1} has disappeared in sintered bovine bones compared to unsintered sample. This suggests a dehydroxylation during sintering. Sintering has also caused decomposition of organic carbonate matters. Figure 4.12 showed the missing of absorption peaks of carbonate at 870 to 880 cm^{-1} and 1300 to 1700 cm^{-1}in all sintered BHA samples. Formation of phosphate characteristic peaks in all sintered samples could be seen at (1020–1040 cm − 1) for $PO4^{-3}$ bands v_3 and (560–565 cm − 1) for band v_4.

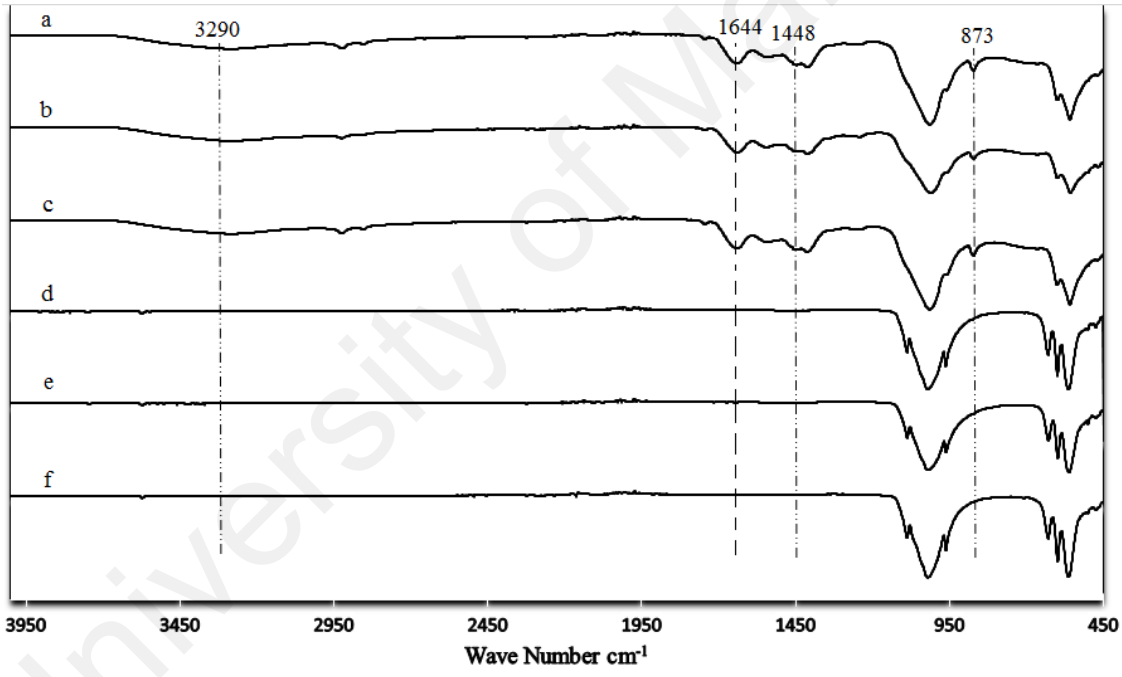

Figure 4.12 FTIR spectra of pre-sintered and post-sintered bovine bones a) Tibia pre-sintered; b) Metatarsus pre-sintered; c) Femur pre-sintered; d) Tibia post-sintered; e) Metatarsus post-sintered; f) Femur post-sintered

4.3.3 Characterization of composite scaffolds of PCL/BHA

4.3.3.1 FTIR spectroscopy of electrospun PCL/BHA

The FT-IR analysis results (Figure 4.13) showed that the intensities of PO_4^{-3} and -OH peaks have increased as the weight % of BHA in the scaffold is increased. The results

also showed that there was no trace of residual solvents in the scaffold, this is also supported by the thermogravimetric analysis (TGA) results.

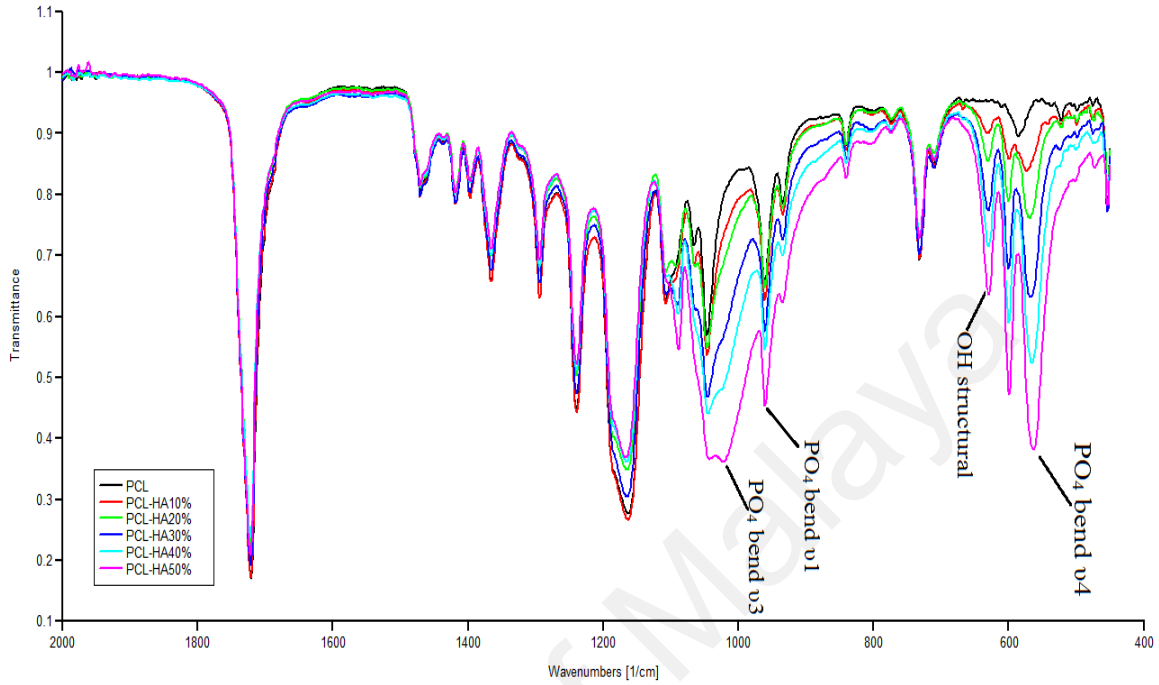

Figure 4.13 FTIR Spectra of electrospun PCL containing 5 different weight ratios of BHA

4.3.3.2 Field emission scanning electron microscopy

Results from Figure 4.14 and Table 4-3 shows the fiber diameter distribution for each sample from image processing technique using ImageJ software based on a minimum of 100 readings for each sample. As can be seen in Table 4, the addition of BHA has caused the average fiber diameters to increase, compared to pure PCL. However, this increase in fiber diameter is less in higher concentrations of BHA in the composite scaffold. Addition of the insoluble BHA particles at a micron size to the PCL solution has resulted in a suspension. At higher concentrations of BHA, a more uniform suspension would be formed, and therefore, the fluctuation in fiber diameter for the sample containing 50% of BHA is the least. Another important observation in FESEM images is the phase separation which happens due to a lack of adhesion at the surfaces of PCL and BHA.

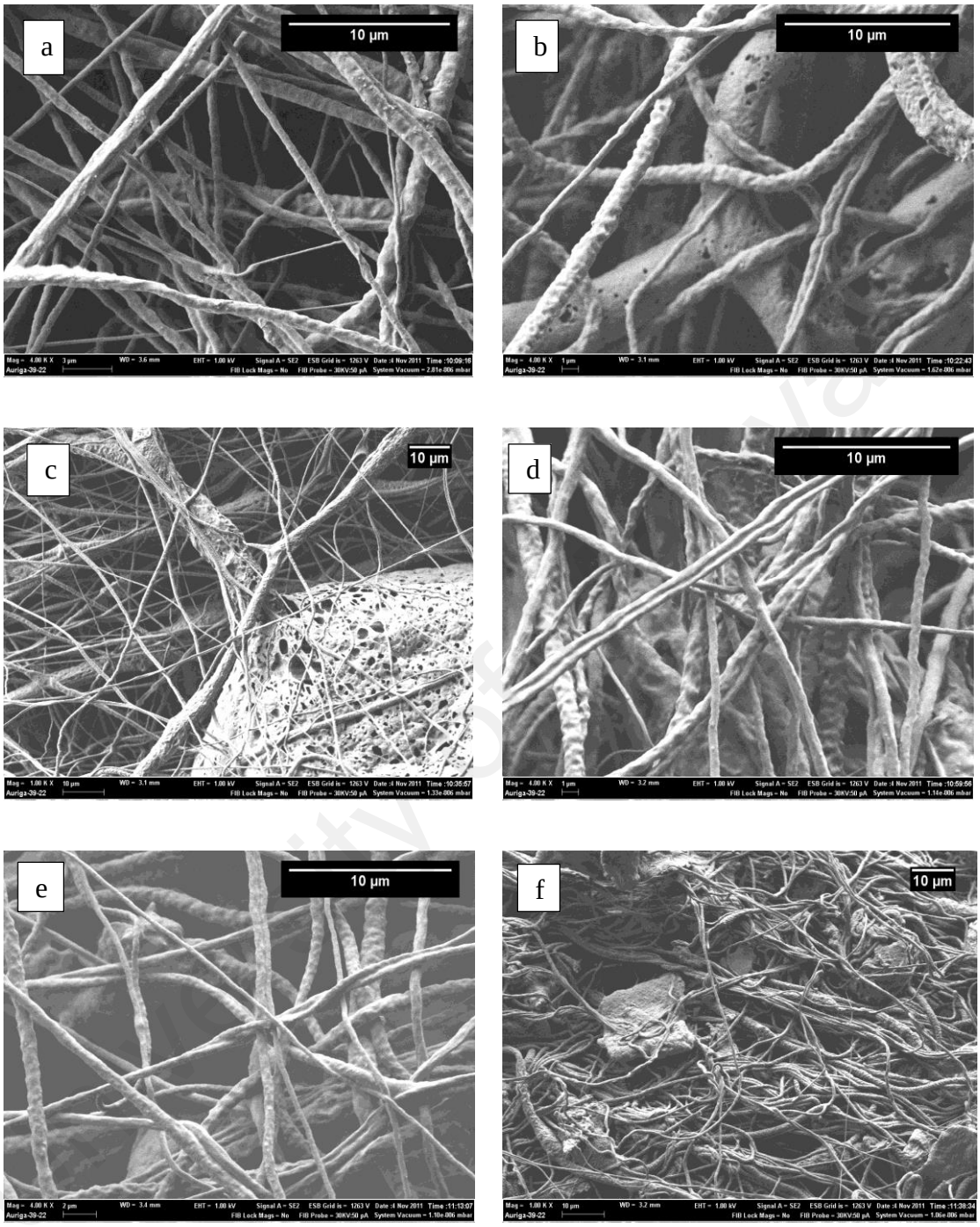

Figure 4.14 FESEM micrographs of blank scaffolds of PCL/BHA a) PCL; b) PCL-BHA10%; c) PCL-BHA20%; d) PCL-BHA30%; e) PCL-BHA40%; f)PCL-BHA50%

Table 4-3 Diameter range of the fibers for blank PCL-BHA scaffolds

Sample	Fiber Diameter (μm)			
	Mean	Standard Deviation	Min	max
PCL	0.63	0.29	0.15	1.84
PCL-BHA10%	1.05	0.76	0.32	4.41
PCL-BHA20%	0.89	0.48	0.26	2.05
PCL-BHA30%	0.84	0.38	0.25	1.78
PCL-BHA40%	0.80	0.20	0.29	1.18
PCL-BHA50%	0.72	0.23	0.22	1.51

Figure 4.15 and Figure 4.16 shows the cells seeded on the scaffolds after 7 and 14 days respectively. All the scaffold have been capable of promoting cell attachment and cell growth. We can observe some calcification occurring in PCL-BHA50% scaffold, which is probably due to the high concentration of BHA. This is a common phenomenon when BHA is exposed to culture medium.

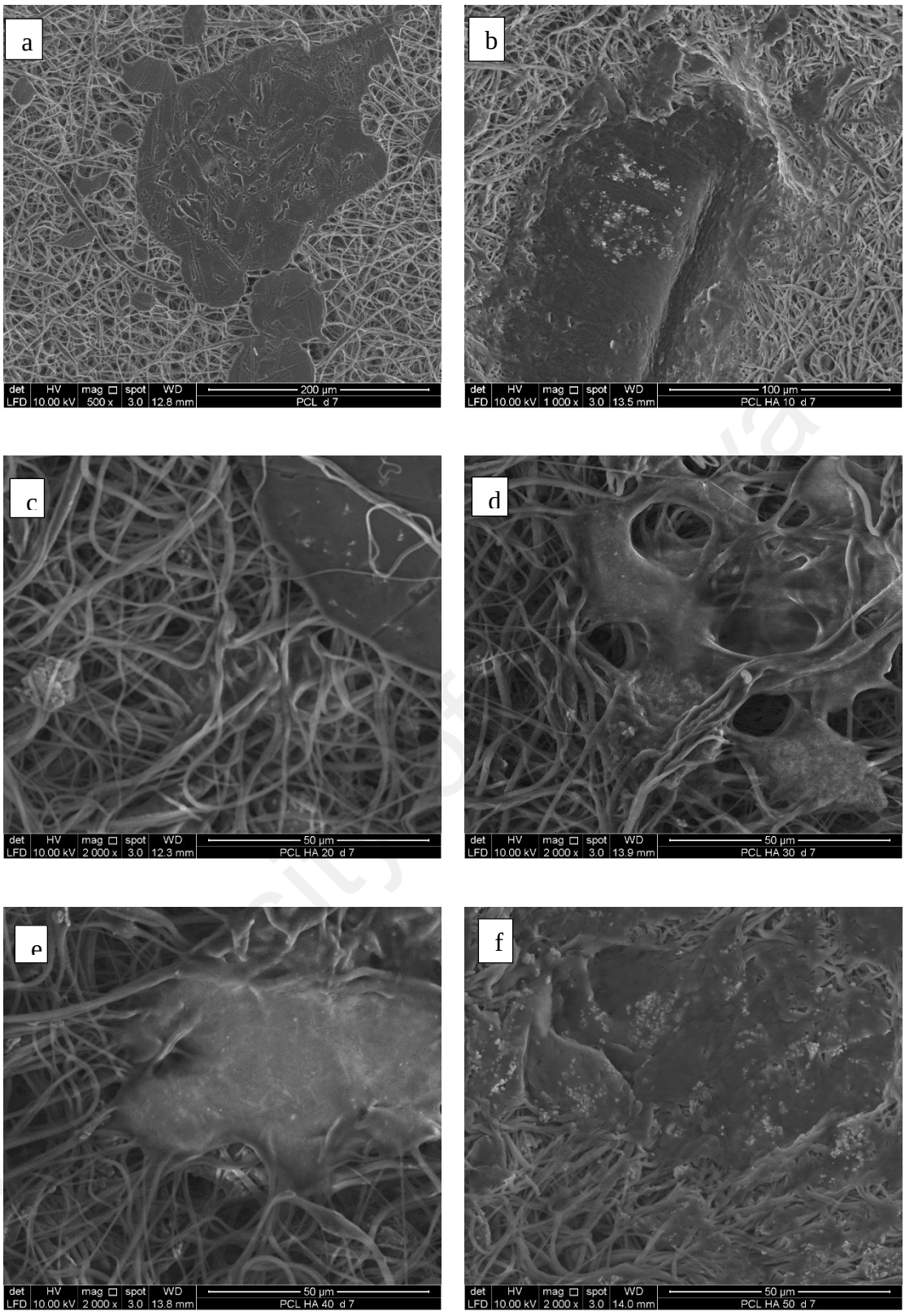

Figure 4.15 FESEM images of seeded scaffolds captured 7 days after seeding; a) PCL; b) PCL-BHA10%; c)PCL-BHA20%; d)PCL-BHA30%; e)PCL-BHA40%; f)PCL-BHA50%

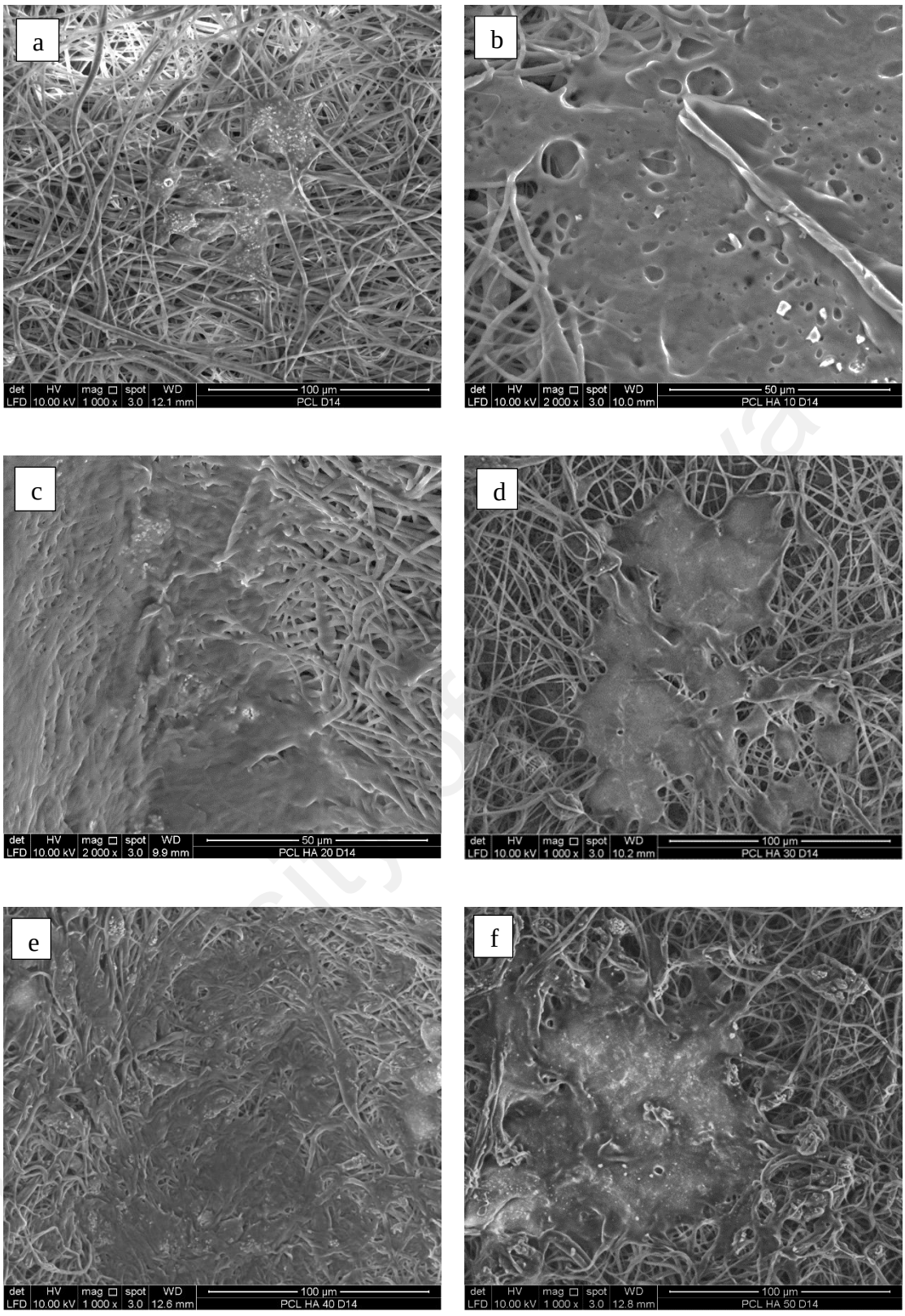

Figure 4.16 FESEM images of seeded scaffolds. The images were captured 14 days after seeding: a) PCL; b)PCL-BHA10%; c)PCLBHA20%; d)PCL-BHA30%; e)PCL-BHA40%; f)PCL-BHA50%

4.3.3.3 Thermogravimetric Analysis

Thermogravimetric analysis was carried out as a quantitative method for measuring the distribution of BHA within the sample. The samples were chosen randomly from different parts of scaffolds. Thermogravimetric analysis results did not show any trace of residual solvents in the scaffold since no weight loss was observed between 30 to 200ºC. The remaining content at 900ºC corresponds to the amount of BHA in each sample. As can be seen in Figure 4.17, all the samples with an extent of deviation (±4.4%) follow the weight percentage used in spinning dope preparation. The results indicate that by usage of particles in the micron range it is also possible to reach an acceptable level of uniformity in terms of particle distribution.

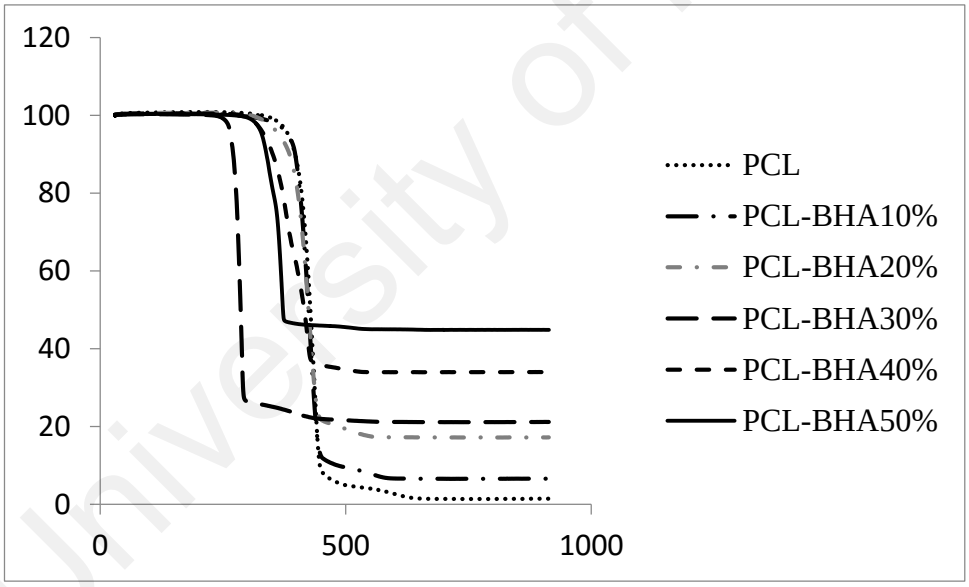

Figure 4.17 Thermogravimetric peaks of composite scaffolds of PCL-BHA; the remaining amount at 900˚C corresponds to weight of BHA present in the sample

4.3.3.4 Contact angle measurement

Contact angle measurements corresponds to surface hydrophilic properties; the lower the contact angle the more hydrophilic it is. Figure 4.18 shows the contact angle readings of scaffold plotted against the weight ratio of BHA. As the graph suggests addition of BHA had a positive effect on decreasing the contact angle and over all decreased the hydrophobicity. A hydrophilic surface encourages cell to scaffold attachment (Webb et al., 1998) and addition of BHA might have a positive effect on cell – scaffold interactions as it is reducing surface hydrophobicity.

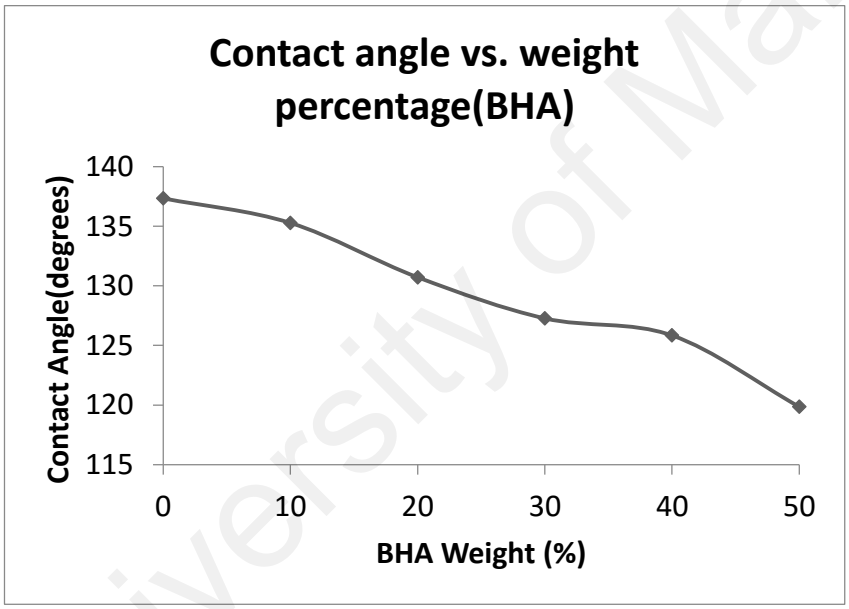

Figure 4.18 Water contact angle of the droplet on the scaffold plotted against the weight ratio of the BHA in the scaffold composition

4.3.3.5 Confocal laser microscopy

Figure 4.19 shows the roughness profile of all scaffolds obtained by confocal microscopy. The roughness was measured by the instrument based on the deviations in a vector direction from an ideal surface. Samples for the measurement were chosen randomly from the electrospun sheet. As Figure 4.19 suggests PCL-BHA30% has the roughest surface

among the samples. It could be due to compositional ratio and distribution of micron sized BHA within the sample.

Figure 4.20 shows the average surface roughness measured by confocal laser microscope. Addition of BHA in lower concentration has decreased surface roughness maybe because of the filling effect of BHA within the porous scaffold. It reached its peak by PCL-BHA30% as the roughest surface, while increasing the concentration of BHA further more started a reducing trend. At higher concentrations of BHA it is expected that the particles distribute more uniformly within the sample resulting in formation of a smoother surface compared to PCL-BHA30%.

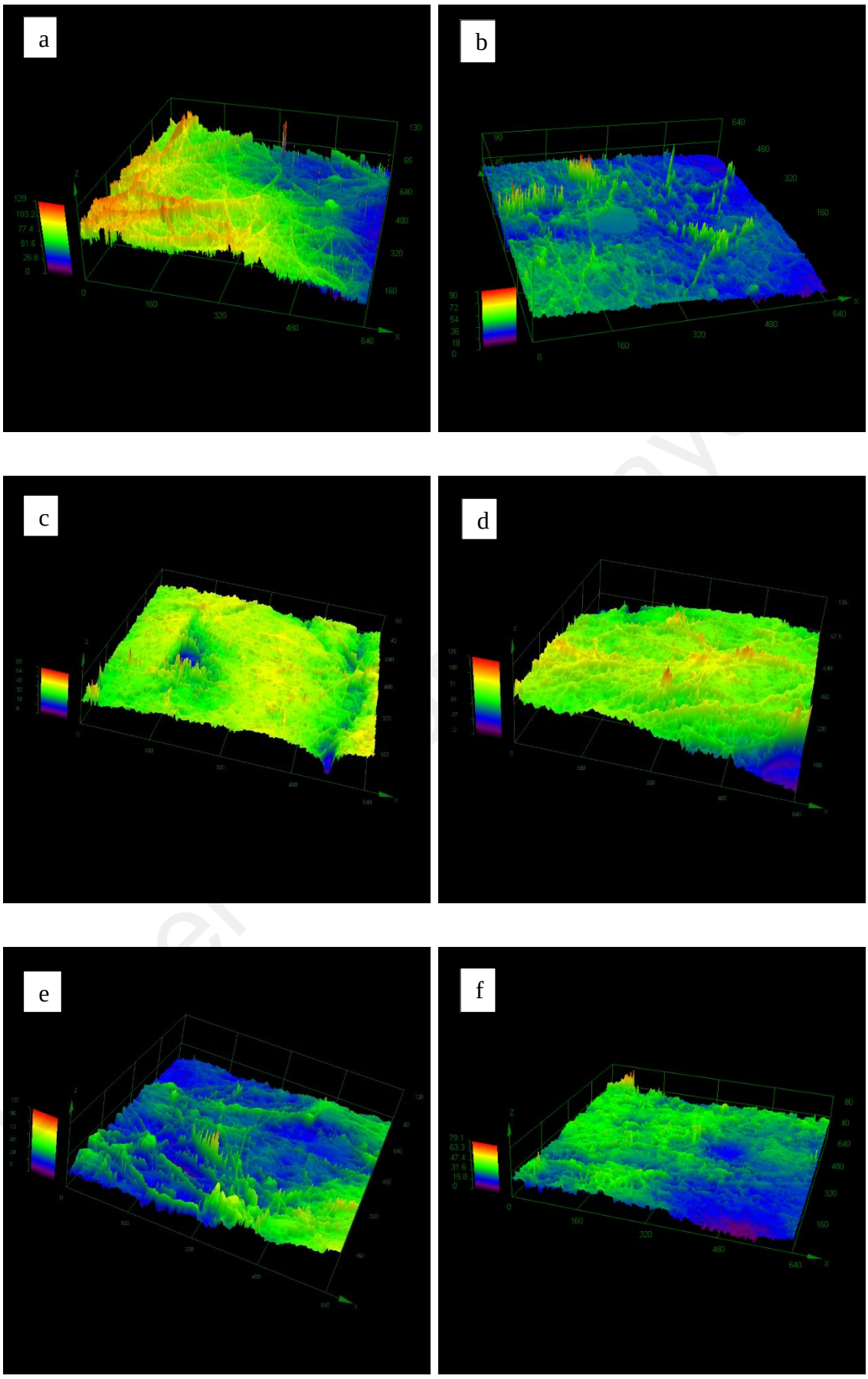

Figure 4.19 Roughness profile of the blank scaffolds; a) PCL; b)PCL-BHA10%; c)PCLBHA20%; d)PCL-BHA30%; e)PCL-BHA40%; f)PCL-BHA50%

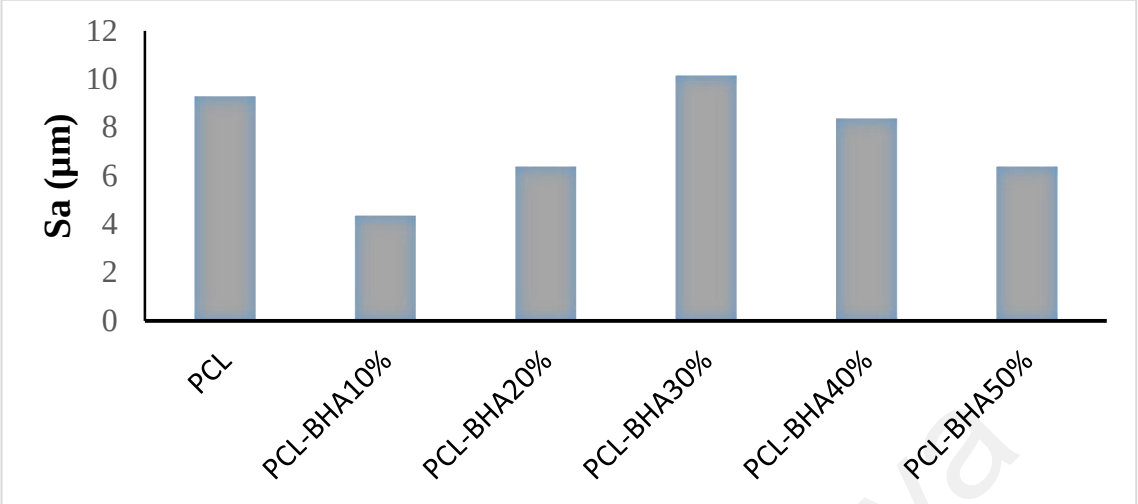

Figure 4.20 Average surface roughness for blank scaffolds

4.3.4 Biological assays

4.3.4.1 Alamar Blue assay

FESEM as a qualitative method already provided the proof for presence of the BMSCs on the scaffolds. However, in order to quantify the proliferation rates of BMSCs on the scaffolds, Alamar Blue assay also known as Resazurin assay was performed as explained in 2.5.4.1. The Alamar Blue profile measures the metabolic activity of cells based on the reduction in resazurin dye i.e. the higher the dye is reduced, the more the metabolic activity of cells. Cell metabolism can be translated to the number of cells. Figure 4.21 shows BMSCs metabolic activity over a period of 14 days.

On day 1 the reading for reduction of Resazurin dye is almost similar and there was no significant difference between the groups. It suggests that the seeding density was the same for all the groups.

On day 7 PCL-BHA30% was significantly lower ($P<0.05$) when compared to Thermanox which was used as positive control in this study. The rest of the samples didn't show any significant difference compared to Thermanox.

On day 14, the cell number on all the scaffolds except for PCL was significantly higher compared to day 1 after performing a paired T-Test ($P<0.05$), suggesting that addition of BHA to electrospun PCL supports cell growth and has a positive effect on cell growth and metabolism. The highest reading on day 14 belonged to PCL-BHA40% which suggests the cells interacted with that compositional ratio better than the others after a period of two weeks.

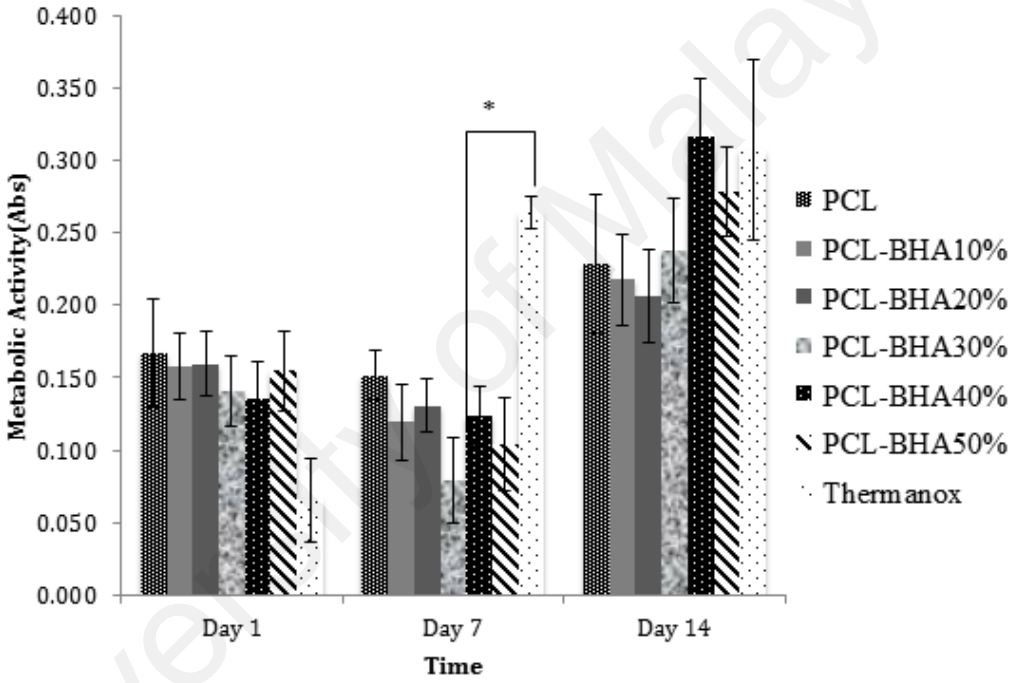

Figure 4.21 Alamar Blue activity of the BMSCs seeded on PCL-BHA scaffolds over a period of two weeks

4.3.4.2 Alkaline phosphate (ALP) assay

Alkaline phosphate activity of the BMSCs provides information about their osteogenic differentiation. Figure 4.22 shows the alkaline phosphate activity of the cells measured on day 7 and day 14 of culturing. The result suggests that all the samples are osteoinductive and osteocunductive. The amount of ALP remained almost constant over

a period of 14 days, which would suggest the concentrations of BHA used did not induce a significant increase in osteogenic differentiation but indicated trace osteogenic activity.

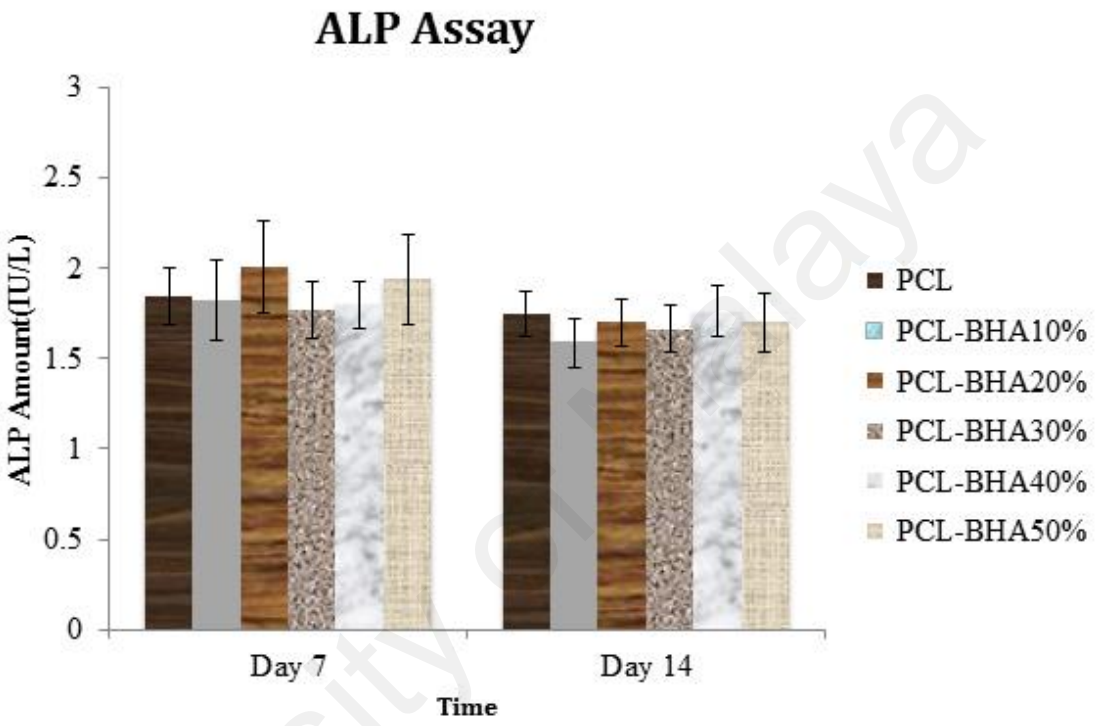

Figure 4.22 Alkaline phosphate activity of the BMSCs over a period of two weeks

4.4 Project 4: A combination micro particles of hydroxyapatite and electrospun PHB as scaffolding materials for bone tissue regeneration

4.4.1 Introduction

In this research we have developed composite scaffolds based on PHB and BHA at five different compositional ratios (10%, 20%, 30%, 40% and 50%) of BHA (Dv50=28.5 µm). The particles were dispersed into the polymeric solution of PHB in chloroform and DMF followed by electrospinning. The details of blending are provided in part 2.2.4. The fabricated scaffolds are characterized by various chemical methods and biological evaluation is carried out *in vitro* using rat derived BMSCs. PHB has good biodegradability and biocompatibility as well as reasonable costs of production which makes it an inevitable option for scaffolding materials in tissue engineering. Previous studies have confirmed its non-toxicity and potential for promoting cell attachment and growth when used as scaffolding material (Heidarkhan Tehrani et al., 2010; Sombatmankhong et al., 2007; Suwantong et al., 2007). The incorporation of nano Hydroxyapatite into electrospun PHB has also been studied briefly (Ito et al., 2005). However, there was no study on the possibility of incorporation micron sized BHA at various ratios to provide a substantial understanding of the compositional ratios and their effect on the cell attachment and proliferation.

4.4.2 Field emission scanning electron microscopy

Figure 4.23 shows the FESEM images of blank scaffolds and their relevant fiber diameter distribution. The histograms of fiber diameter analysis show that addition of BHA did not change the distribution patterns of the samples and they are more or less in the same range. This could be due to high crystallinity and stiffness of PHB, which retained its morphology despite addition of BHA. The BHA particles are easier to see compared to PCL samples mainly due to more uniform morphology of the fibers.

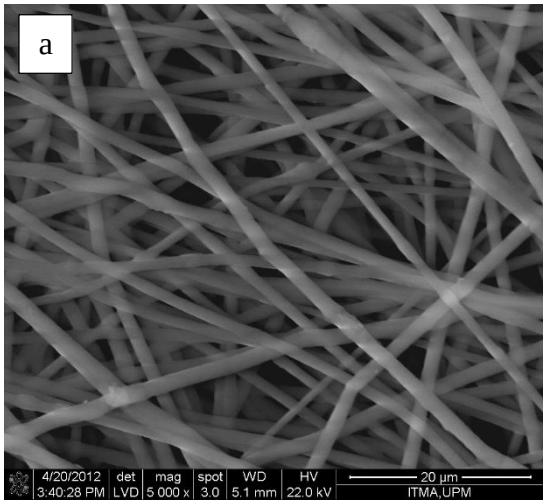

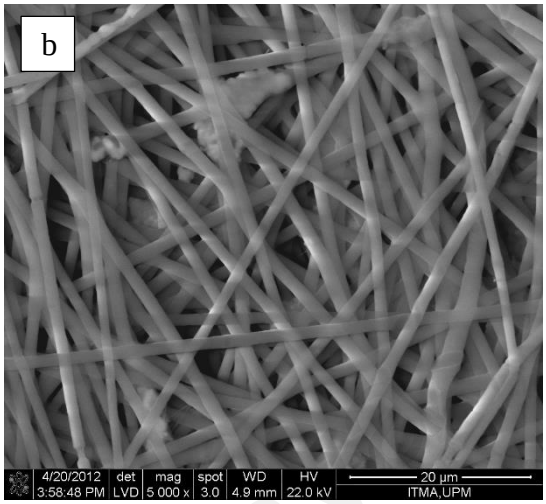

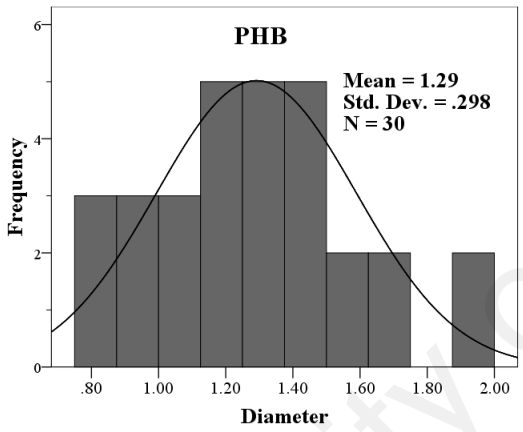

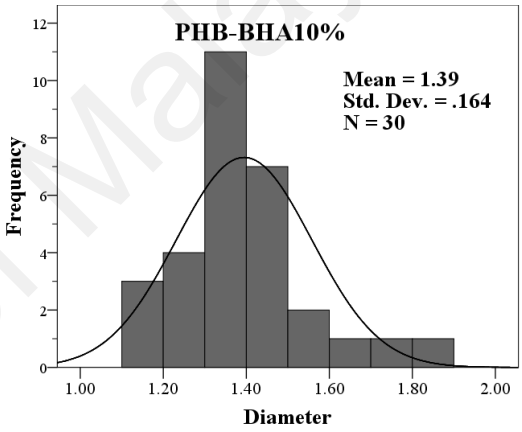

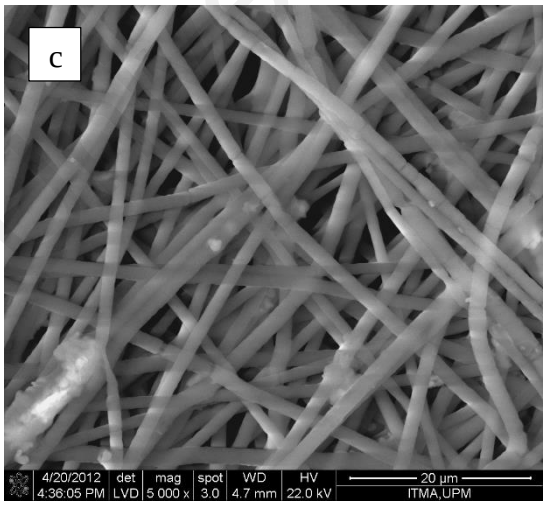

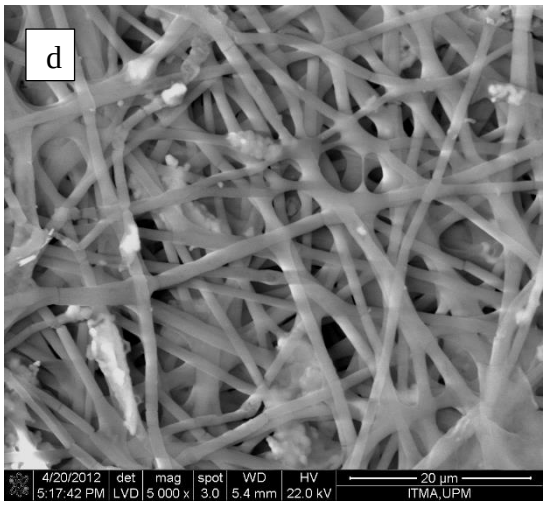

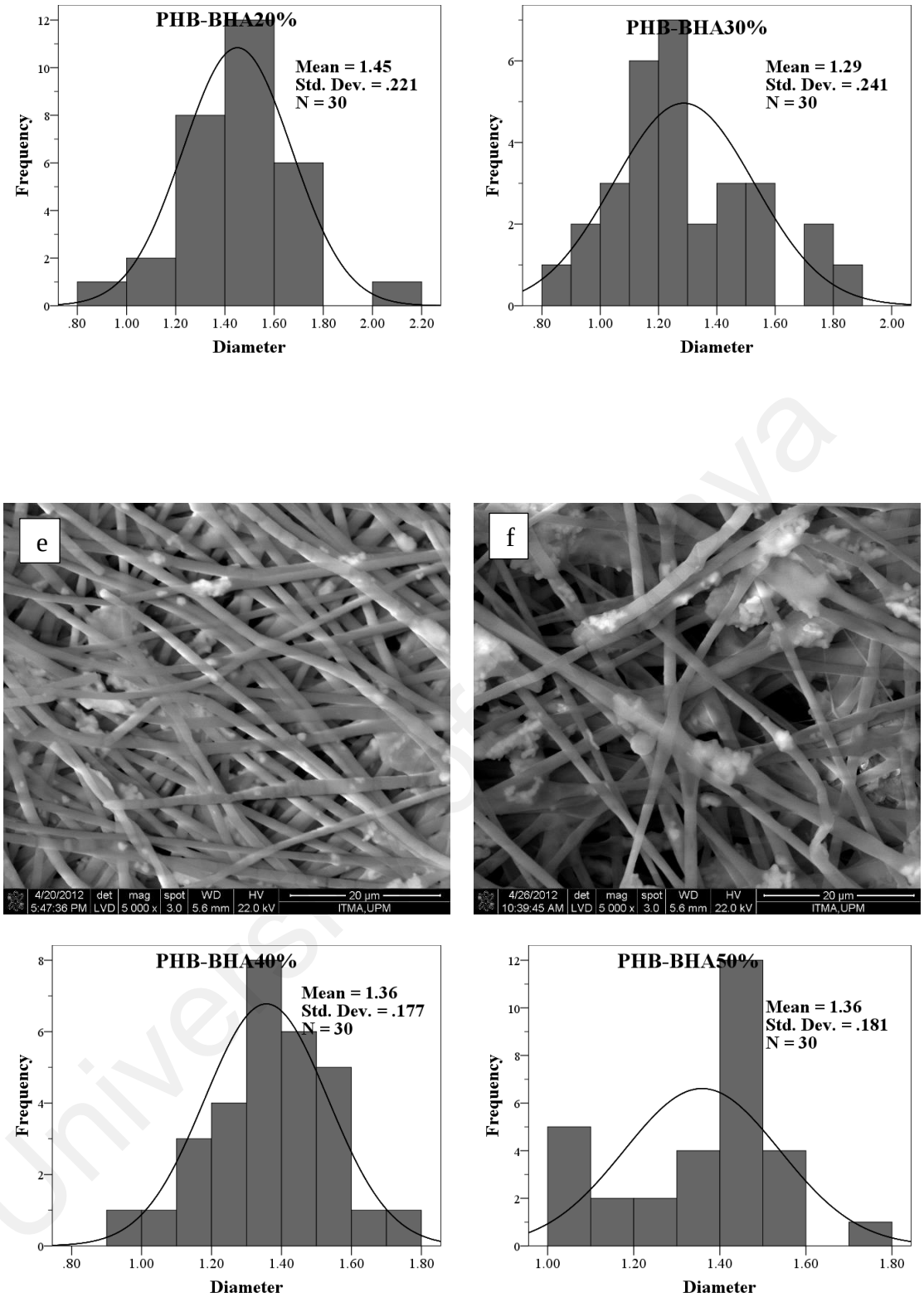

Figure 4.23 FESEM images of the blank scaffolds and their relevant fiber diameter analysis a)PHB; b)PHB-BHA10%; c)PHB-BHA20%; d)PHB-BHA30%; e)PHB-BHA40%; f)PHB-BHA50%

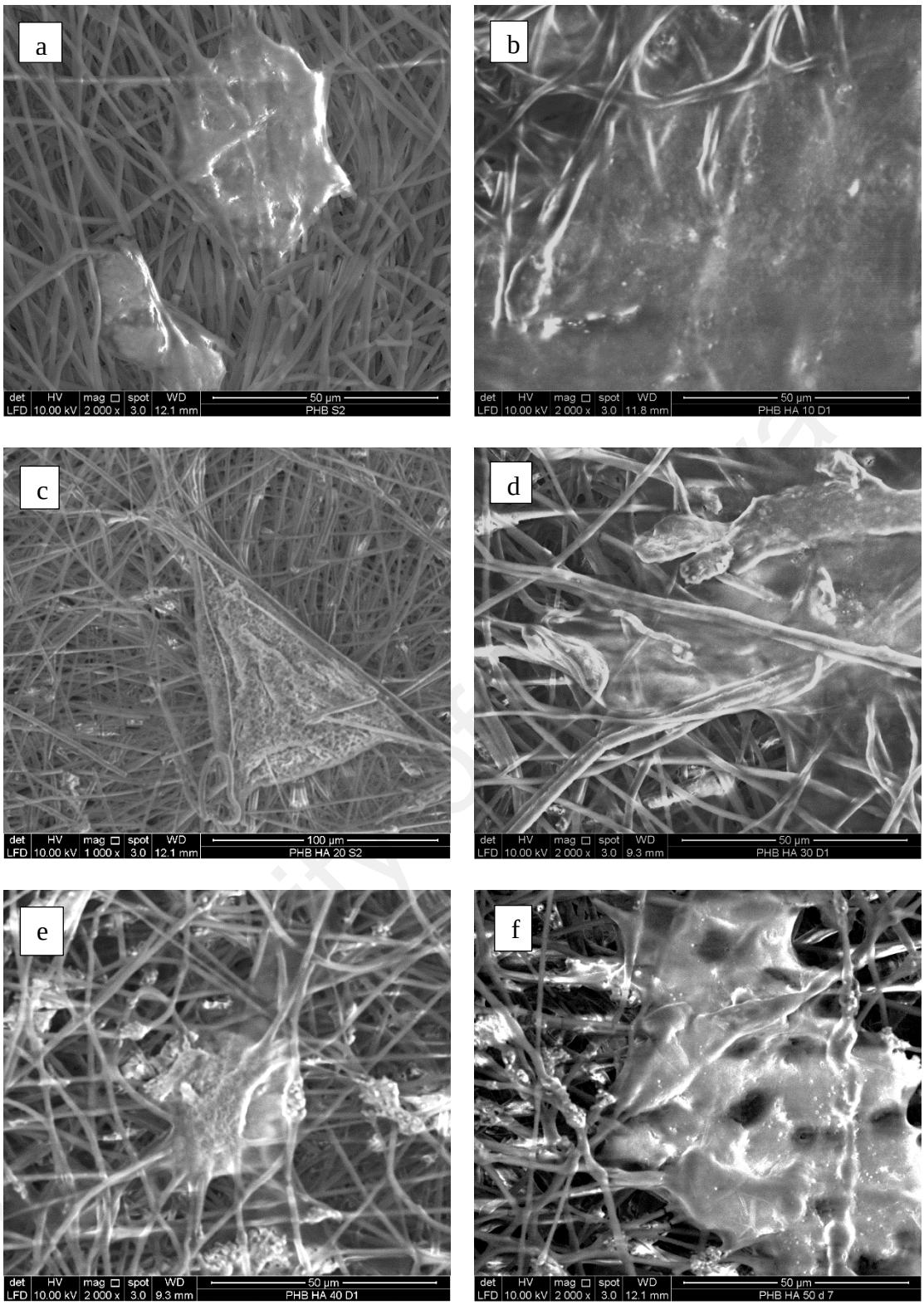

Figure 4.24 BMSC Seeded PHB-BHA scaffolds after 7 days a) PHB; b) PHB-BHA10%; c) PHB-BHA20%; d) PHB-BHA30%; e)PHB-BHA40%; f) PHB-BHA50%

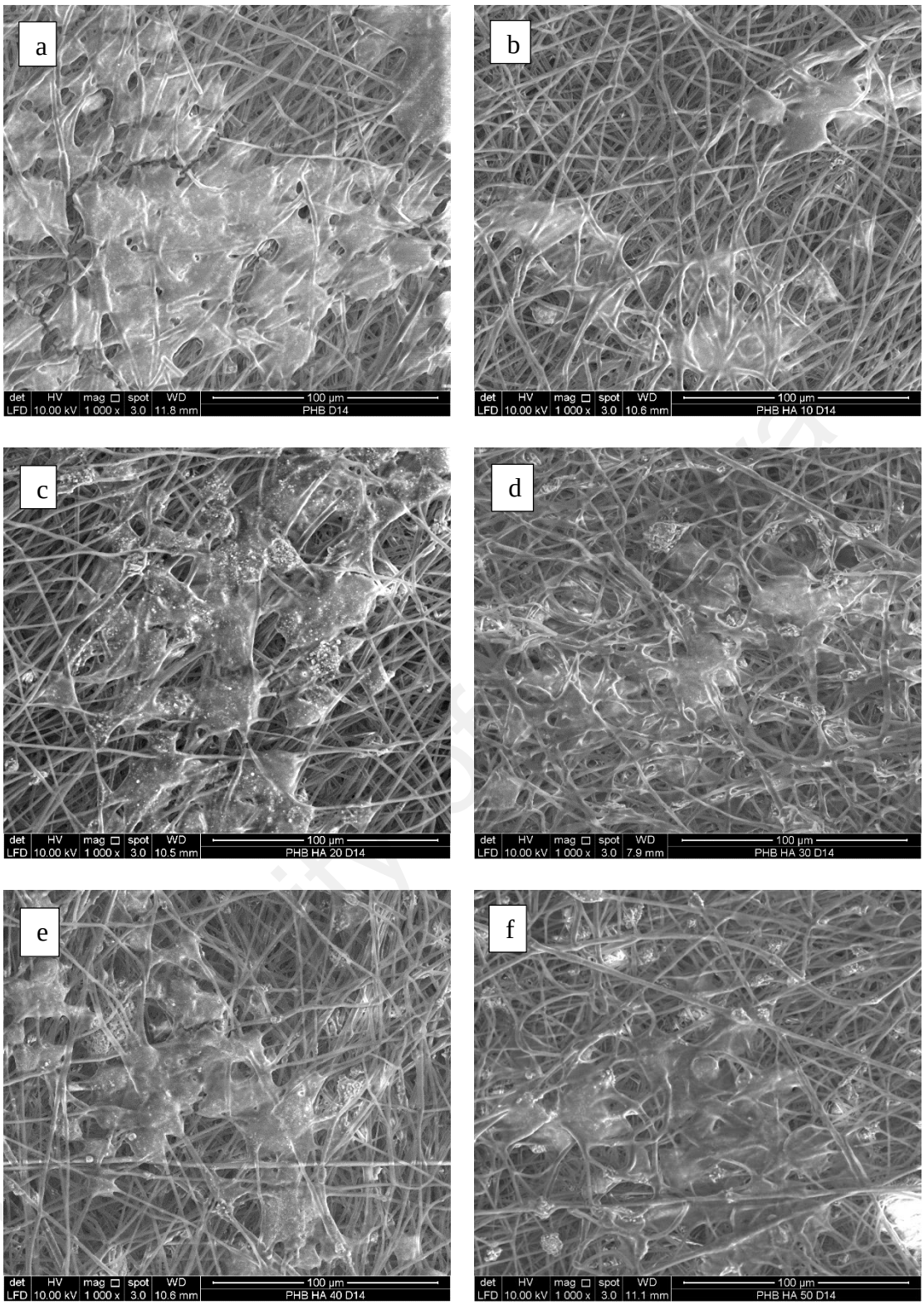

Figure 4.25 BMSC Seeded PHB-BHA scaffolds after 14 days a) PHB; b) PHB-BHA10%; c) PHB-BHA20%; d) PHB-BHA30%; e)PHB-BHA40%; f) PHB-BHA50%

Figure 4.24 and Figure 4.25 show the BMSC seeded scaffolds after 7 and 14 days, respectively. The images show that all the scaffolds were capable of interactions with the

cells in terms of attachment and proliferation. The scaffolds supported cell growth over a period of two weeks and the traces could be observed in FESEM images. Some of the samples show calcification which is a common phenomenon while BHA is incorporated inside.

4.4.3 Confocal laser microscopy

Figure 4.26 shows the 3D morphology of the samples obtained by confocal laser microscopy. As the images suggest addition of BHA reduced the surface roughness of the samples while PHB showing the roughest surface. That is mainly due to the filling effect of BHA particles within the fiber pores. Figure 4.27 shows the average surface roughness of each sample. Among the samples containing BHA, PHB-BHA50% has the highest surface roughness with an average reading of 7.494 µm. The samples PHB-BHA10% and PHB-BHA20% are almost at the same range while the roughness of PHB-BHA40% is slightly lower than PHB-BHA30%. Overall the samples show an ascending trend with addition of BHA with an exception for PHB-BHA40%. The reason for that could be the distribution pattern of BHA which caused that slight deviation in PHB-BHA40% sample. However, the deviation is minute and less than 1 µm.

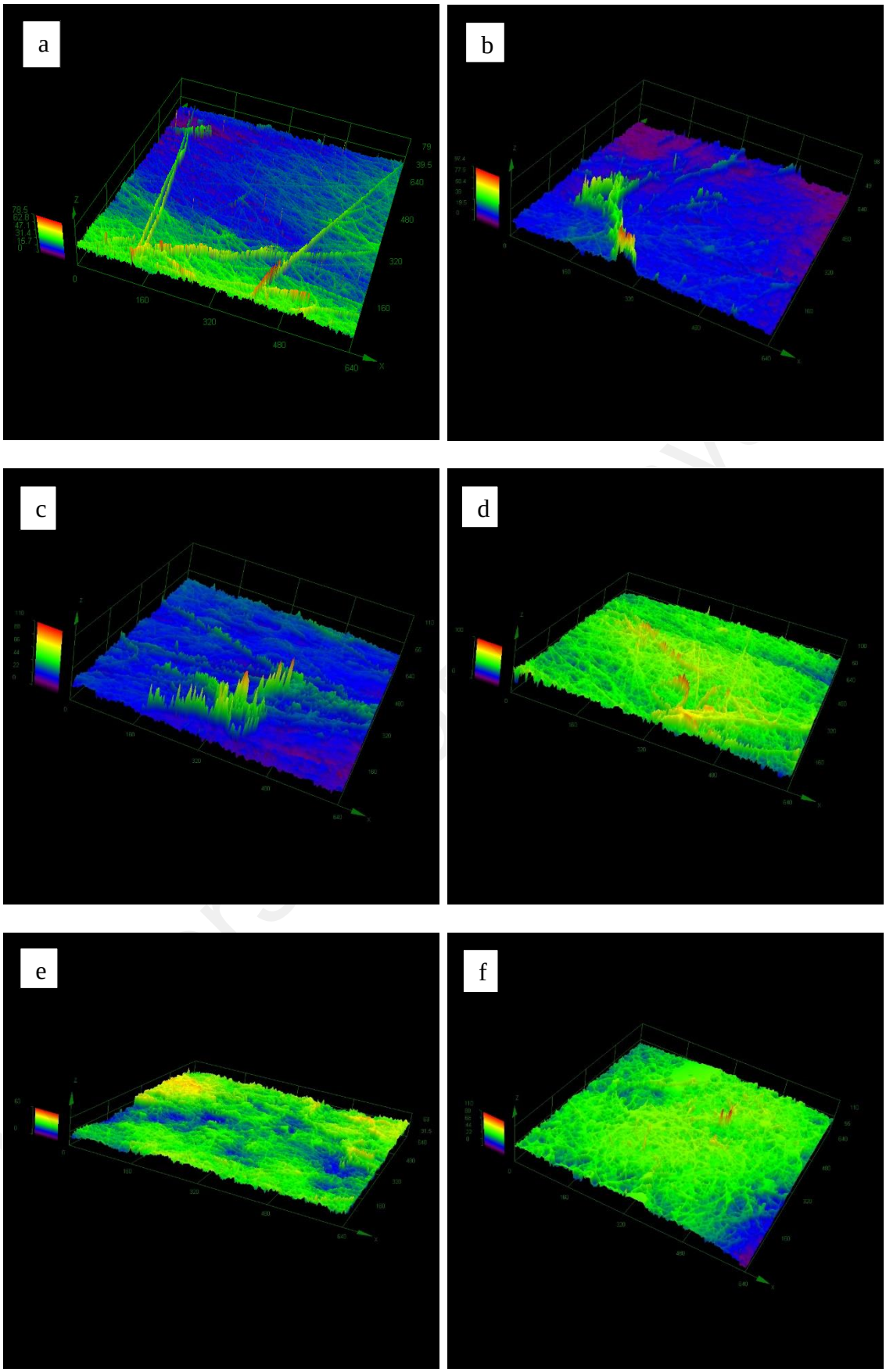

Figure 4.26 3D morphology of the scaffolds obtained by laser microscopy a) PHB; b) PHB-BHA10%; c) PHB-BHA20%; d) PHB-BHA30%; e)PHB-BHA40%; f) PHB-BHA50%

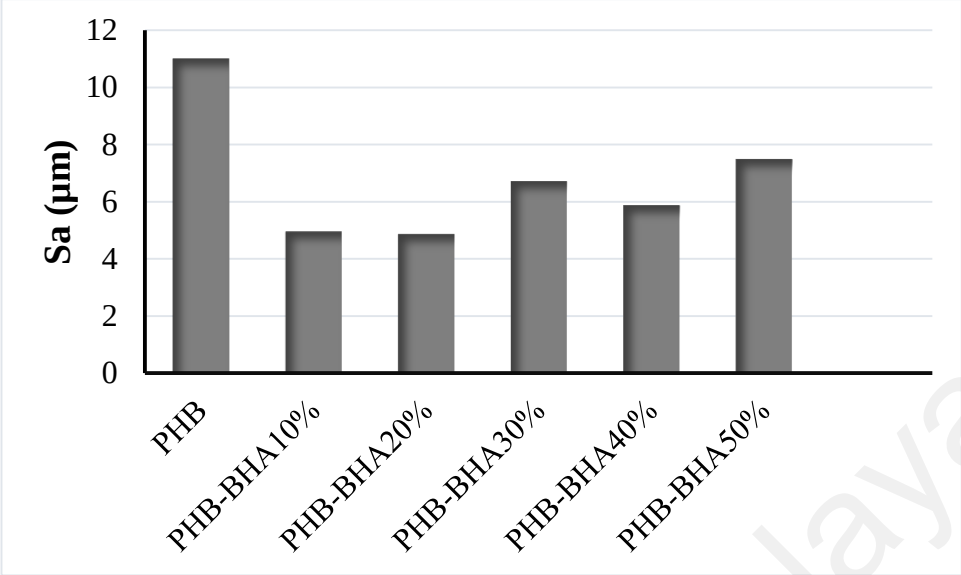

Figure 4.27 Average surface roughness of the blank PHB-BHA scaffolds

4.4.4 FTIR spectroscopy of blank scaffolds

Figure 4.28 shows the FTIR absorbance spectra of blank PHB-BHA scaffolds. The image shows a gradual increase in the intensity of the phosphate peaks along with the increase in concentrations of BHA. This observation can suggest that distribution of BHA inside the scaffolds has been in line with the predesigned amounts as the samples were chosen randomly.

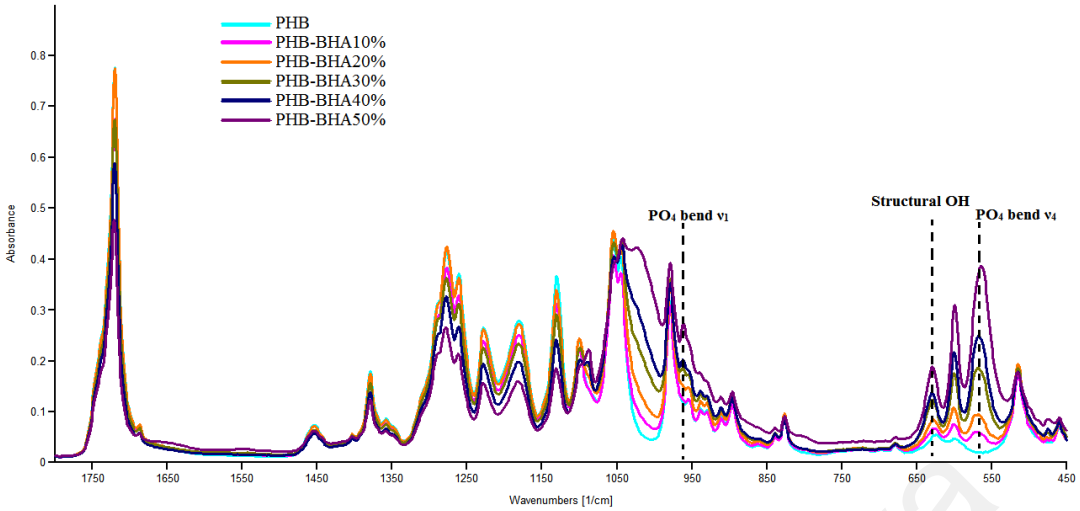

Figure 4.28 FTIR absorbance spectra of blank PHB-BHA scaffolds

4.4.5 Thermogravimetric analysis of PHB-BHA scaffolds

Figure 4.29 shows the TGA analysis of PHB-BHA scaffolds with different compositional ratios of BHA. The remaining weight percentage at 900˚C shows the weight percentage of BHA present in the composite sample which was randomly selected. The remaining amount of BHA at 900˚C shows a gradual increase in line with predesigned amount. The highest deviation from the predesigned amount was observed in sample PCL-BHA30% which was about 9%. The other samples show more accuracy toward the predesigned amount of BHA with a deviation about 5%. Overall, the result suggests that it is possible to obtain samples with homogenous distribution with accuracy of ±4.5%. This result is in line with the results of our previous study on PCL-BHA which was reported in previous chapter.

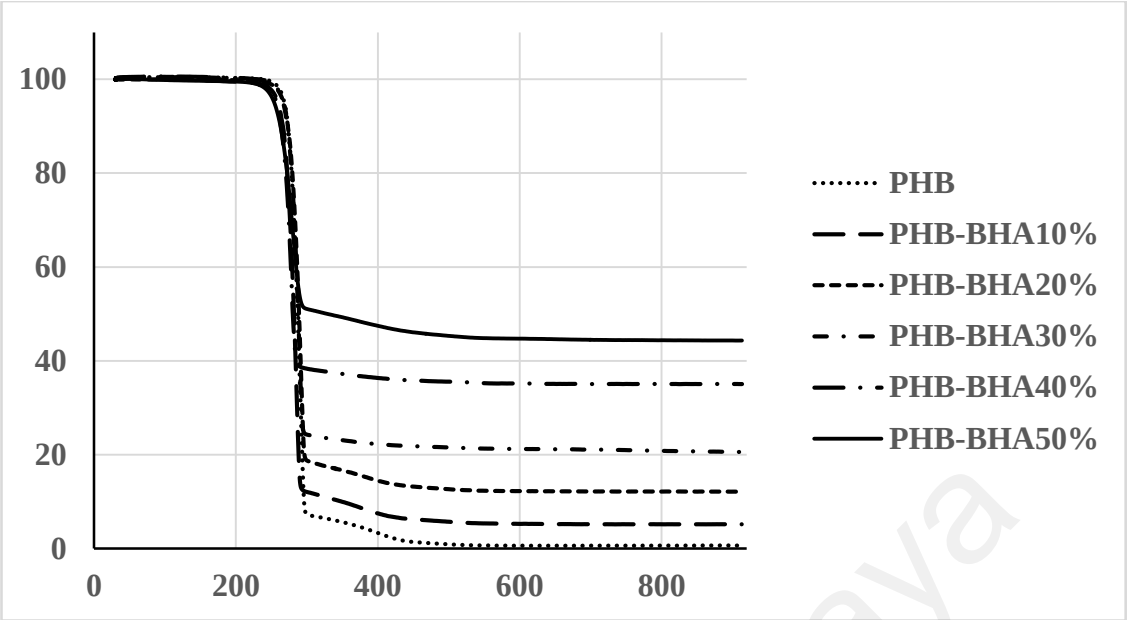

Figure 4.29 TGA analysis of PHB-BHA scaffolds

4.4.6 Biological evaluation of PHB-BHA scaffolds

4.4.6.1 Alamar Blue assay

Alamar Blue provides quantitative information about the number of cells on the scaffold as well as rate of proliferation. Alamar Blue assay also known as Resazurin assay was performed as explained in 3.6.4.1. In Alamar Blue assay, the reduction of resazurin dye is measured; the higher amount of reduction corresponds to more metabolic activity of the cells which is translated to the number of cells. Cell metabolism can be translated to the number of cells. Figure 4.30 shows BMSCs metabolic activity over a period of 14 days. All the samples show biocompatibility, and they promote cell growth.

A one way ANOVA analysis showed that day 1 the reading for reduction of Resazurin dye is almost similar between the groups and there was no significant difference. It suggests that the seeding density was almost the same for all the sample groups.

On day 7 and day 14 also there was no significant difference between the groups. On day 7 the best result was obtained by sample PHB-BHA40% which showed the highest

metabolic activity. However this sample along with PHB-BHA20% and PHB-BHA50% showed a decrease on day 14. It is possible that in the time between day 7 and 14, the culturing medium has reached confluence which resulted in the reduction in cell population on these samples.

On day 14 the highest metabolic activity belonged to PHB-BHA10%, which showed a constant increase from day 1 to day 14. It is necessary to mention that the seeding density on day 1 for PHB-BHA10% was lower than the samples which showed reduction in metabolic activity on day 14. We presume that the lower seeding density has delayed the confluence limit of the sample. Therefore, over a period of two weeks it showed constant increase.

The comparison between the same groups on different day showed that only PHB-BHA20% showed significant difference in metabolic activity on day 1, 7 and 14. The sample PHB showed significant difference in metabolic activity between day 1 and 14 as well as day 7 and 14. PHB-BHA10% showed significant difference between day 1 and 14, while on PHB-BHA40% the difference was significant between day 1 and 7.

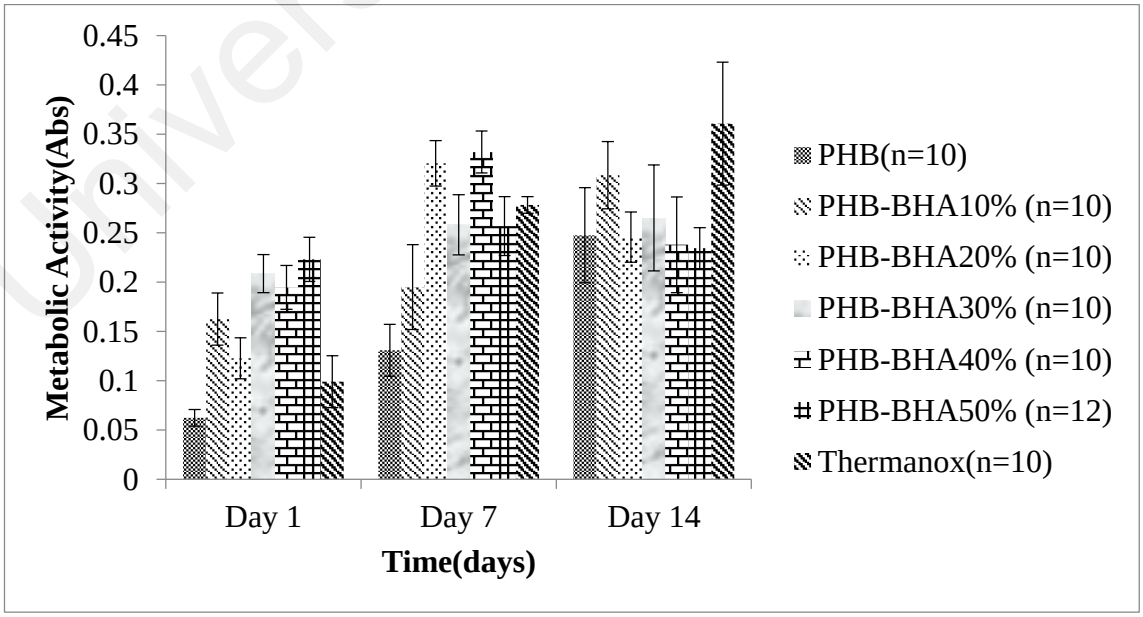

Figure 4.30 Alamar Blue activity of the BMSCs seeded on PHB-BHA scaffolds over a period of two weeks

4.4.6.2 Alkaline phosphate assay

Figure 4.31shows the alkaline phosphate activity of the cells on days 7 and 14. Alkaline phosphate activity of the BMSCs is translated to osteogenic differentiation of the cells. As could be seen in Figure 4.31, all the samples show osteoinductive and osteocunductive properties. The amount of ALP did not show a significant change over a period of 14 days, which suggests the concentrations of BHA did not cause a significant increase in osteogenic differentiation. However, it indicated traces of osteogenic activity within the samples. On day 14 the samples containing the highest amount of HA (PHB-BHA40% and PHB-BHA50%) showed the highest alkaline phosphate activity.

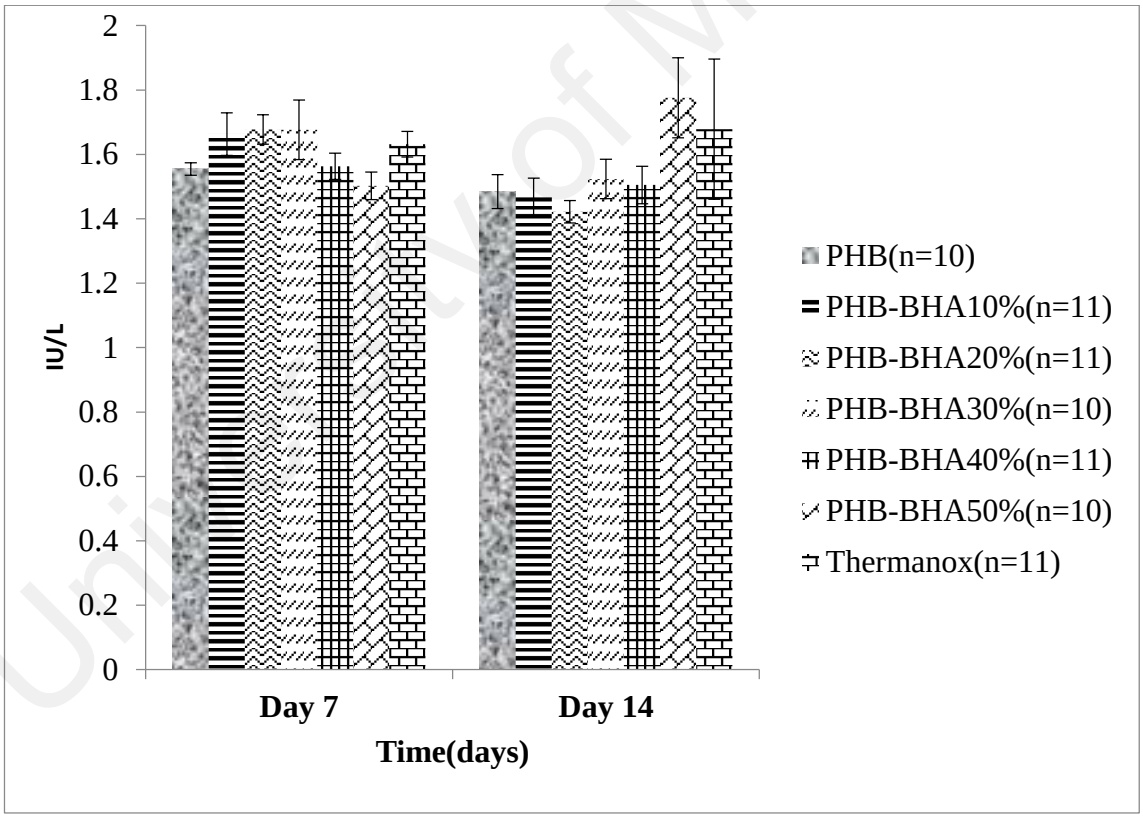

Figure 4.31 Alkaline phosphate activity of the cells seeded PHB-BHA scaffolds

4.5 Project 5: A study on the potential of Electrospun biopolyesters as drug screening platforms for corneal keratocytes

4.5.1 Introduction

In order to assess the toxicity of any novel treatment, animal experimentation is needed. Besides being costly, animal experimentation requires a large number of animals to be sacrificed (Piersma, 2004). As an alternative to animal tests, *in vitro* drug screening could be considered, a method which has the benefits of ease of application, simplicity of testing, and straightforward data interpretation as well as not involving animals. It provides rapid and cost effective screening with good sensitivity (Kirkpatrick et al., 1990) Although accurate extrapolation of the *in vitro* results to *in vivo* conditions remains challenging, it can still be very useful at the preliminary stages of studies as well as saving a lot of animals.

An important part of any *in vitro* drug screening platform is a biomaterial that is capable of promoting cell growth and proliferation. In this study, the potential of electrospun scaffolds made of Polyhydroxybutyrate (PHB), Poly (3-hydroxybutyric acid-co-3-hydroxyvaleric acid) (PHBV) and Polycaprolactone (PCL) was studied to serve as drug screening platrform for corneal keratocyte tissues. All these biopolymers are members of polyester family and have been used previously as cell carriers for biomedical applications, suggesting a possible application here as well (Guan et al., 2008; Heidarkhan Tehrani et al., 2010; Ito et al., 2005; Sombatmankhong et al., 2007). The selection was based on commercial availability as well as low cost of synthesis. These polymers can degrade easily under *in vivo* conditions through hydrolysis of ester bonds, and produce non-toxic degradation products (Abadi et al., 2014; Gunatillake & Adhikari, 2003a). In this comparative study we have subjected these three different biopolyesters to the same electrospinning parameters and obtained different morphologies and the potential of these materials in terms of corneal keratocyte proliferation and differentiation was studied. The

scaffolds were seeded with rabbit corneal keratocytes and evaluated by cell proliferation and gene expression assays.

The choice of corneal keratocytes was based on the fact that there are so many cases of corneal function disorders due to infection, trauma, viral and atopic disease as well as genetic deficiencies (Wilson, 1998; Wilson et al., 2003) which lead to corneal blindness of more than 45 million individuals all around the world annually (Whitcher et al., 2001). Although mild injuries can be cured by the natural immune system response or via clinically available techniques, severe cases still await the development of novel drugs (Zainal Abidin et al., 2011). keratocytes make up about 90% of the volume of corneal stroma, being bonded to an extracellular matrix of highly regular collageneous lamella. Notably, keratocytes usually stay in the quiescent state and maintain non crystalline structures to make the corneal transparent and have optimal refraction. However, they are able to undergo transition into repair phenotypes, namely activated fibroblasts or myofibroblasts in respond to specific environmental signals, example injury and wound healing (West-Mays et al., 2006). It is important for keratocyte to differentiate because it helps in retaining corneal transparency and determining the corneal response to injury (Jester et al., 2003). This clearly established that keratocytes are sensitive to the changes in environmental condition, therefore, understanding the behaviors of keratocytes in different testing conditions will greatly increase our knowledge in corneal wound healing and regeneration.

4.5.2 FESEM

Figure 4.32 shows a microscopic view of blank electrospun scaffolds. As the image suggests, PCL leads to the formation of fibers with a smaller diameter than those of PHB and PHBV under the same conditions. PCL, due to its lower molecular weight, resulted in less viscose solution with less chain entanglement (Figure 4.32 a). Therefore, during electrospinning it could be stretched to a much lower diameter. However, a lower

viscosity could result in less stable jet, with formation of more random fibers, and formation of beads within the electrospun fibers (Shenoy et al., 2005). In agreement with this, fiber diameter distribution patterns of the fibers confirm PCL exhibits the lowest diameter, at 300nm, followed by PHB at 1.12 µm and PHBV at 1.35 µm. PHB, comparatively, is more rigid and stiff because of its high crystallinity, formed more straight fibers (Wang et al., 2007) (Figure 4.32 b). As a result of the incorporation of hydroxyvalerate into PHBV, the polymer is also more elastic. PHBV fibers show good uniformity as well as porosity, and have a looped shape rather than just being straight.

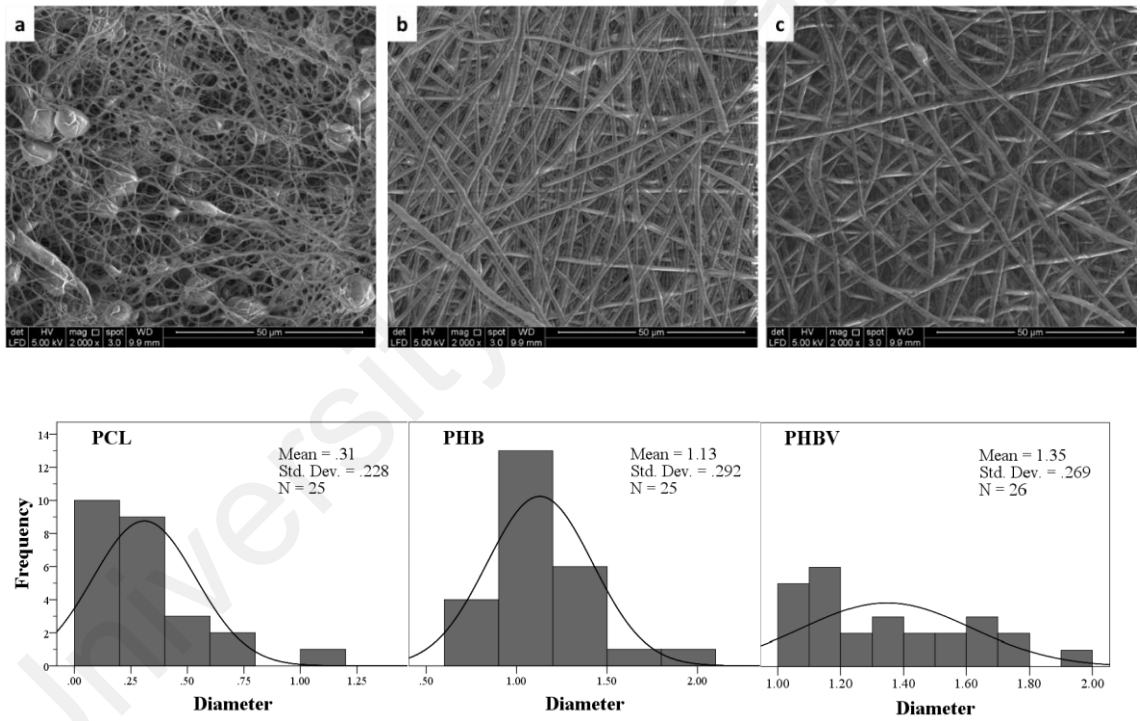

Figure 4.32 FESEM microscopy of the blank scaffolds a) PC; b) PHB; c) PHBV and their fiber diameter distribution pattern; the scale bars indicate 50 µm

Figure 4.33 shows cell morphology and cell to scaffold interaction at 4 different days 1, 3, 5, 7. The SEM images of cells show cells growing on the electrospun scaffolds. These cells can spread and penetrate into the fibers. The filopedia extend along the fibers on all the scaffolds, as guided by the orientation of the fibers. In PHB scaffolds, the micrographs

showed the cells were larger, flatter and stretched. This latter observation may indicate higher expression of α-SMA2 on PHB. During corneal wound healing, keratocytes are activated and transformed into fibroblasts and eventually become alpha-smooth muscle actin (α-SMA)- expressed myofibroblasts and contribute to the wound contraction (Jester et al., 1995). The micrographs demonstrated that the diameter and alignment of fibers in scaffolds could guide cytoskeleton extension of cells and led to different levels of gene expression, as shown in q-PCR results. These findings also showed that PCL fiber of a smaller diameter has produced a hierarchically ordered scaffold closely imitating that of native collagen fibers. The micrographs clearly showed that the changes in cell morphology depended on the type of scaffold on which it was seeded. The cells on the PCL fiber tend to be bulkier and more on the surface mainly due to the smaller pore size. The cells on PHBV show a planar morphology. Cell penetration inside the scaffold also could be observed on PHBV.

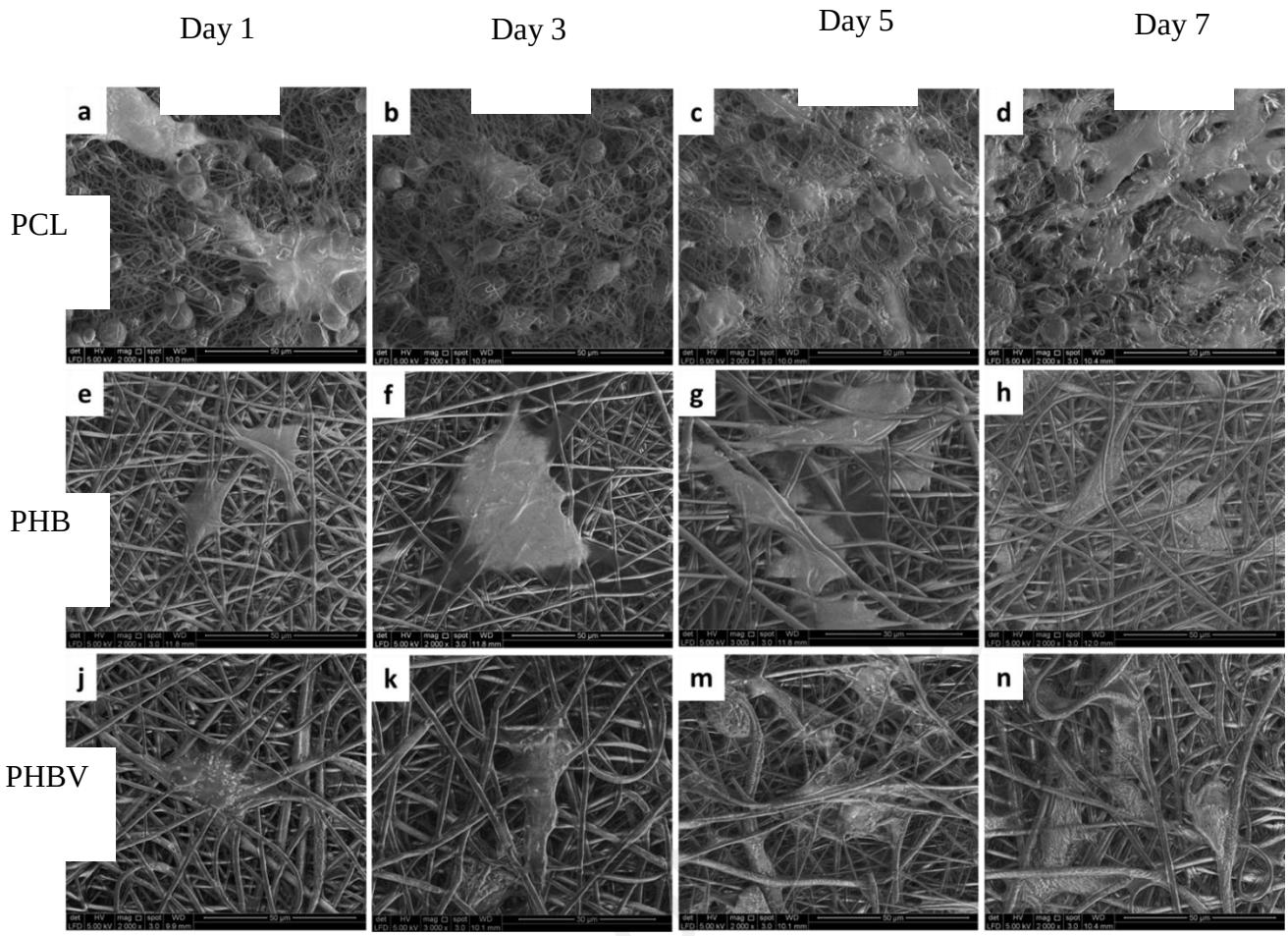

Figure 4.33 FESEM images showing the morphology of keratocytes cultured on PCL (a-d) day 1-7, PHB (e-h) day 1-7 and PHBV (j-n) day 1-7 with magnifications of 2000; the scale bars indicate 50µm

4.5.3 Cell viability and cytotoxicity

Figure 4.34 shows the average MTT activity of the scaffolds (n=5) at 10 different concentrations of leachate solution. As can be seen, none of the scaffolds show signs of inhibition of cell proliferation, and the MTT activity for all scaffolds at different concentrations of leachate solution remains positive. The concerns over solvent residue in the electrospun fibers can be safely dismissed.

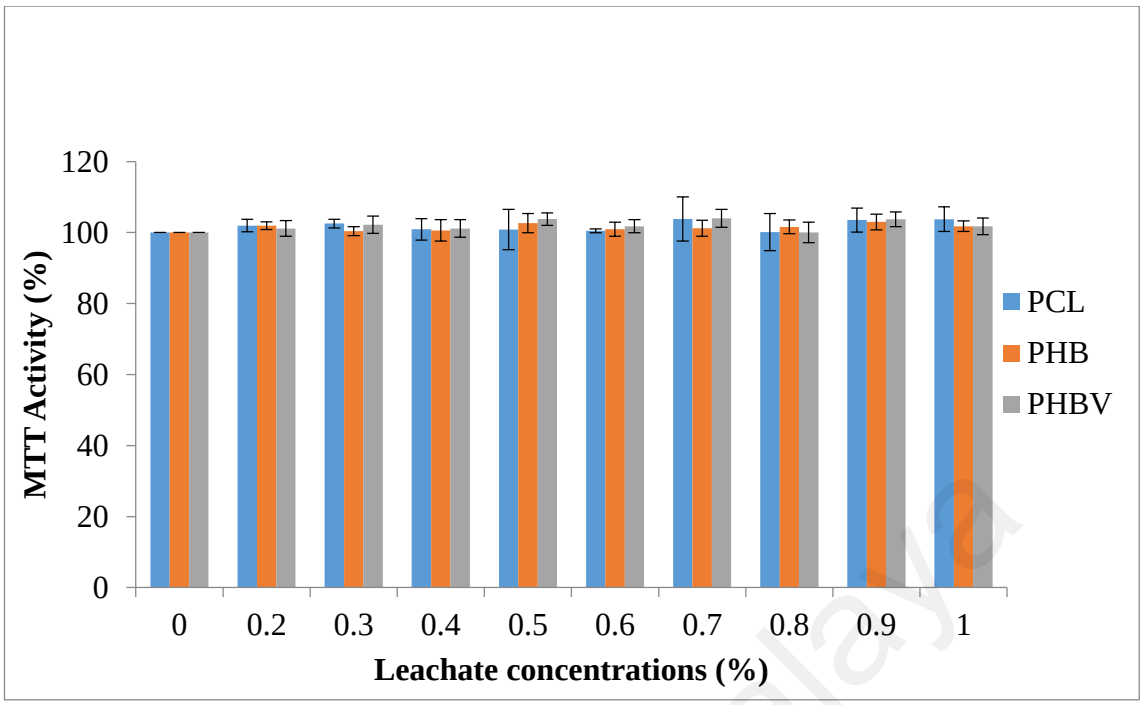

Figure 4.34 Keratocytes' proliferation in several dilutions of scaffold leechate

4.5.4 Alamar Blue assay

Keratocyte interactions between different scaffolds were assessed *in vitro* by seeding cells in PCL, PHB and PHBV at various time points. Figure 4.35 shows average keratocyte proliferation measurements on different days and scaffolds (n=6), based on the Alamar Blue proliferation assay. This cell population shows an ascending trend on PCL, PHB and PHBV, and all the scaffolds support keratocyte proliferation. As could be seen in Figure 4.35, the number of keratocytes increased on all scaffolds as a function of time, however there is no significant difference for days 5 and 7 for PHB and PHBV ($P>0.05$). No significance difference in cell numbers was observed among the different scaffolds, except on day 5, PHB and PHBV exhibit higher cell numbers compare to PCL and it is statistically significant based on paired sample T test.

Figure 4.36 shows the average Alamar Blue readings of each individual scaffold on different days. The significance differences ($P<0.05$) are indicated by # in the Figure 4.36.

The increase in the number of cells on PCL was significant for all days. However, for PHB and PHBV this increase was significant until day 5 and there was no significant difference between day 5 and day 7. The results suggest that the cells may have reached confluency after day 5 on PHB and PHBV. The keratocytes have reached confluence by day 7 in all scaffolds, although the comparison between groups showed some differences on day 5 (Figure 4.35). Overall, the results suggested that the cell proliferation rates on PCL, PHB and PHBV were almost the same and there was no significant difference between them on day 7.

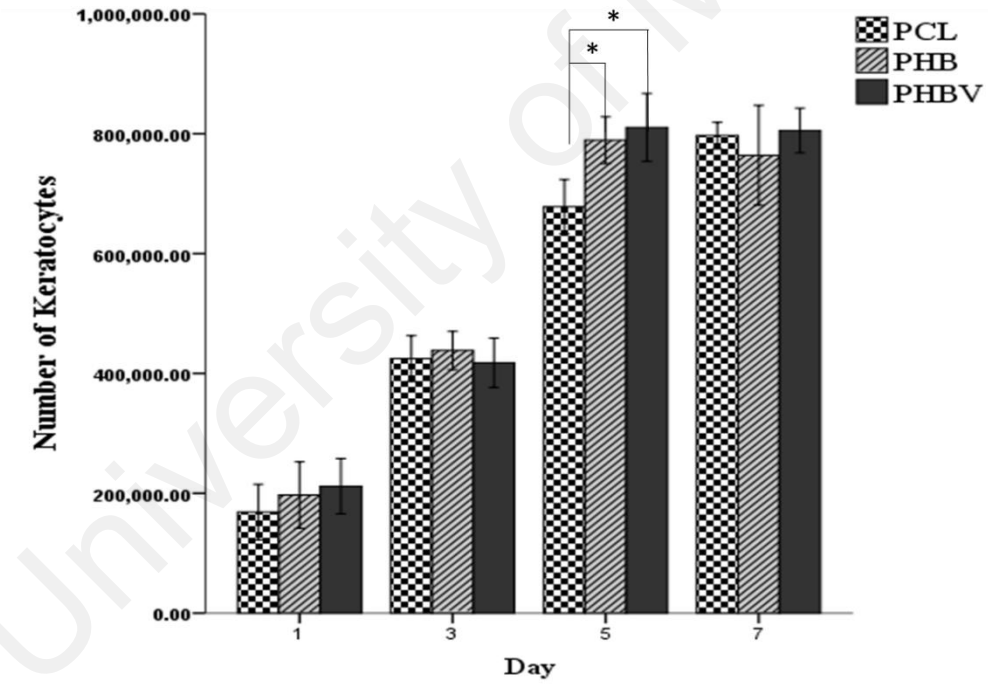

Figure 4.35 Alamar Blue proliferation assay results for keratocytes seeded on PCL, PHB and PHBV at different days; ($P<0.05$). *: Indicates significance difference

a)

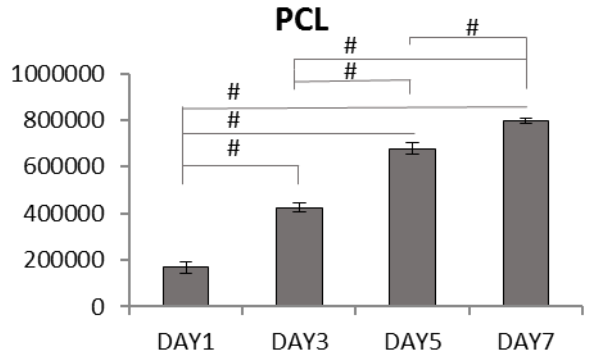

b)

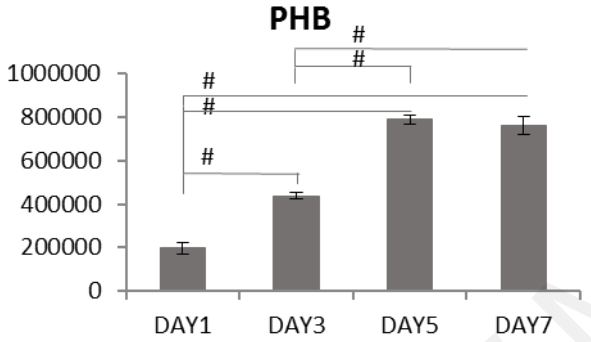

c)

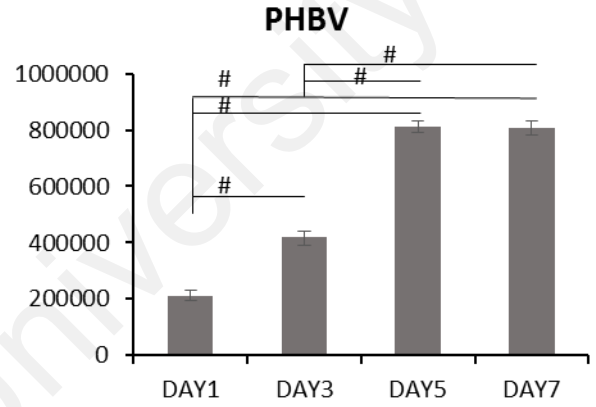

Figure 4.36 AlamarBlue proliferation assay plotted separately for each individual scaffold (a)PCL, b)PHB and c)PHBV) on different days.

4.5.5 Real-time- PCR

Figure 4.37 shows gene expression for five targeted genes; lumican (LUM), aldehyde dehyrogenase ALDH), vimentin(VIM), collagen type 1 (COL.1) and α-SMA2. PCL shows good potential for maintaining cell phenotype with high expression of LUM, ALDH, VIM, COL.1 and α-SMA2. All these genes were significantly higher in expression on PCL, compared to PHBV. Among the three scaffolds, PCL expressed the highest LUM. LUM, a small leucine-rich repeat proteoglycan (SLRP) is a major keratan sulfate proteoglycan in maintaining corneal transparency (Nikitovic et al., 2008). LUM also regulates collagen fibrillogenesis and modulates corneal epithelial cell migration (Saika et al., 2000). Meanwhile, ALDH is abundantly expressed by corneal stromal keratocytes in PCL as well. ALDH is responsible for the production of corneal crystallins, which contributes to cellular transparency (Chen et al., 2013). The high level of expression of α-SMA2 in PHB suggests that this scaffold is good for wound healing. However, over expression of α-SMA2 may result in corneal scar formation and affects optical transparency (Tomasek et al., 2002). It is postulated that the higher expression of α-SMA2 is the result of cell stretching over the PHB sample. Expression of vimentin (VIM), a mesenchymal cell marker characterised as fibroblast is important to show the transition of keratocytes to activated fibroblasts, providing structural properties of cell and enhancing the cell migration in the corneal wound healing (Ritchey et al., 2011). COL 1 is the main extracellular matrix in corneal stroma, while the well-organised collagen 1 fibrils are necessary to regulate corneal transparency (Michelacci, 2003). Overall, PCL was shown to be the best option as a scaffold from those tested, as it is able to maintain corneal stromal cell functionality better than PHB or PHBV.

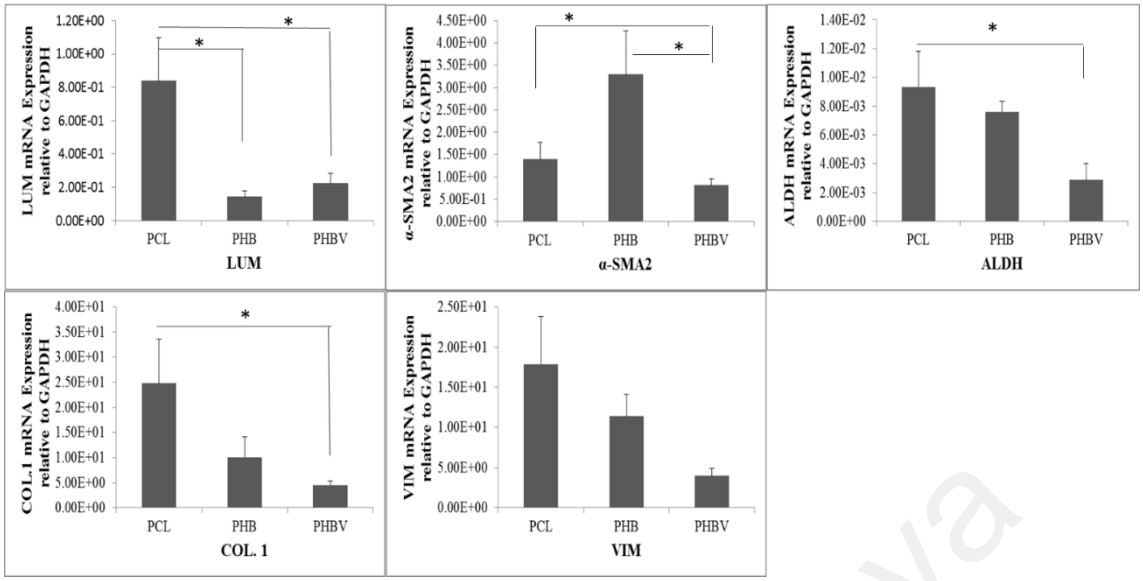

Figure 4.37 Quantitative gene expression of cultured corneal keratocytes for Lumican (LUM), α-SMA2, ALDH, Collagen type 1 (COL.1) and Vimentin (VIM) relative to the expression values of GAPDH as the internal control *: Indicates significant difference PCL, PHB and PHBV ($p<0.05$).

4.6 Project 6: Fabrication of a functionally graded composite scaffold based on combination of salt leaching and electrospinning in a single construct for guided bone tissue regeneration

4.6.1 Introduction

Fabrication of synthetic scaffolds which can be functionally graded in composition distribution to serve as support for cellular function and proliferation while mimicking the native tissue in terms of structure, composition and functionality, is a significant part of tissue engineering (Erisken et al., 2008; Moradi et al., 2013). Polymeric constructs capable of directing the growth of new tissue during bone reconstruction process have found application in orthopedic and dental applications with promising results (Caffesse et al., 1994; Murphy et al., 2003). Citric acid (CA) based elastomers are biodegradable hydrophilic elastomers that can be applied in tissue engineering with minimum risk of host tissue immunological response from host tissues (Djordjevic et al., 2009; Qiu et al., 2006; J. Yang et al., 2006). Hydroxyapatie (HA) micro particles as a key ingredient of bone, can be incorporated into elastomers to fabricate composite materials suitable for bone healing with controlled compositional ratio as well as mechanical properties (Yang et al., 2004; J. Yang et al., 2006). HA as a mineral which promotes stem cell differentiation and osteoblast proliferation can be incorporated inside the scaffolds for guided tissue regeneration (Jang et al., 2009). In this research we have tried to fabricate a scaffolding material which is functionally graded in terms of HA content, by using a citric acid based polycaprolactone triol (PCLT) elastomer. The eleastomeric PCLT-CA-HA compositions were put together in the form of layered cake. Sheets of electrospun PHB was placed in between the layers as a distinction and inhibition of possible HA sinking during esterification reaction. Electrospun PHB sheets also provide the support for holding different layers together in a single construct. Figure 4.38 shows schematic illustration of the scaffold construct that we have fabricated; a three layered scaffold and

its constituent layers structure; while Microscopic and macroscopic views of the scaffold constituents could be seen in Figure 4.38 a-c. This scaffold contains different compositional ratios HA in a single construct which can create a gradient for guided tissue regeneration. Furthermore, all these layers are incorporated in a single construct.

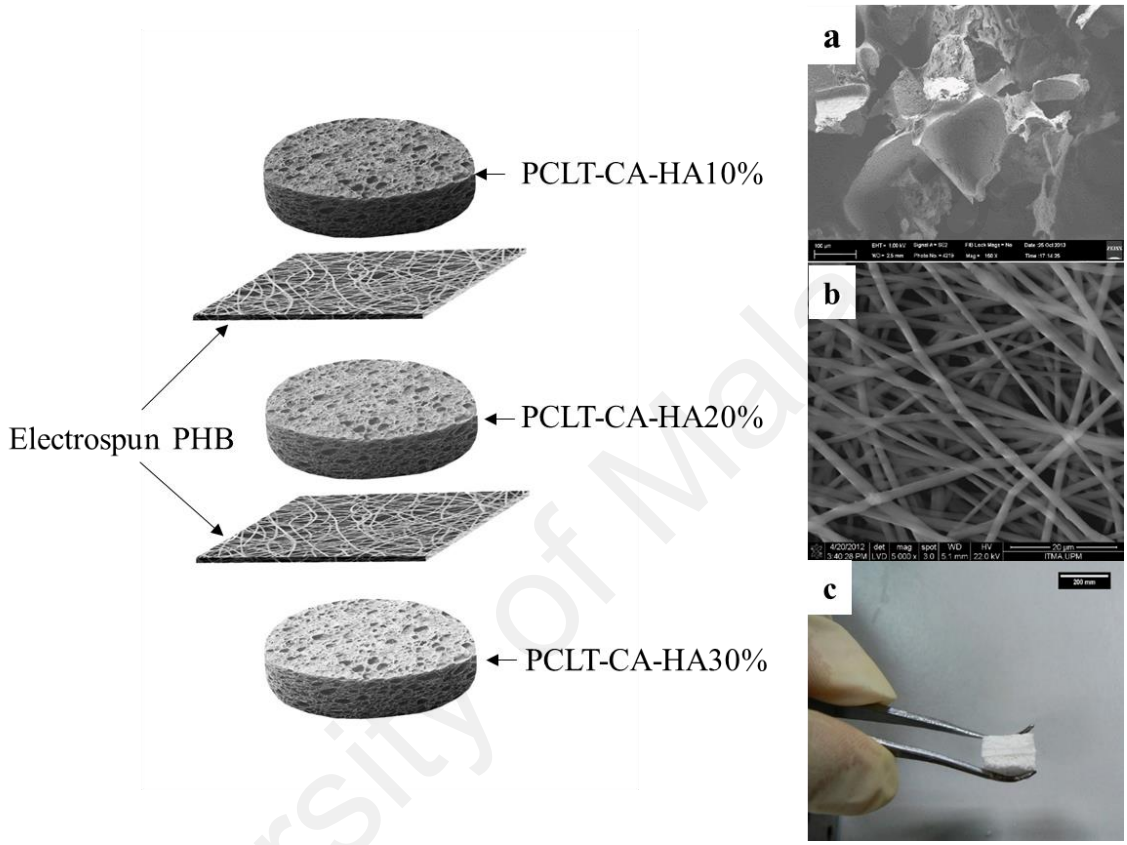

Figure 4.38 Schematic illustration of an individual scaffold constituents a) PCLT-HA morphology b) Electrospun PHB c) Macroscopic view of the three layered scaffold

4.6.2 Morphology of scaffolds by FESEM

Figure 4.39 shows FESEM micrographs of the structure of the three layered scaffold. Figure 4.39 a shows the microscopic overview of the three layer construct. The sample is showing a porous morphology with interconnected pores. It shows homogenous pore distribution all around (average Dimension 100-200 µm) which is favorable for tissue engineering applications (Figure 4.39 b-d) (Moroni et al., 2006). The observed cubic shape of the pores as well as the size of them are in line with the porogen (NaCl) used in

the scaffold fabrication process (Figure 4.39). There is no trace of porogen and it has successfully been removed. Figure 4.40 shows the interface of the electrospun PHB sheet with PCLTHA scaffolds.

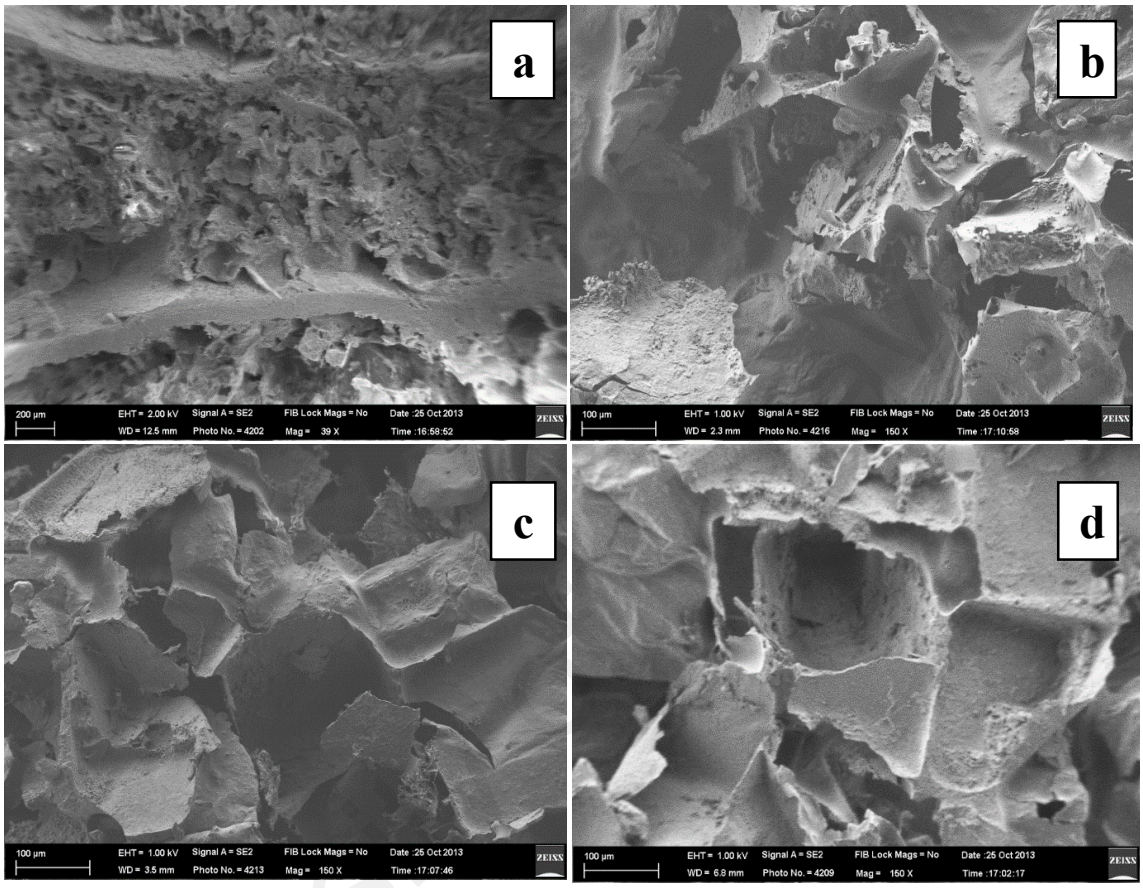

Figure 4.39 Scanning electron microscopy of the three layered scaffold and a)morphology of the three layer b) PCLT-CA-HA10% c)PCLT-CA-HA20% d)PCLT-CA-HA30%

As the image suggests, PCLT-CA-HA has been able to cover PHB sheet (Figure 4.40) creating the bonding required to hold the scaffold together (Figure 4.40 a, b). However, PCLT-CA-HA covering remains on the surface and doesn't penetrate deep inside the electrospun fiber (Figure 4.40d). Therefore, Electrospun fibers maintained their porous structure which is an important feature for scaffolding materials. The interfacial connection between PCLT-CA-HA and PHB fibers has the role of holding the three layers together. Although because of the porous nature of the PCLT the connection is randomly

happening at various spots, yet it was strong enough to hold the scaffold together throughout salt leaching and freeze drying process.

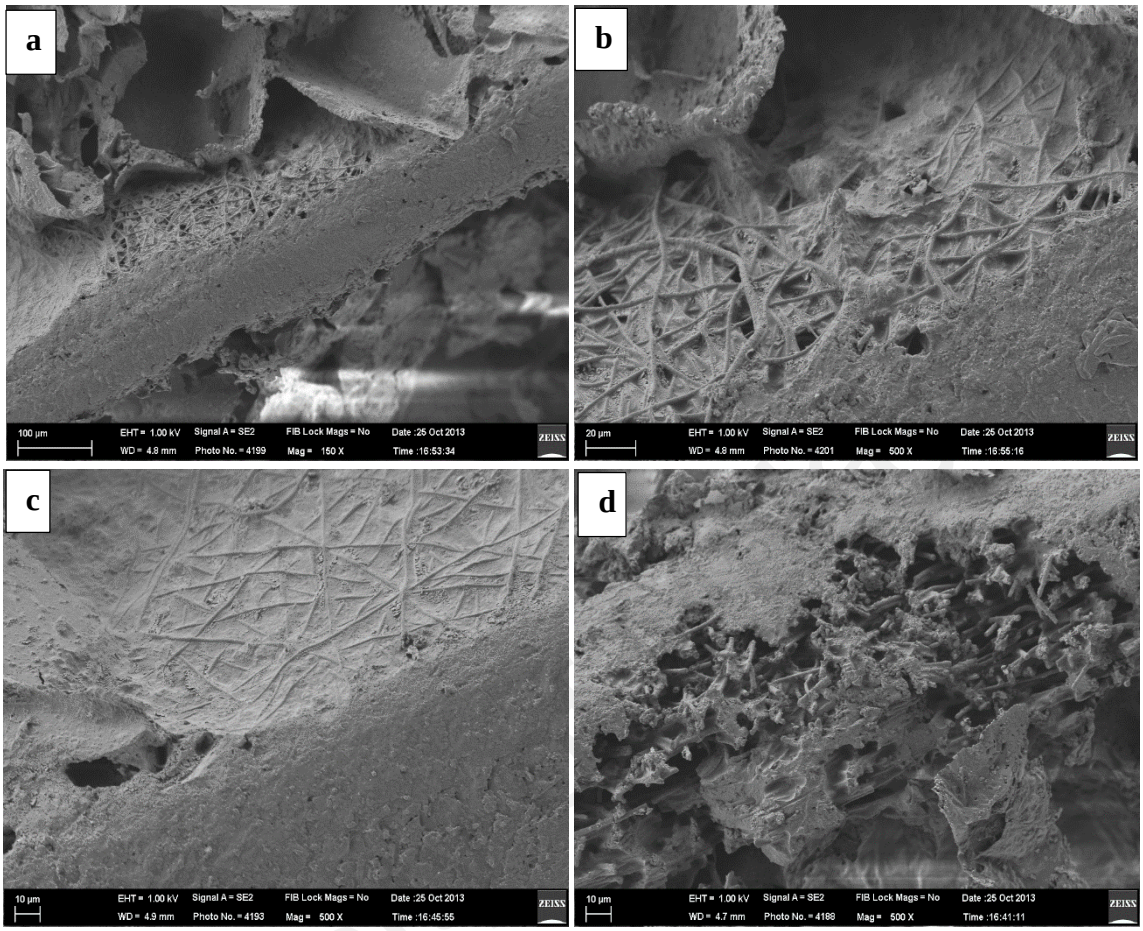

Figure 4.40 Scanning electron microscopy image of the electrospun PHB sheet interface with PCLT-HA

4.6.3 FTIR Spectroscopy

Figure 4.41 shows the infra-red reflectance spectrum of PCLT-HA scaffolds. The peaks at 1727cm^{-1} and 3457cm^{-1} confirm that polymerization was successful and ester bonds have been formed (J. Yang et al., 2006). The bands at 560cm^{-1}, 601cm^{-1} and 1030 cm^{-1} correspond to the phosphate groups of HA (Chang et al., 2002; Pekounov et al., 2009). As could be seen in Figure 4.41, the increase in intensity of the peaks of hydroxyapatite is in line with the increase in HA concentration in scaffolding material. The peaks at 1602 cm^{-1} could be the carboxyl groups which have formed ionic interaction with calcium ions

released from hydroxyapatite. Figure 4.42 shows the possible ionic interactions between calcium ions and carboxyl groups present on PCLT.

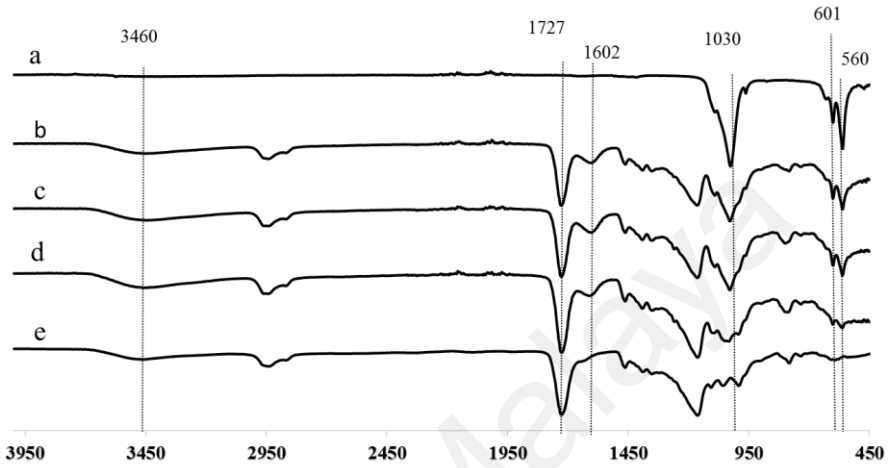

Figure 4.41 FTIR spectra of the HA and PCLT-CA-HA scaffolds a) HA; b) PCLT-CA-HA10%; c)PCLT-CA-HA20%; d)PCLT-CA-HA30%; e)PCLT

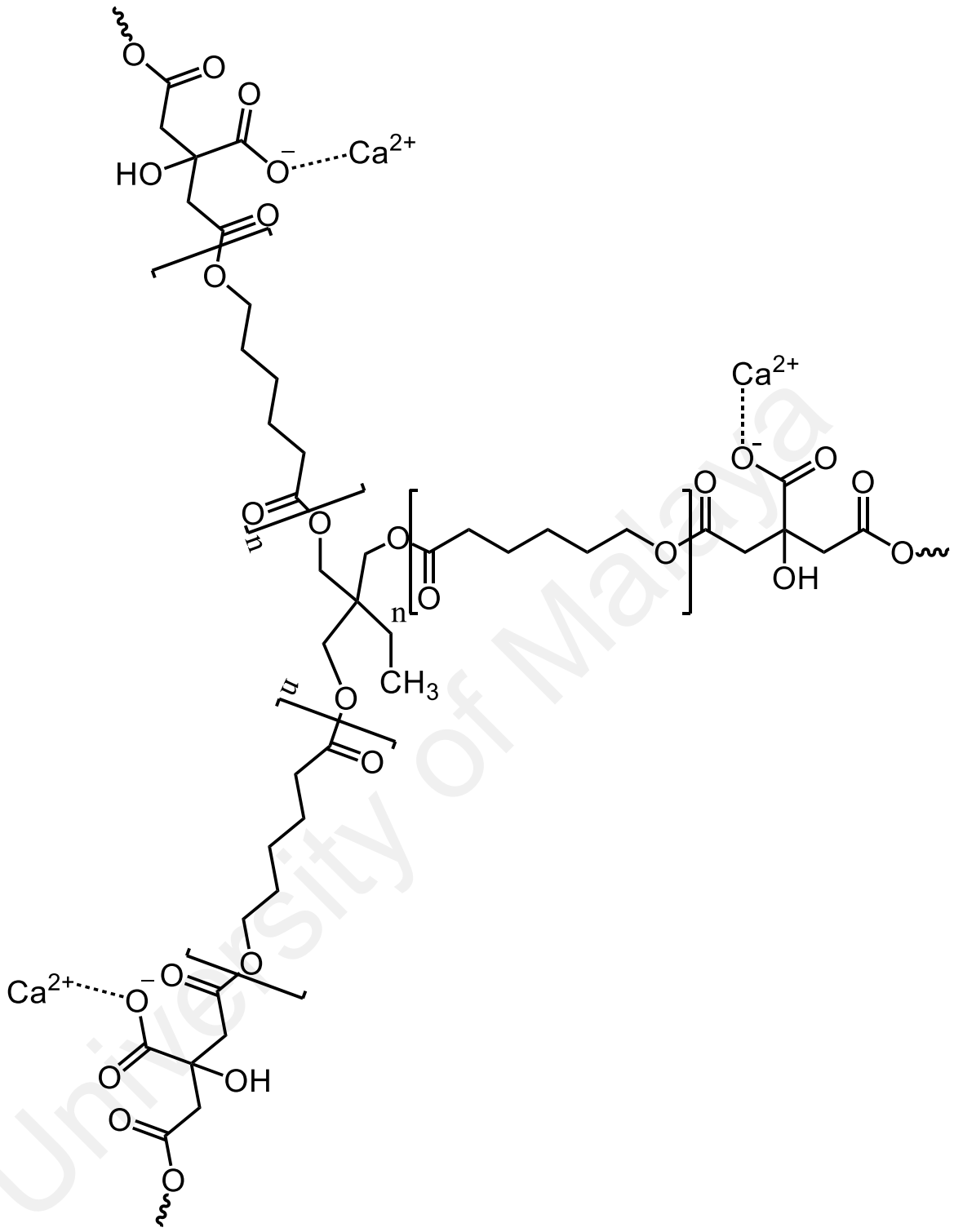

Figure 4.42 Ionic interaction between carboxyl groups and calcium ions

4.6.4 Thermogravimetric analysis

Figure 4.43.a shows the thermogravimetric analysis results of the PCLT-CA-HA reference scaffolds while figure 4.43.b shows the thermogravimetric analysis results for each individual layer separated from the three layer scaffold. The onset of degradation for pure PCLT-CA was at 233ºC. As the concentration of HA increased, the onset of degradation also increased accordingly and the highest amount was measured for PCLT-CA-HA30% at 247 ºC. Addition of HA has contributed to the thermostability of the scaffolds. No trace of the unreacted monomers could be detected in the samples thermograms. Both the TGA and FTIR results confirmed the concentration of HA increases according to the predesigned concentration. The remaining amount at 900 ºC corresponds to the predesigned weight ratio of HA. Figure 4.43 shows a gradual increase of HA weight from 10% to 20% and 30% as it was designed. Since the samples were randomly chosen, it can infer that HA has been distributed uniformly throughout the sample. By comparing the TGA thermograms of reference samples and the three layer scaffold, we can see that the HA distribution within the three layer has been uniform and HA sinking within layers has not happened and each layer kept the predesigned concentration gradient.

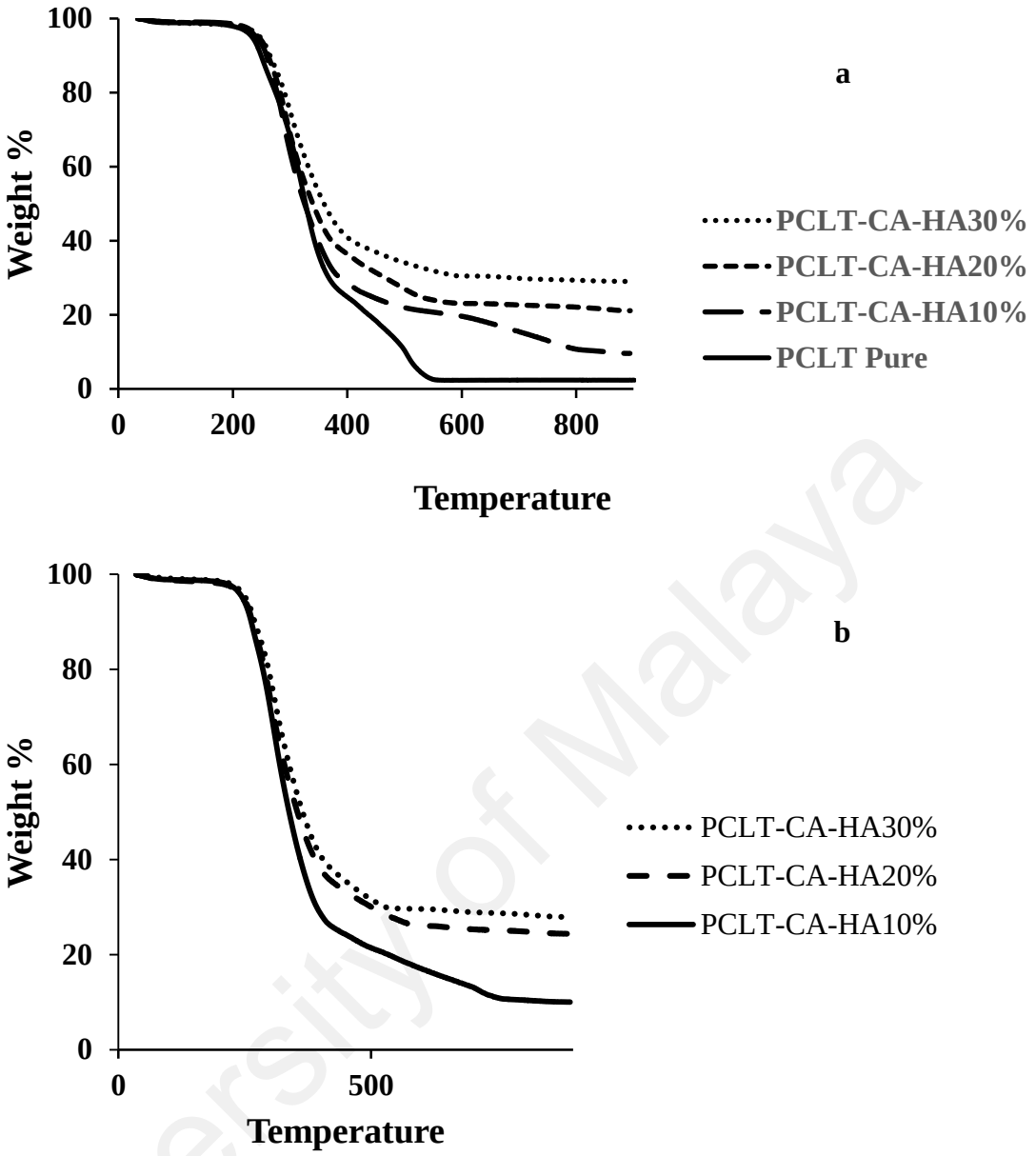

Figure 4.43 TGA Analysis of PCLT-CA-HA scaffolds a) Reference samples; b) Individual layer separated from the three layered sample

4.6.5 Mechanical Testing

Disk-shaped porous scaffolds with thickness of 3mm and diameter of 6 mm were compressed at a rate of 1 mm/min by INSTRON machine model 5544 mechanical taster. The results reported in Table 4-4 are based on the mean value and standard deviation for five different samples in each ratio. Initial slope of compressive stress-extension data and 60% of the original thickness was used to calculate compressive modulus (E_c) and

compressive strength (S_c), respectively. The percentage of recovery was measured based on the thickness regain of the samples in 1 minute from removal of pressure.

There was no significant difference between compressive modulus values of the pure PCLT and PCLT-CA- HA10% samples. However, by increasing the concentration of HA in the PCLT-CA-HA composites, compressive strength and modulus of the samples were increased. It is reported that, variation of the concentration of the HA particles in the samples have significant effect on biocompatibility and mechanical properties of the samples (Chung, Sugimoto, et al., 2011; Qiu et al., 2006). In this study, the highest compressive properties was shown by PCLT-HA30% which has the highest amount of HA among all the samples. The possibility of formation of covalent bonds between free carboxyl groups of PCLT and hydroxyl groups of HA microparticles during the curing process (7 days, 80ºC) should be considered. This can lead to higher crosslinking density and therefore higher compressive modulus and strength while decreasing recovery from deformation. The lowest recovery rate is reported for PCL-CA- HA30% (56.76%) which is in line with the compressive strength of this sample (Chung, Qiu, et al., 2011). The previous studies have also indicated that the increase in amount of HA can result in increasing the compressive properties (Moradi et al., 2013). Results in table 1 show that a considerable amount of elasticity could still be achieved even at the higher compositional ratios of HA. The solvent casting particulate leaching technique contributes to formation of a three dimensional porous architecture with improved biological activity due to presence of HA particles. The application of salt crystals regulate the shape of PCLT-CA-HA by creating uniformly distributed pores all over the three dimensional structure.

Table 4-4 Compression properties of the PCLT-CA-HA scaffolds

Scaffold	Compressive Modulus (kPa)	Compressive Strength (kPa)	Recovery (%)
Pure PCLT	11.87 ± 1	22.47 ± 1.9	98.65 ± 1.1
PCLT-CA-HA 10%	11.09 ± 1.1	59.93 ± 9.7	92.28 ± 2
PCLT-CA-HA 20%	20.07 ± 1.9	140.53 ± 15	91.19 ± 2
PCLT-CA-HA 30%	52.44 ± 5.9	262.56 ± 33	56.76 ± 4

CONCLUSIONS AND SUGGESTIONS FOR FURTHER RESEARCH

5.1 Optimizing the processing parameters

The electrospinning setup was based on semi-rectified DC high voltage, it was important to explore the processing parameters. The application of 10 kV, needle to collector distance of 18 cm, feeding rate of 3ml/h and the needle 20 G (0.9 mm) led to formation of uniform and bead free fibrous morphology of PHB. The obtained morphology could be suitable for tissue engineering applications. Depending on the type of polymer, these settings with some minor changes were used in other projects included in this research.

5.2 Processability improvement of electrospun PHB with mcl-PHA

Blending PHB and mcl-PHA was successfully carried out at 4 different ratios followed by electrospinning. FESEM images have shown that the presence of mcl-PHA can contribute to formation of smaller diameter nanofibers presumably by plasticizing the blend into a more flexible and stretchable material. On the other hand, due to its amorphous structure it cannot maintain the whipping instability, which leads to jet breakage and formation of beaded fibers at higher weight ratios of mcl-PHA (30% & 40%). DSC results showed that addition of mcl-PHA to PHB has led to lower enthalpy of fusion and crystallinity. Overall, based on structural and morphological analysis, blends containing mcl-PHA (10% &20%) could be suggested for their improved processability. Lower crystallinity of the electrospun scaffolds can be beneficial for certain applications such as neural or fibroblast tissue engineering (Chen et al., 2011).

Despite the presence of beads in fiber for blends containing mcl-PHA (30% & 40%), they could benefit from better permeability and porosity mainly due to their smaller fiber diameter. Porosity and permeability are some of the key features of scaffolds which

improve cell attachment and penetration as well as waste release (Liang et al., 2007; Prabhakaran et al., 2009; Soliman et al., 2011).

In vitro cell cultivation using fibroblasts could be suggested for future work on these fabricated scaffolds to evaluate their biological potential.

5.3 Electrospun Composite scaffolds of PCL and BHA

It is possible to produce electrospun composite scaffolds of PCL containing microparticles of BHA in desirable ratios. The scaffolds were tested *in vitro*, and these scaffolds support the growth and proliferation of BMSCs. Alamar Blue assay showed there was cell proliferation over a period of two weeks on all fabricated scaffolds, which suggests these scaffolds are biocompatible and noncytotoxic. Furthermore, the results indicate that there is no presence of residual solvent, and there is no variation in BHA purity between donor sites, which is excellent news as that means that as BHA has very high bioavailability. This is a confirmation of FTIR and WAXRD results which were carried out on the synthesized BHA.

Based on the TGA and FTIR analysis, the scaffolds also showed uniformity of distribution of BHA powder in the polymeric phase scaffold, which led to a well formed electrospun scaffold, suitable for cell cultivation.

Alkaline phosphate is one of the common bone cell-specific markers used to assess the presence of bone cells, and from our preliminary study, we have shown these scaffolds are osteoinductive based on the alkaline phosphate activity and in a manner which is not yet shown to vary based upon the relative proportions. To further confirm the differentiation of BMSC to bone cells, additional analysis of bone cell-specific markers like osteocalcin, and collagen type I or detection of fuctional mineralization needs to be conducted. Future works with human stem cells or osteoblasts could be suggested.

5.4 Electrospun composite scaffolds of PHB and BHA

Electrospun composite scaffolds of PHB containing microparticles of BHA in predesigned ratios were successfully produced. The biological properties of the scaffolds were evaluated *in vitro*, which showed these scaffolds could support the growth and proliferation of rat derived BMSCs. Alamar Blue assay provided information about the rates of cell proliferation in two weeks on all fabricated scaffolds, suggesting these scaffolds are biocompatible and noncytotoxic.

The TGA results suggested a uniformity of distribution of BHA powder whithin the polymeric phase of the scaffold. It has led to a well formed electrospun scaffold, ideal for cell cultivation. Alkaline phosphate is one of the common bone cell-specific markers used to assess the presence of bone cells, and in this study, we have shown these scaffolds are osteoinductive based on the alkaline phosphate activity. However, it is not yet shown to vary based upon the relative proportions. To further confirm the differentiation of BMSC to bone cells, additional analysis of bone cell-specific markers like osteocalcin, and collagen type I or detection of fuctional mineralization needs to be conducted.

For furture work, cultivation of human stem cells or osteoblast on the fabricated scaffolds could be investigated.

5.5 Electrospun scaffolds of PCL, PHB and PHBV as templates for corneal keratocytes

The electro-spinning technique can produce fibers that are able to support keratocyte growth and proliferation. All of the scaffolds are capable of promoting corneal keratocytes attachment and growth. There is a preference for up-regulation of gene expression when PCL scaffolds are used, including an up-regulation of LUM, ALDH, VIM, and COL 1. This could be due to the similarity of PCL fiber orientation to native collagen in extracellular matrix in terms of fiber morphology and diameter. PHB showed

a better α-SMA2 expression which makes it a suitable material for corneal wound healing applications. This study shows that the selection of biopolymer for scaffolding material can have an important influence upon gene expression, and requires careful consideration in the design of drug-screening technologies.

5.6 Composite multilayered scaffolds for guided tissue regeneration

A novel of composite scaffold consisting of three layers with different HA concentration has been successfully formed. Two major methods of scaffold fabrication was applied to achieve a favorable 3D construct with interconnected pores; electrospinning and salt-leaching. TGA results proved that HA could be uniformly dispersed within PCLT. Good interfacial connection between PCLT-CA-HA and electrospun PHB could be established during crosslinking reaction. The interfacial connections are strong enough interfacial connection between PCLT-CA-HA and electrospun PHB to undergo salt leaching and freeze drying without separation to fabricate a functionally graded scaffold. Mechanical test results showed that the scaffold fabricated by our method, shows elastomeric nature and mechanical properties suitable for bone tissue engineering. Different pore sizes and HA concentrations can be easily fabricated according to a predesigned amount without any limitation in a single composite construct.

References

Abadi, F. J. H., Tehran, M. A., Zamani, F., Nematollahi, M., Mobarakeh, L. G., & Nasr-Esfahani, M. H. (2014). Effect of Nanoporous Fibers on Growth and Proliferation of Cells on Electrospun Poly (epsilon-caprolactone) Scaffolds. *International Journal of Polymeric Materials and Polymeric Biomaterials, 63*(2), 57-64. doi:10.1080/00914037.2013.769248

Abd-el-haleem, D. A. M., & Alma, M. A. (2007). Physical and Chemical Properties of Polyhydroxyalkanotes Biodegradable Polymers Produced in Transgenic Yeasts. *Environmental Studies, 1*, 69-73.

Adamson, A. W., & Gast, A. P. (1967). Physical chemistry of surfaces.

Agarwal, S., Wendorff, J. H., & Greiner, A. (2008). Use of electrospinning technique for biomedical applications. *Polymer, 49*(26), 5603-5621. doi:10.1016/j.polymer.2008.09.014

Akram, H., Azari, P., Abas, W. A. B. W., Zain, N. M., Gan, S. N., Yahya, R., . . . Pingguan-Murphy, B. (2014). An in-vitro study on the proliferative potential of rat bone marrow stem cells on electrospun fibrous polycaprolactone scaffolds containing micro-hydroxyapatite particles. *Materials Research Innovations, 18*(S6), 520-524. doi:10.1179/1432891714z.0000000001039

Amini, A. R., Laurencin, C. T., & Nukavarapu, S. P. (2012). Bone tissue engineering: recent advances and challenges. *Critical Reviews in Biomedical Engineering, 40*(5), 363-408. Retrieved from http://www.ncbi.nlm.nih.gov/pubmed/23339648

Andrady, A. L. (2008). *Science and technology of polymer nanofibers*: John Wiley & Sons.

Araujo, P. L. B. (2010). Biodegradable conductive composites of poly(3-hydroxybutyrate) and polyaniline nanofibers: Preparation, characterization and radiolytic effects. *eXPRESS Polymer Letters, 5*(1), 12-22. doi:10.3144/expresspolymlett.2011.3

Avérous, L., & Pollet, E. (2012). *Green nano-biocomposites*: Springer.

Azari, P., Luan, N. S., Gan, S. N., Yahya, R., Wong, C. S., Chua, K. H., & Pingguan-Murphy, B. (2015). Electrospun Biopolyesters as Drug Screening Platforms for Corneal Keratocytes. *International Journal of Polymeric Materials and Polymeric Biomaterials, 64*(15), 785-791. doi:10.1080/00914037.2015.1030648

Balmayor, E. R., Tuzlakoglu, K., Azevedo, H. S., & Reis, R. (2009). Preparation and characterization of starch-poly-ε-caprolactone microparticles incorporating bioactive agents for drug delivery and tissue engineering applications. *Acta Biomaterialia, 5*(4), 1035-1045.

Blumm, E., & Owen, A. J. (1995). Miscibility, Crystallization and Melting of Poly(3-Hydroxybutyrate)/Poly(L-Lactide) Blends. *Polymer, 36*(21), 4077-4081. doi:Doi 10.1016/0032-3861(95)90987-D

Buchko, C. J., Chen, L. C., Shen, Y., & Martin, D. C. (1999). Processing and microstructural characterization of porous biocompatible protein polymer thin films. *Polymer, 40*(26), 7397-7407. doi:Doi 10.1016/S0032-3861(98)00866-0

Burr, D. B., Martin, R. B., Schaffler, M. B., & Radin, E. L. (1985). Bone remodeling in response to< i> in vivo</i> fatigue microdamage. *Journal of Biomechanics, 18*(3), 189-200.

Caffesse, R. G., Nasjleti, C. E., Morrison, E. C., & Sanchez, R. (1994). Guided tissue regeneration: comparison of bioabsorbable and non-bioabsorbable membranes. Histologic and histometric study in dogs. *Journal of Periodontology, 65*(6), 583-591. doi:10.1902/jop.1994.65.6.583

Casper, C. L., Stephens, J. S., Tassi, N. G., Chase, D. B., & Rabolt, J. F. (2004). Controlling surface morphology of electrospun polystyrene fibers: Effect of humidity and molecular weight in the electrospinning process. *Macromolecules, 37*(2), 573-578. doi:10.1021/ma0351975

Chan Sin, M., Gan, S. N., Mohd Annuar, M. S., & Ping Tan, I. K. (2010). Thermodegradation of medium-chain-length poly(3-hydroxyalkanoates) produced by Pseudomonas putida from oleic acid. *Polymer Degradation and Stability, 95*(12), 2334-2342. doi:10.1016/j.polymdegradstab.2010.08.027

Chan Sin, M., Gan, S. N., Mohd Annuar, M. S., & Ping Tan, I. K. (2011). Chain cleavage mechanism of palm kernel oil derived medium-chain-length poly(3-hydroxyalkanoates) during high temperature decomposition. *Polymer Degradation and Stability, 96*(9), 1705-1710. doi:10.1016/j.polymdegradstab.2011.06.004

Chang, M. C., & Tanaka, J. (2002). FT-IR study for hydroxyapatite/collagen nanocomposite cross-linked by glutaraldehyde. *Biomaterials, 23*(24), 4811-4818. Retrieved from http://www.ncbi.nlm.nih.gov/pubmed/12361620

Chapekar, M. S. (2000). Tissue engineering: challenges and opportunities. *Journal of Biomedial Materials Research, 53*(6), 617-620. Retrieved from http://www.ncbi.nlm.nih.gov/pubmed/11074418

Chawla, K. K. (2005). *Fibrous materials*: Cambridge University Press.

Chen, G. Q., & Wu, Q. (2005). The application of polyhydroxyalkanoates as tissue engineering materials. *Biomaterials, 26*(33), 6565-6578. doi:10.1016/j.biomaterials.2005.04.036

Chen, Y., Thompson, D. C., Koppaka, V., Jester, J. V., & Vasiliou, V. (2013). Ocular aldehyde dehydrogenases: Protection against ultraviolet damage and maintenance of transparency for vision. *Progress in retinal and eye research, 33*, 28-39.

Chen, Y., Zhou, S., & Li, Q. (2011). Microstructure design of biodegradable scaffold and its effect on tissue regeneration. *Biomaterials, 32*(22), 5003-5014. doi:10.1016/j.biomaterials.2011.03.064

Cheng, M. L., Lin, C. C., Su, H. L., Chen, P. Y., & Sun, Y. M. (2008). Processing and characterization of electrospun poly(3-hydroxybutyrate-co-3-hydroxyhexanoate) nanofibrous membranes. *Polymer, 49*(2), 546-553. doi:10.1016/j.polymer.2007.11.049

Choi, J. S., Lee, S. W., Jeong, L., Bae, S.-H., Min, B. C., Youk, J. H., & Park, W. H. (2004). Effect of organosoluble salts on the nanofibrous structure of electrospun poly (3-hydroxybutyrate-< i> co</i>-3-hydroxyvalerate). *International Journal of Biological Macromolecules, 34*(4), 249-256.

Chun, Y. S., & Kim, W. N. (2000). Thermal properties of poly (hydroxybutyrate-co-hydroxyvalerate) and poly (e-caprolactone) blends. *Polymer, 41*, 2305-2308.

Chung, E. J., Qiu, H., Kodali, P., Yang, S., Sprague, S. M., Hwong, J., . . . Ameer, G. A. (2011). Early tissue response to citric acid-based micro- and nanocomposites. *Journal of Biomedical Materials Research, Part A, 96*(1), 29-37. doi:10.1002/jbm.a.32953

Chung, E. J., Sugimoto, M. J., & Ameer, G. A. (2011). The role of hydroxyapatite in citric acid-based nanocomposites: surface characteristics, degradation, and osteogenicity in vitro. *Acta Biomaterialia, 7*(11), 4057-4063. doi:10.1016/j.actbio.2011.07.001

Cipitria, A., Skelton, A., Dargaville, T. R., Dalton, P. D., & Hutmacher, D. W. (2011). Design, fabrication and characterization of PCL electrospun scaffolds-a review. *Journal of Materials Chemistry, 21*(26), 9419-9453. doi:10.1039/c0jm04502k

Croisier, F., Duwez, A. S., Jerome, C., Leonard, A. F., van der Werf, K. O., Dijkstra, P. J., & Bennink, M. L. (2012). Mechanical testing of electrospun PCL fibers. *Acta Biomaterialia, 8*(1), 218-224. doi:10.1016/j.actbio.2011.08.015

Dalton, P. D., Grafahrend, D., Klinkhammer, K., Klee, D., & Moller, M. (2007). Electrospinning of polymer melts: Phenomenological observations. *Polymer, 48*(23), 6823-6833. doi:10.1016/j.polymer.2007.09.037

Deitzel, J. M., Kleinmeyer, J., Harris, D., & Tan, N. C. B. (2001). The effect of processing variables on the morphology of electrospun nanofibers and textiles. *Polymer, 42*(1), 261-272. doi:Doi 10.1016/S0032-3861(00)00250-0

Deitzel, J. M., Kleinmeyer, J. D., Hirvonen, J. K., & Tan, N. C. B. (2001). Controlled deposition of electrospun poly(ethylene oxide) fibers. *Polymer, 42*(19), 8163-8170. doi:Doi 10.1016/S0032-3861(01)00336-6

Demir, M. M., Yilgor, I., Yilgor, E., & Erman, B. (2002). Electrospinning of polyurethane fibers. *Polymer, 43*(11), 3303-3309. doi:Pii S0032-3861(02)00136-2

Doi 10.1016/S0032-3861(02)00136-2

Diba, M., Kharaziha, M., Fathi, M. H., Gholipourmalekabadi, M., & Samadikuchaksaraei, A. (2012). Preparation and characterization of polycaprolactone/forsterite nanocomposite porous scaffolds designed for bone tissue regeneration. *Composites Science and Technology, 72*(6), 716-723. doi:10.1016/j.compscitech.2012.01.023

Djordjevic, I., Choudhury, N. R., Dutta, N. K., & Kumar, S. (2009). Synthesis and characterization of novel citric acid-based polyester elastomers. *Polymer, 50*(7), 1682-1691. doi:10.1016/j.polymer.2009.01.045

Doshi, J., & Reneker, D. H. (1993). *Electrospinning process and applications of electrospun fibers.* Paper presented at the Industry Applications Society Annual Meeting, 1993., Conference Record of the 1993 IEEE.

Doyle, C., Tanner, E., & Bonfield, W. (1991). < i> In vitro</i> and< i> in vivo</i> evaluation of polyhydroxybutyrate and of polyhydroxybutyrate reinforced with hydroxyapatite. *Biomaterials, 12*(9), 841-847.

Erisken, C., Kalyon, D. M., & Wang, H. (2008). Functionally graded electrospun polycaprolactone and beta-tricalcium phosphate nanocomposites for tissue engineering applications. *Biomaterials, 29*(30), 4065-4073. doi:10.1016/j.biomaterials.2008.06.022

Fabbri, P., Cannillo, V., Sola, A., Dorigato, A., & Chiellini, F. (2010). Highly porous polycaprolactone-45S5 Bioglass (R) scaffolds for bone tissue engineering. *Composites Science and Technology, 70*(13), 1869-1878. doi:10.1016/j.compscitech.2010.05.029

Fetters, L. J., Lohse, D. J., Richter, D., Witten, T. A., & Zirkel, A. (1994). Connection between Polymer Molecular-Weight, Density, Chain Dimensions, and Melt Viscoelastic Properties. *Macromolecules, 27*(17), 4639-4647. doi:DOI 10.1021/ma00095a001

Fridrikh, S. V., Yu, J. H., Brenner, M. P., & Rutledge, G. C. (2003). Controlling the fiber diameter during electrospinning. *Physical Review Letters, 90*(14), 144502. Retrieved from http://www.ncbi.nlm.nih.gov/pubmed/12731920

Furukawa, T., Sato, H., Murakami, R., Zhang, J. M., Duan, Y. X., Noda, I., . . . Ozaki, Y. (2005). Structure, dispersibility, and crystallinity of poly(hydroxybutyrate)/poly(L-lactic acid) blends studied by FT-IR

microspectroscopy and differential scanning calorimetry. *Macromolecules, 38*(15), 6445-6454. doi:10.1021/ma0504668

Galego, N., Rozsa, C., Sánchez, R., Fung, J., Vázquez, A. a., & Santo Tomas, J. (2000). Characterization and application of poly (< i> β</i>-hydroxyalkanoates) family as composite biomaterials. *Polymer Testing, 19*(5), 485-492.

Ghafar, N. A., Hamzah, J. C., Othman, F., & Bhi, R. (2007). Rabbit limbal epithelial cells maintains its stemness in serum-free and feeder layer-free culture system. *조직공학과 재생의학, 4*(4), 557-565.

Ghasemi-Mobarakeh, L., Prabhakaran, M. P., Morshed, M., Nasr-Esfahani, M. H., & Ramakrishna, S. (2008). Electrospun poly(epsilon-caprolactone)/gelatin nanofibrous scaffolds for nerve tissue engineering. *Biomaterials, 29*(34), 4532-4539. doi:10.1016/j.biomaterials.2008.08.007

Gibson, P., Schreuder-Gibson, H., & Rivin, D. (2001). Transport properties of porous membranes based on electrospun nanofibers. *Colloids and Surfaces a-Physicochemical and Engineering Aspects, 187*, 469-481. doi:Doi 10.1016/S0927-7757(01)00616-1

Godbole, S., Gote, S., Latkar, M., & Chakrabarti, T. (2003). Preparation and characterization of biodegradable poly-3-hydroxybutyrate-starch blend films. *Bioresource Technology, 86*(1), 33-37. Retrieved from http://www.ncbi.nlm.nih.gov/pubmed/12421006

Gualandi, C. (2011). *Porous polymeric bioresorbable scaffolds for tissue engineering*: Springer.

Guan, D. H., Chen, Z. Q., Huang, C. P., & Lin, Y. H. (2008). Attachment, proliferation and differentiation of BMSCs on gas-jet/electrospun nHAP/PHB fibrous scaffolds. *Applied Surface Science, 255*(2), 324-327. doi:10.1016/j.apsusc.2008.06.093

Gunatillake, P. A., & Adhikari, R. (2003a). Biodegradable synthetic polymers for tissue engineering. *Eur Cell Mater, 5*, 1-16; discussion 16. Retrieved from http://www.ncbi.nlm.nih.gov/pubmed/14562275

Gunatillake, P. A., & Adhikari, R. (2003b). Biodegradable synthetic polymers for tissue engineering. *Eur Cell Mater, 5*(1), 1-16; discussion 16. Retrieved from http://www.ncbi.nlm.nih.gov/pubmed/14562275

Gupta, P., Elkins, C., Long, T. E., & Wilkes, G. L. (2005). Electrospinning of linear homopolymers of poly(methyl methacrylate): exploring relationships between fiber formation, viscosity, molecular weight and concentration in a good solvent. *Polymer, 46*(13), 4799-4810. doi:10.1016/j.polymer.2005.04.021

Hahn, S. K., Chang, Y. K., & Lee, S. Y. (1995). Recovery and characterization of poly(3-hydroxybutyric acid) synthesized in Alcaligenes eutrophus and recombinant Escherichia coli. *Applied and Environment Microbiology, 61*(1), 34-39. Retrieved from http://www.ncbi.nlm.nih.gov/pubmed/7887612

Hartgerink, J. D., Beniash, E., & Stupp, S. I. (2001). Self-assembly and mineralization of peptide-amphiphile nanofibers. *Science, 294*(5547), 1684-1688. doi:10.1126/science.1063187

Heidarkhan Tehrani, A., Zadhoush, A., Karbasi, S., & Sadeghi-Aliabadi, H. (2010). Scaffold percolative efficiency: in vitro evaluation of the structural criterion for electrospun mats. *Journal of Materials Science: Materials in Medicine, 21*(11), 2989-2998. doi:10.1007/s10856-010-4149-7

Herliansyah, M. K., Hamdi, M., Ide-Ektessabi, A., Wildan, M. W., & Toque, J. A. (2009). The influence of sintering temperature on the properties of compacted bovine hydroxyapatite. *Materials Science & Engineering C-Biomimetic and Supramolecular Systems, 29*(5), 1674-1680. doi:10.1016/j.msec.2009.01.007

Hildebrand, J., & Scott, R. (1964). The solubility of nonelectrolytes, 1950. *Reinhold, New York*, 411.

Hill, P. A. (1998). Bone remodelling. *British Journal of Orthodontics, 25*(2), 101-107. Retrieved from http://www.ncbi.nlm.nih.gov/pubmed/9668992

Hsu, C. M., & Shivkumar, S. (2004). N, N-Dimethylformamide Additions to the Solution for the Electrospinning of Poly (ε-caprolactone) Nanofibers. *Macromolecular Materials and Engineering, 289*(4), 334-340.

Huang, Z. M., Zhang, Y. Z., Kotaki, M., & Ramakrishna, S. (2003). A review on polymer nanofibers by electrospinning and their applications in nanocomposites. *Composites Science and Technology, 63*(15), 2223-2253. doi:10.1016/S0266-3538(03)00178-7

Hutmacher, D. W. (2000). Scaffolds in tissue engineering bone and cartilage. *Biomaterials, 21*(24), 2529-2543. Retrieved from http://www.ncbi.nlm.nih.gov/pubmed/11071603

Ikegame, M., Tajima, K., & Aida, T. (2003). Template Synthesis of Polypyrrole Nanofibers Insulated within One-Dimensional Silicate Channels: Hexagonal versus Lamellar for Recombination of Polarons into Bipolarons. *Angewandte Chemie International Edition, 42*(19), 2154-2157.

Ito, Y., Hasuda, H., Kamitakahara, M., Ohtsuki, C., Tanihara, M., Kang, I. K., & Kwon, O. H. (2005). A composite of hydroxyapatite with electrospun biodegradable nanofibers as a tissue engineering material. *Journal of Bioscience and Bioengineering, 100*(1), 43-49. doi:10.1263/jbb.100.43

Jang, J. H., Castano, O., & Kim, H. W. (2009). Electrospun materials as potential platforms for bone tissue engineering. *Adv Drug Deliv Rev, 61*(12), 1065-1083. doi:10.1016/j.addr.2009.07.008

Jester, J. V., & Ho-Chang, J. (2003). Modulation of cultured corneal keratocyte phenotype by growth factors/cytokines control in vitro contractility and extracellular matrix contraction. *Experimental Eye Research, 77*(5), 581-592. Retrieved from http://www.ncbi.nlm.nih.gov/pubmed/14550400

Jester, J. V., Petroll, W. M., Barry, P. A., & Cavanagh, H. D. (1995). Expression of alpha-smooth muscle (alpha-SM) actin during corneal stromal wound healing. *Investigative ophthalmology & visual science, 36*(5), 809-819.

Johnson, J., Andy Niehaus, Sylvain Nichols, David Lee , J. K., David Anderson & John, LannuttiJohnson, J., Niehaus, A., Nichols, S., Lee, D., . . . Anderson, D. (2012). Electrospun PCL in Vitro : a Microstructural Basis for Mechanical Property Changes. *Journal of Biomaterials Science, Polymer Edition, 20:4*, 467-481.

Jokinen, V., Suvanto, P., & Franssila, S. (2012). Oxygen and nitrogen plasma hydrophilization and hydrophobic recovery of polymers. *Biomicrofluidics, 6*(1), 16501-1650110. doi:10.1063/1.3673251

Kenawy, E.-R., Abdel-Hay, F. I., El-Newehy, M. H., & Wnek, G. E. (2009). Processing of polymer nanofibers through electrospinning as drug delivery systems. *Materials Chemistry and Physics, 113*(1), 296-302. doi:10.1016/j.matchemphys.2008.07.081

Kim, G. H., & Yoon, H. (2008). A direct-electrospinning process by combined electric field and air-blowing system for nanofibrous wound-dressings. *Applied Physics a-Materials Science & Processing, 90*(3), 389-394. doi:10.1007/s00339-007-4330-0

Kimakhe, S., Bohic, S., Larrose, C., Reynaud, A., Pilet, P., Giumelli, B., . . . Daculsi, G. (1999). Biological activities of sustained polymyxin B release from calcium phosphate biomaterial prepared by dynamic compaction: an in vitro study. *Journal of Biomedial Materials Research, 47*(1), 18-27. Retrieved from http://www.ncbi.nlm.nih.gov/pubmed/10400876

Kirkpatrick, C., & Mittermayer, C. (1990). Theoretical and practical aspects of testing potential biomaterialsin vitro. *Journal of Materials Science: Materials in Medicine, 1*(1), 9-13.

Koutsopoulos, S. (2002). Synthesis and characterization of hydroxyapatite crystals: a review study on the analytical methods. *Journal of Biomedial Materials Research, 62*(4), 600-612. doi:10.1002/jbm.10280

Krishnappa, R. V. N., Desai, K., & Sung, C. M. (2003). Morphological study of electrospun polycarbonates as a function of the solvent and processing voltage.

Journal of Materials Science, 38(11), 2357-2365. doi:Doi 10.1023/A:1023984514389

Kroeze, R. J., Helder, M. N., Govaert, L. E., & Smit, T. H. (2009). Biodegradable Polymers in Bone Tissue Engineering. *Materials, 2*(3), 833-856. doi:10.3390/ma2030833

Labet, M., & Thielemans, W. (2009). Synthesis of polycaprolactone: a review. *Chemical Society Reviews, 38*(12), 3484-3504. doi:10.1039/b820162p

Lee, H., & Kim, G. (2010). Biocomposites electrospun with poly(epsilon-caprolactone) and silk fibroin powder for biomedical applications. *Journal of Biomaterials Science, Polymer Edition, 21*(13), 1687-1699. doi:10.1163/092050609X12548956645680

Lee, J. S., Choi, K. H., Do Ghim, H., Kim, S. S., Chun, D. H., Kim, H. Y., & Lyoo, W. S. (2004). Role of molecular weight of atactic poly(vinyl alcohol) (PVA) in the structure and properties of PVA nanofabric prepared by electrospinning. *Journal of Applied Polymer Science, 93*(4), 1638-1646. doi:10.1002/app.20602

Lemstra, P., Kirschbaum, R., Ohta, T., & Yasuda, H. (1987). High-strength/high-modulus structures based on flexible macromolecules: gel-spinning and related processes *Developments in Oriented Polymers—2* (pp. 39-77): Springer.

Li, X. R., Xie, J. W., Yuan, X. Y., & Xia, Y. N. (2008). Coating Electrospun Poly(epsilon-caprolactone) Fibers with Gelatin and Calcium Phosphate and Their Use as Biomimetic Scaffolds for Bone Tissue Engineering. *Langmuir, 24*(24), 14145-14150. doi:10.1021/la802984a

Liang, D., Hsiao, B. S., & Chu, B. (2007). Functional electrospun nanofibrous scaffolds for biomedical applications. *Adv Drug Deliv Rev, 59*(14), 1392-1412. doi:10.1016/j.addr.2007.04.021

Lin, F.-H., Liao, C.-J., Chen, K.-S., & Sun, J.-S. (1999). Preparation of a biphasic porous bioceramic by heating bovine cancellous bone with Na 4 P 2 O 7· 10H 2 O addition. *Biomaterials, 20*(5), 475-484.

Liu, C., Xia, Z., & Czernuszka, J. T. (2007). Design and development of three-dimensional scaffolds for tissue engineering. *Chemical Engineering Research & Design, 85*(A7), 1051-1064. doi:10.1205/cherd061915

Liu, X., & Ma, P. X. (2009). Phase separation, pore structure, and properties of nanofibrous gelatin scaffolds. *Biomaterials, 30*(25), 4094-4103. doi:10.1016/j.biomaterials.2009.04.024

Lovera, D., Marquez, L., Balsamo, V., Taddei, A., Castelli, C., & Muller, A. J. (2007). Crystallization, morphology, and enzymatic degradation of polyhydroxybutyrate/polycaprolactone (PHB/PCL) blends. *Macromolecular Chemistry and Physics, 208*(9), 924-937. doi:10.1002/macp.200700011

Luklinska, Z. B., & Bonfield, W. (1997). Morphology and ultrastructure of the interface between hydroxyapatite-polyhydroxybutyrate composite implant and bone. *Journal of Materials Science-Materials in Medicine, 8*(6), 379-383. doi:Doi 10.1023/A:1018589018205

Lyons, J., Li, C., & Ko, F. (2004). Melt-electrospinning part I: processing parameters and geometric properties. *Polymer, 45*(22), 7597-7603. doi:10.1016/j.polymer.2004.08.071

Ma, Z. W., Kotaki, M., Inai, R., & Ramakrishna, S. (2005). Potential of nanofiber matrix as tissue-engineering scaffolds. *Tissue Engineering, 11*(1-2), 101-109. doi:DOI 10.1089/ten.2005.11.101

Martins, A., Pinho, E. D., Faria, S., Pashkuleva, I., Marques, A. P., Reis, R. L., & Neves, N. M. (2009). Surface modification of electrospun polycaprolactone nanofiber meshes by plasma treatment to enhance biological performance. *Small, 5*(10), 1195-1206. doi:10.1002/smll.200801648

McClure, M. J., Sell, S. A., Simpson, D. G., Walpoth, B. H., & Bowlin, G. L. (2011). Tri-layered Electrospinning to Mimic Native Arterial Architecture using Polycaprolactone, Elastin, and Collagen: A Preliminary Study. *Jove-Journal of Visualized Experiments*(47). doi:UNSP e2084

10.3791/2084

Megelski, S., Stephens, J. S., Chase, D. B., & Rabolt, J. F. (2002). Micro- and nanostructured surface morphology on electrospun polymer fibers. *Macromolecules, 35*(22), 8456-8466. doi:10.1021/ma020444a

Michelacci, Y. (2003). Collagens and proteoglycans of the corneal extracellular matrix. *Brazilian journal of medical and biological research, 36*(8), 1037-1046.

Mit-uppatham, C., Nithitanakul, M., & Supaphol, P. (2004). Ultrafine Electrospun Polyamide-6 Fibers: Effect of Solution Conditions on Morphology and Average Fiber Diameter. *Macromolecular Chemistry and Physics, 205*(17), 2327-2338.

Mo, X. M., Xu, C. Y., Kotaki, M., & Ramakrishna, S. (2004). Electrospun P(LLA-CL) nanofiber: a biomimetic extracellular matrix for smooth muscle cell and endothelial cell proliferation. *Biomaterials, 25*(10), 1883-1890. Retrieved from http://www.ncbi.nlm.nih.gov/pubmed/14738852

Mondrinos, M. J., Dembzynski, R., Lu, L., Byrapogu, V. K., Wootton, D. M., Lelkes, P. I., & Zhou, J. (2006). Porogen-based solid freeform fabrication of polycaprolactone-calcium phosphate scaffolds for tissue engineering. *Biomaterials, 27*(25), 4399-4408. doi:10.1016/j.biomaterials.2006.03.049

Moradi, A., Dalilottojari, A., Pingguan-Murphy, B., & Djordjevic, I. (2013). Fabrication and characterization of elastomeric scaffolds comprised of a citric acid-based polyester/hydroxyapatite microcomposite. *Materials & Design, 50*, 446-450. doi:10.1016/j.matdes.2013.03.026

Moroni, L., de Wijn, J. R., & van Blitterswijk, C. A. (2006). 3D fiber-deposited scaffolds for tissue engineering: influence of pores geometry and architecture on dynamic mechanical properties. *Biomaterials, 27*(7), 974-985. doi:10.1016/j.biomaterials.2005.07.023

Muhammad, K. B., Abas, W. A., Kim, K. H., Pingguan-Murphy, B., Zain, N. M., & Akram, H. (2012). In vitro comparative study of white and dark polycaprolactone trifumarate in situ cross-linkable scaffolds seeded with rat bone marrow stromal cells. *Clinics (Sao Paulo), 67*(6), 629-638. Retrieved from http://www.ncbi.nlm.nih.gov/pubmed/22760903

Murphy, K. G., & Gunsolley, J. C. (2003). Guided tissue regeneration for the treatment of periodontal intrabony and furcation defects. A systematic review. *Annals of Periodontology, 8*(1), 266-302. doi:10.1902/annals.2003.8.1.266

Nain, A. S., Wong, J. C., Amon, C., & Sitti, M. (2006). Drawing suspended polymer micro-/nanofibers using glass micropipettes. *Applied Physics Letters, 89*(18), 183105. doi:Artn 183105

10.1063/1.2372694

Nakajima, T. (1994). *Advanced fiber spinning technology*: Elsevier.

Ni, J., & Wang, M. (2002). In vitro evaluation of hydroxyapatite reinforced polyhydroxybutyrate composite. *Materials Science & Engineering C-Biomimetic and Supramolecular Systems, 20*(1-2), 101-109. doi:Pii S0928-4931(02)00019-X

Doi 10.1016/S0928-4931(02)00019-X

Nikitovic, D., Katonis, P., Tsatsakis, A., Karamanos, N. K., & Tzanakakis, G. N. (2008). Lumican, a small leucine-rich proteoglycan. *IUBMB life, 60*(12), 818-823.

Nisbet, D. R., Forsythe, J. S., Shen, W., Finkelstein, D. I., & Horne, M. K. (2009). Review paper: a review of the cellular response on electrospun nanofibers for tissue engineering. *Journal of Biomaterials Applications, 24*(1), 7-29. doi:10.1177/0885328208099086

Oh, S. H., Park, I. K., Kim, J. M., & Lee, J. H. (2007). In vitro and in vivo characteristics of PCL scaffolds with pore size gradient fabricated by a centrifugation method. *Biomaterials, 28*(9), 1664-1671. doi:10.1016/j.biomaterials.2006.11.024

Ooi, C. Y., Hamdi, M., & Ramesh, S. (2007). Properties of hydroxyapatite produced by annealing of bovine bone. *Ceramics International, 33*(7), 1171-1177. doi:10.1016/j.ceramint.2006.04.001

Park, A., & Cima, L. G. (1996). In vitro cell response to differences in poly-L-lactide crystallinity. *Journal of Biomedial Materials Research, 31*(1), 117-130. Retrieved from http://www.ncbi.nlm.nih.gov/pubmed/8731156

Pekounov, Y., Chakarova, K., & Hadjiivanov, K. (2009). Surface acidity of calcium phosphate and calcium hydroxyapatite: FTIR spectroscopic study of low-temperature CO adsorption. *Materials Science & Engineering C-Biomimetic and Supramolecular Systems, 29*(4), 1178-1181. doi:10.1016/j.msec.2008.10.011

Piersma, A. H. (2004). Validation of alternative methods for developmental toxicity testing. *Toxicology letters, 149*(1), 147-153.

Pouton, C. W., & Akhtar, S. (1996). Biosynthetic polyhydroxyalkanoates and their potential in drug delivery. *Advanced Drug Delivery Reviews, 18*(2), 133-162. doi:10.1016/0169-409x(95)00092-l

Prabhakaran, M. P., Venugopal, J., & Ramakrishna, S. (2009). Electrospun nanostructured scaffolds for bone tissue engineering. *Acta Biomaterialia, 5*(8), 2884-2893. doi:10.1016/j.actbio.2009.05.007

Purane, S. V., & Panigrahi, N. R. (2007). Microfibers, microfilaments and their applications. *AUTEX RESEARCH JOURNAL, 7*(3), 148-158.

Qiu, H., Yang, J., Kodali, P., Koh, J., & Ameer, G. A. (2006). A citric acid-based hydroxyapatite composite for orthopedic implants. *Biomaterials, 27*(34), 5845-5854. doi:10.1016/j.biomaterials.2006.07.042

Rainer, A., Spadaccio, C., Sedati, P., De Marco, F., Carotti, S., Lusini, M., . . . Trombetta, M. (2011). Electrospun hydroxyapatite-functionalized PLLA scaffold: potential applications in sternal bone healing. *Annals of Biomedical Engineering, 39*(7), 1882-1890. doi:10.1007/s10439-011-0289-2

Ramakrishna, S., Fujihara, K., Teo, W.-E., Lim, T.-C., & Ma, Z. (2005). *An introduction to electrospinning and nanofibers* (Vol. 90): World Scientific.

Reneker, D. H., & Yarin, A. L. (2008). Electrospinning jets and polymer nanofibers. *Polymer, 49*(10), 2387-2425. doi:10.1016/j.polymer.2008.02.002

Reneker, D. H., Yarin, A. L., Fong, H., & Koombhongse, S. (2000). Bending instability of electrically charged liquid jets of polymer solutions in electrospinning. *Journal of Applied Physics, 87*(9), 4531-4547. doi:Doi 10.1063/1.373532

Ritchey, E. R., Code, K., Zelinka, C. P., Scott, M. A., & Fischer, A. J. (2011). The chicken cornea as a model of wound healing and neuronal re-innervation.

Rose, F. R., & Oreffo, R. O. (2002). Bone tissue engineering: hope vs hype. *Biochemical and Biophysical Research Communications, 292*(1), 1-7. doi:10.1006/bbrc.2002.6519

Rutledge, G. C., & Fridrikh, S. V. (2007). Formation of fibers by electrospinning. *Adv Drug Deliv Rev, 59*(14), 1384-1391. doi:10.1016/j.addr.2007.04.020

Saika, S., Shiraishi, A., Saika, S., Liu, C.-Y., Funderburgh, J. L., Kao, C. W.-C., . . . Kao, W. W.-Y. (2000). Role of lumican in the corneal epithelium during wound healing. *Journal of Biological Chemistry, 275*(4), 2607-2612.

Shenoy, S. L., Bates, W. D., Frisch, H. L., & Wnek, G. E. (2005). Role of chain entanglements on fiber formation during electrospinning of polymer solutions: good solvent, non-specific polymer-polymer interaction limit. *Polymer, 46*(10), 3372-3384. doi:10.1016/j.polymer.2005.03.011

Shih, W. J., Chen, Y. H., Shih, C. J., Hon, M. H., & Wang, M. C. (2007). Structural and morphological studies on poly(3-hydroxybutyrate acid) (PHB)/chitosan drug releasing microspheres prepared by both single and double emulsion processes. *Journal of Alloys and Compounds, 434*, 826-829. doi:10.1016/j.jallcom.2006.08.210

Shin, M., Yoshimoto, H., & Vacanti, J. P. (2004). In vivo bone tissue engineering using mesenchymal stem cells on a novel electrospun nanofibrous scaffold. *Tissue Engineering, 10*(1-2), 33-41. doi:Doi 10.1089/107632704322791673

Shin, Y. M., Hohman, M. M., Brenner, M. P., & Rutledge, G. C. (2001). Experimental characterization of electrospinning: the electrically forced jet and instabilities. *Polymer, 42*(25), 9955-9967. doi:Doi 10.1016/S0032-3861(01)00540-7

Sobczak, A., Kowalski, Z., & Wzorek, Z. (2009). Preparation of hydroxyapatite from animal bones. *Acta Bioeng Biomech, 11*(4), 23-28. Retrieved from http://www.ncbi.nlm.nih.gov/pubmed/20405812

Soliman, S., Sant, S., Nichol, J. W., Khabiry, M., Traversa, E., & Khademhosseini, A. (2011). Controlling the porosity of fibrous scaffolds by modulating the fiber diameter and packing density. *Journal of Biomedical Materials Research, Part A, 96*(3), 566-574. doi:10.1002/jbm.a.33010

Sombatmankhong, K., Sanchavanakit, N., Pavasant, P., & Supaphol, P. (2007). Bone scaffolds from electrospun fiber mats of poly (3-hydroxybutyrate), poly(3-hydroxybutyrate-co-3-hydroxyvalerate) and their blend. *Polymer, 48*(5), 1419-1427. doi:10.1016/j.polymer.2007.01.014

Sombatmankhong, K., Suwantong, O., Waleetorncheepsawat, S., & Supaphol, P. (2006). Electrospun fiber mats of poly(3-hydroxybutyrate), poly(3-hydroxybutyrate-co-3-hydroxyvalerate), and their blends. *Journal of Polymer Science Part B-Polymer Physics, 44*(19), 2923-2933. doi:10.1002/polb.20915

Song, W., Markel, D. C., Wang, S., Shi, T., Mao, G., & Ren, W. (2012). Electrospun polyvinyl alcohol-collagen-hydroxyapatite nanofibers: a biomimetic extracellular matrix for osteoblastic cells. *Nanotechnology, 23*(11), 115101. doi:10.1088/0957-4484/23/11/115101

Stevenson, S., Emery, S. E., & Goldberg, V. M. (1996). Factors affecting bone graft incorporation. *Clinical Orthopaedics and Related Research, 324*(324), 66-74. Retrieved from http://www.ncbi.nlm.nih.gov/pubmed/8595779

Subbiah, T., Bhat, G. S., Tock, R. W., Pararneswaran, S., & Ramkumar, S. S. (2005). Electrospinning of nanofibers. *Journal of Applied Polymer Science, 96*(2), 557-569. doi:10.1002/app.21481

Subramanian, A., Vu, D., Larsen, G. F., & Lin, H. Y. (2005). Preparation and evaluation of the electrospun chitosan/PEO fibers for potential applications in cartilage tissue engineering. *Journal of Biomaterials Science, Polymer Edition, 16*(7), 861-873. Retrieved from http://www.ncbi.nlm.nih.gov/pubmed/16128293

Sultana, N. (2013). *Biodegradable Polymer-Based Scaffolds for Bone Tissue Engineering*: Springer.

Sun, J. S., Tsuang, Y. H., Chang, W. H., Li, J., Liu, H. C., & Lin, F. H. (1997). Effect of hydroxyapatite particle size on myoblasts and fibroblasts. *Biomaterials, 18*(9), 683-690. Retrieved from http://www.ncbi.nlm.nih.gov/pubmed/9152000

Suwantong, O., Waleetorncheepsawat, S., Sanchavanakit, N., Pavasant, P., Cheepsunthorn, P., Bunaprasert, T., & Supaphol, P. (2007). In vitro biocompatibility of electrospun poly(3-hydroxybutyrate) and poly(3-hydroxybutyrate-co-3-hydroxyvalerate) fiber mats. *International Journal of Biological Macromolecules, 40*(3), 217-223. doi:10.1016/j.ijbiomac.2006.07.006

Tan, I. K. P., Kumar, K. S., Theanmalar, M., Gan, S. N., & Gordon, B. (1997). Saponified palm kernel oil and its major free fatty acids as carbon substrates for the production of polyhydroxyalkanoates in Pseudomonas putida PGA1. *Applied Microbiology and Biotechnology, 47*(3), 207-211. doi:10.1007/s002530050914

Taylor, G. (1969). Electrically driven jets. *Proceedings of the Royal Society of London. A. Mathematical and Physical Sciences, 313*(1515), 453-475.

Tehrani, A. H., & Zadhoush, A. (2010). Preparing Nanocomposite Fibrous Scaffolds of P3HB / nHA for Bone Tissue Engineering. *Scanning Electron Microscopy*, 3-4.

Teo, W. E., & Ramakrishna, S. (2006). A review on electrospinning design and nanofibre assemblies. *Nanotechnology, 17*(14), R89-R106. doi:10.1088/0957-4484/17/14/R01

Thiré, R. M., Ribeiro, T. A., & Andrade, C. T. (2006). Effect of starch addition on compression-molded poly (3-hydroxybutyrate)/starch blends. *Journal of Applied Polymer Science, 100*(6), 4338-4347.

Tomasek, J. J., Gabbiani, G., Hinz, B., Chaponnier, C., & Brown, R. A. (2002). Myofibroblasts and mechano-regulation of connective tissue remodelling. *Nature Reviews Molecular Cell Biology, 3*(5), 349-363.

Tong, H. W., Wang, M., & Lu, W. W. (2011). In Vitro Biological Evaluation of Fibrous PHBV Polymer and CHA/PHBV Nanocomposite Scaffolds Developed for Tissue Engineering Applications. *Bioceramics Development and Applications, 1*, 1-3. doi:10.4303/bda/D110168

Tripatanasuwan, S., Zhong, Z. X., & Reneker, D. H. (2007). Effect of evaporation and solidification of the charged jet in electrospinning of poly(ethylene oxide) aqueous solution. *Polymer, 48*(19), 5742-5746. doi:10.1016/j.polymer.2007.07.045

Trotman, E. R. (1984). Dyeing and chemical technology of textile fibres. 1-15.

Um, I. C., Fang, D., Hsiao, B. S., Okamoto, A., & Chu, B. (2004). Electro-spinning and electro-blowing of hyaluronic acid. *Biomacromolecules, 5*(4), 1428-1436. doi:10.1021/bm034539b

Veleirinho, B., Ribeiro-do-Valle, R. M., & Lopes-da-Silva, J. A. (2011). Processing conditions and characterization of novel electrospun poly (3-hydroxybutyrate-co-hydroxyvalerate)/chitosan blend fibers. *Materials Letters, 65*(14), 2216-2219. doi:10.1016/j.matlet.2011.04.058

Vogel, C., Hoffmann, G. G., & Siesler, H. W. (2009). Rheo-optical FT-IR spectroscopy of poly(3-hydroxybutyrate)/poly(lactic acid) blend films. *Vibrational Spectroscopy, 49*(2), 284-287. doi:10.1016/j.vibspec.2008.10.014

Wang, C., Hsu, C. H., & Hwang, I. H. (2008). Scaling laws and internal structure for characterizing electrospun poly[(R)-3-hydroxybutyrate] fibers. *Polymer, 49*(19), 4188-4195. doi:10.1016/j.polymer.2008.07.033

Wang, L., Zhu, W., Wang, X., Chen, X., Chen, G.-q., & Xu, K. (2007). Processability Modifications of Poly (3-hydroxybutyrate) by Plasticizing , Blending , and Stabilizing. *Polymer,* 27-30. doi:10.1002/app

Wang, X. Y., Drew, C., Lee, S. H., Senecal, K. J., Kumar, J., & Sarnuelson, L. A. (2002). Electrospun nanofibrous membranes for highly sensitive optical sensors. *Nano Letters, 2*(11), 1273-1275. doi:10.1021/nl020216u

Wang, Y., Wang, G., Chen, L., Li, H., Yin, T., Wang, B., . . . Yu, Q. (2009). Electrospun nanofiber meshes with tailored architectures and patterns as potential tissue-engineering scaffolds. *Biofabrication, 1*(1), 015001. doi:10.1088/1758-5082/1/1/015001

Wannatong, L., Sirivat, A., & Supaphol, P. (2004). Effects of solvents on electrospun polymeric fibers: preliminary study on polystyrene. *Polymer International, 53*(11), 1851-1859. doi:10.1002/pi.1599

Webb, K., Hlady, V., & Tresco, P. A. (1998). Relative importance of surface wettability and charged functional groups on NIH 3T3 fibroblast attachment, spreading, and

cytoskeletal organization. *Journal of Biomedial Materials Research, 41*(3), 422-430. Retrieved from http://www.ncbi.nlm.nih.gov/pubmed/9659612

Wei, G., & Ma, P. X. (2004). Structure and properties of nano-hydroxyapatite/polymer composite scaffolds for bone tissue engineering. *Biomaterials, 25*(19), 4749-4757. doi:10.1016/j.biomaterials.2003.12.005

West-Mays, J. A., & Dwivedi, D. J. (2006). The keratocyte: corneal stromal cell with variable repair phenotypes. *The international journal of biochemistry & cell biology, 38*(10), 1625-1631.

Whitcher, J. P., Srinivasan, M., & Upadhyay, M. P. (2001). Corneal blindness: a global perspective. *Bulletin of the World Health Organization, 79*(3), 214-221.

Wilkinson, J. H., Boutwell, J. H., & Winsten, S. (1969). Evaluation of a new system for the kinetic measurement of serum alkaline phosphatase. *Clinical Chemistry, 15*(6), 487-495. Retrieved from http://www.ncbi.nlm.nih.gov/pubmed/5786804

Williamson, M. R., & Coombes, A. G. (2004). Gravity spinning of polycaprolactone fibres for applications in tissue engineering. *Biomaterials, 25*(3), 459-465. Retrieved from http://www.ncbi.nlm.nih.gov/pubmed/14585694

Wilson, S. E. (1998). Everett Kinsey Lecture. Keratocyte apoptosis in refractive surgery. *CLAO Journal, 24*(3), 181-185. Retrieved from http://www.ncbi.nlm.nih.gov/pubmed/9684078

Wilson, S. E., Netto, M., & Ambrósio Jr, R. (2003). Corneal cells: chatty in development, homeostasis, wound healing, and disease. *American journal of ophthalmology, 136*(3), 530-536.

Woodruff, M. A., & Hutmacher, D. W. (2010). The return of a forgotten polymer-Polycaprolactone in the 21st century. *Progress in Polymer Science, 35*(10), 1217-1256. doi:10.1016/j.progpolymsci.2010.04.002

Wu, C. C., Huang, S. T., Tseng, T. W., Rao, Q. L., & Lin, H. C. (2010). FT-IR and XRD investigations on sintered fluoridated hydroxyapatite composites. *Journal of Molecular Structure, 979*(1-3), 72-76. doi:10.1016/j.molstruc.2010.06.003

Wutticharoenmongkol, P., Pavasant, P., & Supaphol, P. (2007). Osteoblastic phenotype expression of MC3T3-E1 cultured on electrospun polycaprolactone fiber mats filled with hydroxyapatite nanoparticles. *Biomacromolecules, 8*(8), 2602-2610. doi:10.1021/bm700451p

Wutticharoenmongkol, P., Sanchavanakit, N., Pavasant, P., & Supaphol, P. (2006). Preparation and characterization of novel bone scaffolds based on electrospun polycaprolactone fibers filled with nanoparticles. *Macromolecular Bioscience, 6*(1), 70-77. doi:10.1002/mabi.200500150

Yang, J., Webb, A. R., & Ameer, G. A. (2004). Novel Citric Acid-Based Biodegradable Elastomers for Tissue Engineering. *Advanced Materials, 16*(6), 511-516.

Yang, J., Webb, A. R., Pickerill, S. J., Hageman, G., & Ameer, G. A. (2006). Synthesis and evaluation of poly(diol citrate) biodegradable elastomers. *Biomaterials, 27*(9), 1889-1898. doi:10.1016/j.biomaterials.2005.05.106

Yang, X., Yang, F., Walboomers, X. F., Bian, Z., Fan, M., & Jansen, J. A. (2010). The performance of dental pulp stem cells on nanofibrous PCL/gelatin/nHA scaffolds. *Journal of Biomedical Materials Research, Part A, 93*(1), 247-257. doi:10.1002/jbm.a.32535

Yang, Y., Jia, Z. D., Li, Q., & Guan, Z. C. (2006). Experimental investigation of the governing parameters in the electrospinning of polyethylene oxide solution. *Ieee Transactions on Dielectrics and Electrical Insulation, 13*(3), 580-585. Retrieved from <Go to ISI>://WOS:000239184400018

Yarin, A. L., Koombhongse, S., & Reneker, D. H. (2001). Taylor cone and jetting from liquid droplets in electrospinning of nanofibers. *Journal of Applied Physics, 90*(9), 4836-4846. doi:Doi 10.1063/1.1408260

Yoshimoto, H., Shin, Y. M., Terai, H., & Vacanti, J. P. (2003). A biodegradable nanofiber scaffold by electrospinning and its potential for bone tissue engineering. *Biomaterials, 24*(12), 2077-2082. doi:10.1016/S0142-9612(02)00635-X

Yu, B. Y., Chen, P. Y., Sun, Y. M., Lee, Y. T., & Young, T. H. (2008). The behaviors of human mesenchymal stem cells on the poly(3-hydroxybutyrate-co-3-hydroxyhexanoate) (PHBHHx) membranes. *Desalination, 234*(1-3), 204-211. doi:10.1016/j.desal.2007.09.087

Yu, H. S., Jang, J. H., Kim, T. I., Lee, H. H., & Kim, H. W. (2009). Apatite-mineralized polycaprolactone nanofibrous web as a bone tissue regeneration substrate. *Journal of Biomedical Materials Research Part A, 88*(3), 747-754.

Yu, L. (2009). *Biodegradable polymer blends and composites from renewable resources*: John Wiley & Sons.

Yun, K. M., Hogan, C. J., Mastubayashi, Y., Kawabe, M., Iskandar, F., & Okuyama, K. (2007). Nanoparticle filtration by electrospun polymer fibers. *Chemical Engineering Science, 62*(17), 4751-4759. doi:10.1016/j.ces.2007.06.007

Zainal Abidin, F., Hui, C. K., Luan, N. S., Mohd Ramli, E. S., Hun, L. T., & Abd Ghafar, N. (2011). Effects of edible bird's nest (EBN) on cultured rabbit corneal keratocytes. *BMC Complementary and Alternative Medicine, 11*(1), 94. doi:10.1186/1472-6882-11-94

Zhao, G., Yin, S., Liu, G., Cen, L., Sun, J., Zhou, H., . . . Cao, Y. (2009). < i> In vitro</i> engineering of fibrocartilage using CDMP1 induced dermal fibroblasts and polyglycolide. *Biomaterials, 30*(19), 3241-3250.

Zhao, S. L., Wu, X. H., Wang, L. G., & Huang, Y. (2004). Electrospinning of ethyl-cyanoethyl cellulose/tetrahydrofuran solutions. *Journal of Applied Polymer Science, 91*(1), 242-246. doi:10.1002/app.13196

Zhou, Y., Chen, F., Ho, S. T., Woodruff, M. A., Lim, T. M., & Hutmacher, D. W. (2007). Combined marrow stromal cell-sheet techniques and high-strength biodegradable composite scaffolds for engineered functional bone grafts. *Biomaterials, 28*(5), 814-824. doi:10.1016/j.biomaterials.2006.09.032

Zong, X. H., Kim, K., Fang, D. F., Ran, S. F., Hsiao, B. S., & Chu, B. (2002). Structure and process relationship of electrospun bioabsorbable nanofiber membranes. *Polymer, 43*(16), 4403-4412. doi:Pii S0032-3861(02)00275-6

Doi 10.1016/S0032-3861(02)00275-6

Zuo, W. W., Zhu, M. F., Yang, W., Yu, H., Chen, Y. M., & Zhang, Y. (2005). Experimental study on relationship between jet instability and formation of beaded fibers during electrospinning. *Polymer Engineering and Science, 45*(5), 704-709. doi:10.1002/pen.20304

APPENDIX A

List of ISI Publications

I. **Azari, P**., N. S. Luan, S. N. Gan, R. Yahya, C. S. Wong, K. H. Chua and B. Pingguan-Murphy (2015). "Electrospun Biopolyesters as Drug Screening Platforms for Corneal Keratocytes." International Journal of Polymeric Materials and Polymeric Biomaterials 64(15): 785-791

II. **Azari, P**., R. Yahya, C. Wong and S. Gan (2014). "Improved processability of electrospun poly [(R)-3-hydroxybutyric acid] through blending with medium-chain length poly (3-hydroxyalkanoates) produced by Pseudomonas putida from oleic acid." Materials Research Innovations **18**(S6): S6-345-S346-349

III. Akram, H., **P. Azari**, W. Wan Abas, N. Zain, S. Gan, R. Yahya, C. Wong and B. Pingguan-Murphy (2014). "An in-vitro study on the proliferative potential of rat bone marrow stem cells on electrospun fibrous polycaprolactone scaffolds containing micro-hydroxyapatite particles." Materials Research Innovations 18(S6): S6-520-S526-524

IV. I. Rozila, **P. Azari**, S. Munirah, W. K. Z. Wan Safwani, SN Gan, B. Pingguan-Murphy, K. H Chua (2015) "Differential Osteogenic Potential Of Human Adipose-Derived Stem Cell Co-Cultured With Human Osteoblast On Polymeric Microfiber Scaffolds: An In-Vitro Study" Acta Biomaterialia Under Review Manuscript

APPENDIX B

Conference Oral Presentations

Pedram Azari, Haris Akram, Gan Seng Neon, Rosiyah Yahya, Wong Chiow San, Belinda-Pingguan Murphy, Norita Mohd Zain

Electrospun nanofibers of Poly [(R)-3-hydroxybutyric acid] and hydroxyapatite as scaffolds for tissue engineering, Oral Presentation, 17 Malaysian Chemical congress

Pedram Azari Gan Seng Neon, Rosiyah Yahya, Wong Chiow San

"Construction of electrospinning set up for micron and nano polymeric fiber mats", Oral Presentation, Malaysian Polymer international conference 2009

Pedram Azari, Haris Akram, Gan Seng Neon, Rosiyah Yahya, Wong Chiow San, Belinda-Pingguan Murphy

An in vitro biological evaluation of electrospun poly(3-hydroxybutyrate) and

bovine hydroxyapatite composite scaffold for bone tissue engineering, UM-NUS-Chulangkorn Trilateral Symposium 2014, Poster Presentation

APPENDIX C

SEM Images of PEO

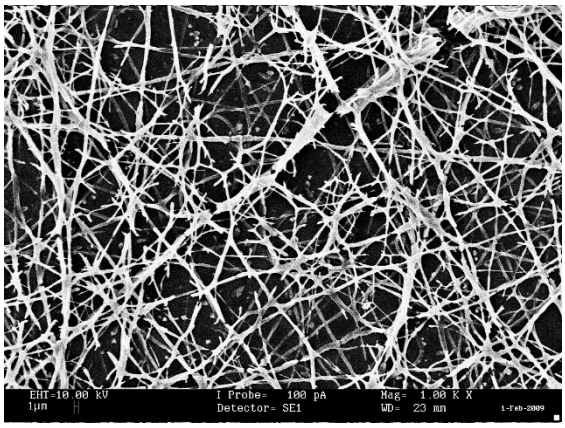

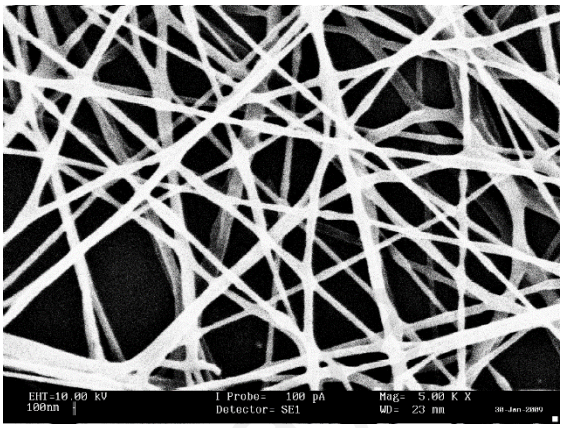

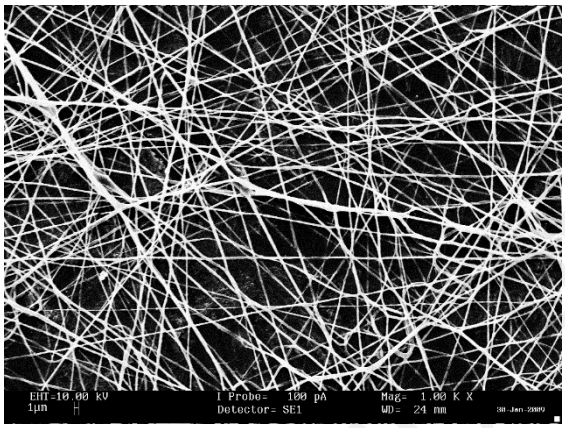

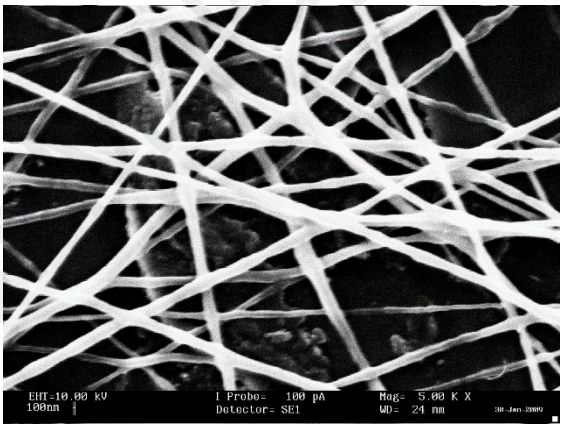

APPENDIX D

Rotating spindle viscometer results for PHB and PCL electrospinning solutions

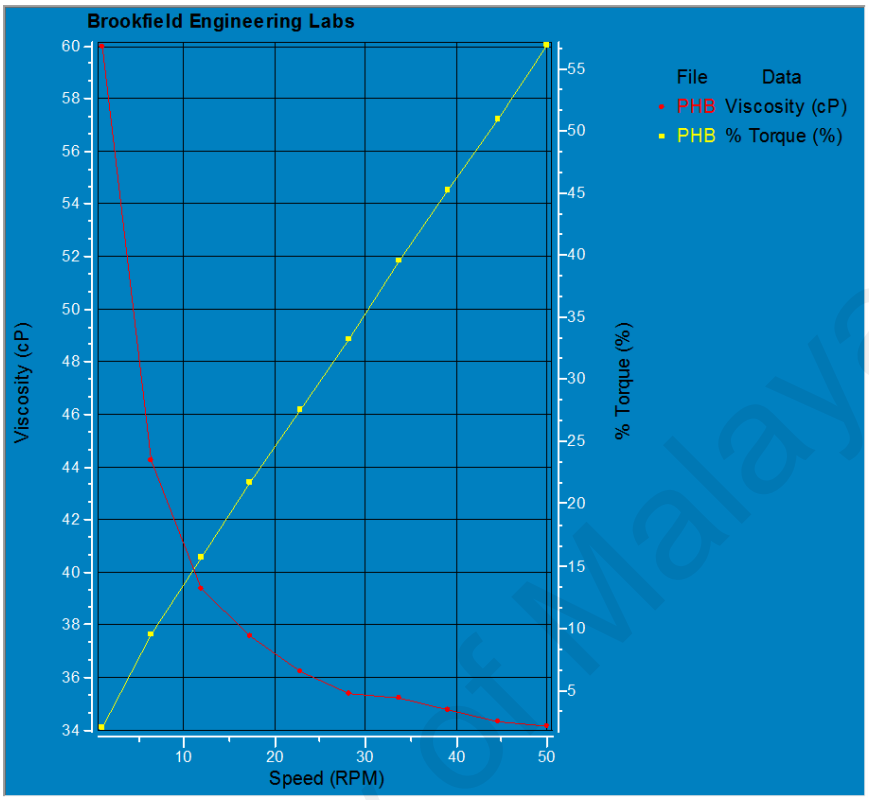

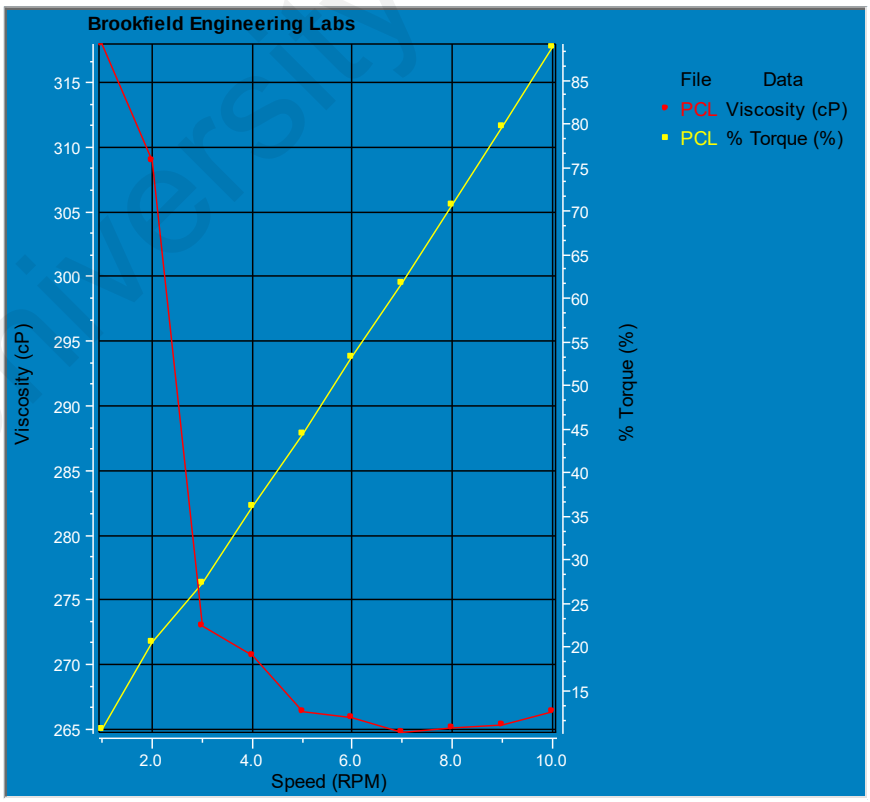

APPENDIX E

Particle size analysis for BHA

Result: Analysis Table

ID: sample 2	Run No: 3	Measured: 11/21/2012 3:53PM
File: PEDRAM	Rec. No: 6	Analysed: 11/21/2012 3:53PM
Path: C:\SIZERS\DATA\		Source: Analysed

Range: 300RF mm	Beam: 2.40 mm	Sampler: None	Obs': 18.1 %
Presentation: 3OHD		Analysis: Polydisperse	Residual: 1.081 %
Modifications: None			

Conc. = 0.0160 %Vol	Density = 1.000 g/cm^3	S.S.A.= 2.7702 m^2/g
Distribution: Volume	D[4, 3] = 28.46 um	D[3, 2] = 2.17 um
D(v, 0.1) = 0.58 um	D(v, 0.5) = 22.81 um	D(v, 0.9) = 63.69 um
Span = 2.767E+00	Uniformity = 8.448E-01	

Size (um)	Volume Under%	Size (um)	Volume Under%	Size (um)	Volume Under%	Size (um)	Volume Under%
0.05	0.00	0.67	10.66	9.00	25.19	120.67	100.00
0.06	0.00	0.78	11.16	10.48	28.28	140.58	100.00
0.07	0.01	0.91	11.59	12.21	31.79	163.77	100.00
0.08	0.02	1.06	11.96	14.22	35.70	190.80	100.00
0.09	0.06	1.24	12.30	16.57	39.97	222.28	100.00
0.11	0.13	1.44	12.62	19.31	44.59	258.95	100.00
0.13	0.28	1.68	12.94	22.49	49.53	301.68	100.00
0.15	0.56	1.95	13.27	26.20	54.79	351.46	100.00
0.17	1.01	2.28	13.62	30.53	60.39	409.45	100.00
0.20	1.70	2.65	14.02	35.56	66.34	477.01	100.00
0.23	2.67	3.09	14.52	41.43	72.66	555.71	100.00
0.27	3.90	3.60	15.16	48.27	79.16	647.41	100.00
0.31	5.29	4.19	16.00	56.23	85.42	754.23	100.00
0.36	6.69	4.88	17.11	65.51	90.94	878.67	100.00
0.42	7.96	5.69	18.54	76.32	95.21		
0.49	9.06	6.63	20.34	88.91	98.23		
0.58	9.97	7.72	22.55	103.58	100.00		

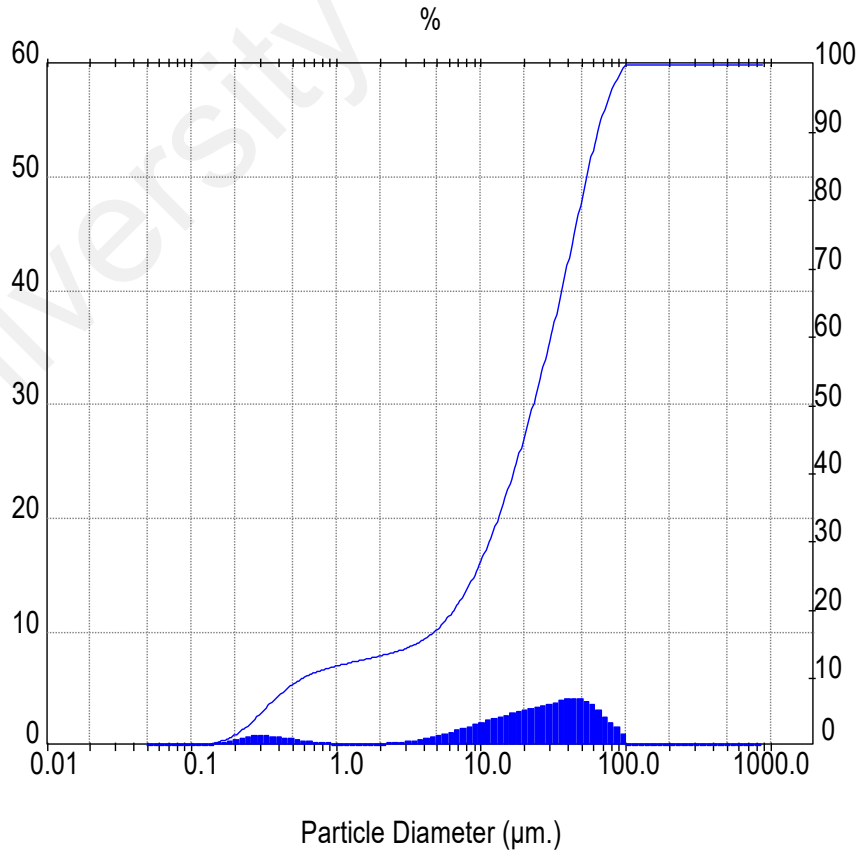

APPENDIX F

GPC results for mcl-PHA

Empower

GPC Report

Reported by User: System

Project Name: UM_GPC1

SAMPLE INFORMATION

Sample Name:	PHA	Acquired By:	System
Sample Type:	Broad Unknown	Date Acquired:	8/7/2009 11:17:58 AM MYT
Vial:	1	Acq. Method Set:	GPC
Injection #:	1	Date Processed:	8/7/2009 2:58:54 PM MYT
Injection Volume:	100.00 ul	Processing Method:	GPC Proc
Run Time:	55.0 Minutes	Channel Name:	410
Sample Set Name:	PEDRAM70809	Proc. Chnl. Descr.:	

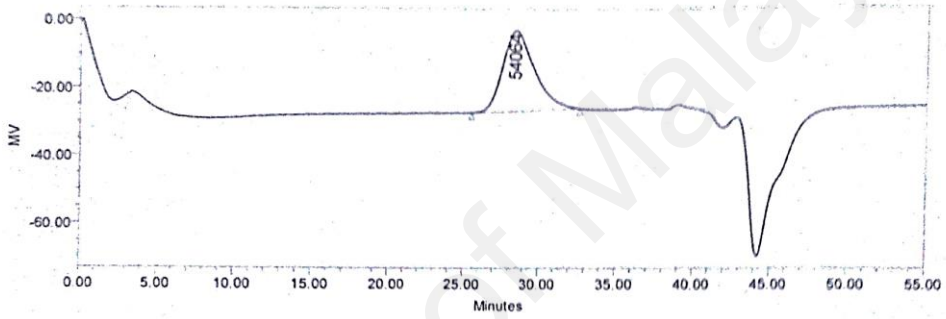

GPC Results

	Mn	Mw	MP	Mz	Mz+1	Mv	Polydispersity
1	34317	56324	54064	83454	115402		1.641293

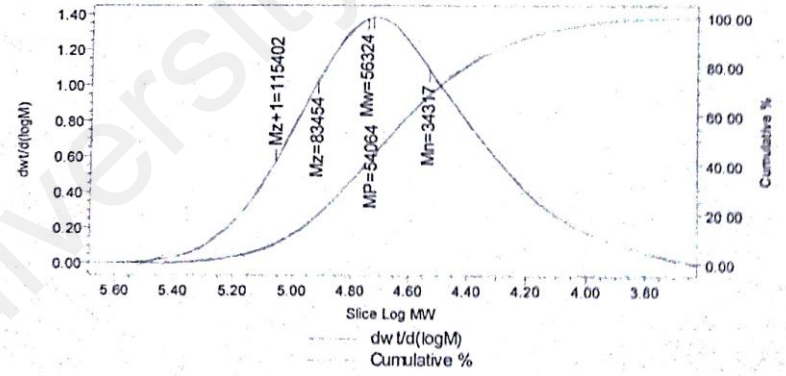

Report Method: GPC Report

Printed 2:59:26 PM As: 8/7/2009

Page: 1 of 1